

# **Optical Design Report**

**WP 2 - Deliverable 2**

**Solar collectors with static concentrator for solar thermal applications at intermediate and medium temperatures**

**Acronym: SCOSCO**

**Date: 30-09-2019**

**Authors:**

**Christian Schorn, Joachim Götsche, Spiros Alexopoulos (SIJ)**

**Athanassios Argiriou, Orestis Panagopoulos, Giorgos Kosmpopoulos, Alex Dokouzis (UPAT)**

Technical report within the framework of „BMBF/GSRT: German-Greek Research and Innovation Programme 2016“

Year of promotion: 2018  
Project executing organisation: BMBF/PTJ  
Support code: 03SF0554A  
Duration: 01.03.2018 to 28.02.2021

Partner of the joint research project

University Patras



Calpak S.A.



Hilger GmbH



Heliokom GmbH



Solar-Institut Jülich

**SIJ | SOLAR-INSTITUT JÜLICH**

GEFÖRDERT VOM



Bundesministerium  
für Bildung  
und Forschung



**GSRT**  
GENERAL SECRETARIAT FOR  
RESEARCH AND TECHNOLOGY

## Table of contents

Executive summary .....	4
Introduction .....	6
Initial Criteria .....	7
Manufacturing errors – defect of fabrication.....	8
Overview Concepts .....	9
Receiver-Concentrator Combinations .....	10
Weather data.....	13
Energy yield calculation.....	14
Complete system simulation .....	15
Concepts .....	18
Concept SCO_1_Tracking_SYM.....	18
Concept SCO_1_Tracking_ASYM.....	19
Concept SCO_1_CYL_CPC .....	20
Concept SCO_4_Micro-mirror concentrator concept .....	28
Results .....	33
Results SCO_1_Tracking_SYM .....	33
Parabolic.....	33
Cylindrical.....	36
CPC .....	38
Results SCO_1_Tracking_SYM and ASYM @ SIJ .....	45
Results SCO_1_CYL_CPC.....	48
Results SCO_2_Multi_SYM/ASYM .....	56
Results SCO_3_FPC/VTC .....	60
Results SCO_4_Micro-mirror concentrator concept.....	60
Results SCO_4_Micro-mirror concentrator concept UPatras .....	72
Conclusion .....	73
Annex .....	76
References .....	79

### Further related documents:

- MA-Thesis “Simulation of solar Thermal Cooling System by means of Annual Energy Yield Calculation” by Aina Attiyah Binti Reiner Karl Lanin, FH Aachen Faculty 10, May 2019.
- Literature survey “190329\_literature\_survey\_SIJ\_LAPUP\_final.docx” from April 2019.

## Executive summary

The concepts examined by the SIJ can both reach the benchmark criteria defined within the project - if the initial parameters are improved. None of the concepts can fully reach all criteria with the initially defined parameters for surface properties and the specific error assumptions, respectively.

The necessary improvements of the concept **SCO\_1\_CYL\_CPC** include a reduction of the error assumptions for the specific surfaces and shapes and the application of an improved reflector.

The reflector should have a reflectivity of at least 95%, which can be reached by state-of-the-art glass mirrors. However, to find a manufacturer to produce glass mirrors of a defined geometry for the primary and secondary reflector, at a reasonable price, appears to be challenging. Aluminium reflectors with a reflectivity of 95% are only available for indoor applications since their surface properties are downgraded after long-term outdoor exposure.

In order to fulfill the criteria, a state-of-the-art receiver with vacuum at the annular gap shall be purchased. The heat loss coefficients should be at least as those of the Himin receiver. The same minimum requirements are required for the absorptance ( $\alpha \geq 85\%$ ) and transmittance ( $\tau \geq 92\%$ ). Since this receiver is already available on the market and its specifications are well documented, the device was considered as a base case for simulations. A receiver without vacuum at the annular gap cannot reach the criteria for the setup of **SCO\_1\_CYL\_CPC**, unless the concentration ratio is raised to a, financially absurd, high level.

The minimum requirement for the construction process and the manufacturing accuracy was examined. The total allowed error per reflector should be  $\sim 7$  mrad; an additional tracking accuracy of 3.5 mrad is feasible in order to reach the benchmark criteria.

The tracking pathway of the concept can be simplified to a circular track if the best of glass and surface materials are used. This might lead to a lower cost, since only one drive motor will be necessary. On the other hand, a higher investment is necessary in order to purchase or manufacture high quality reflectors and receivers.

Further optimization of this concept is required in order to detect the best tracking path with all errors included. Since the tracking pathway of the receiver currently applied was determined for a collector setup without errors and without surface properties, this optimization might lead to a slight improvement of the order of  $\sim 1\%$  zero loss efficiency. This approximate value was derived from a simulation for a static operation point.

The necessary improvement of the **SCO\_4\_Microhelix** concept is an adjustment of the allowed fabrication tolerances. With the initial error assumption, the design point criteria are missing, whereas the annual yield criteria are fulfilled. Hence, the design point is only slightly missed by  $\sim 2\%$  instantaneous efficiency. With a reduced error assumption of  $\sim 7$  mrad the system complies with both criteria.

The SIJ defined initially not only the material properties and specifications of the surfaces, but also the receiver properties for this system. The application of a high-quality absorber coating and an AR-glass is mandatory. The heat loss coefficients of the receiver have been estimated. Typical values of a flat plate collector are considered.

Finally, it must be emphasized at this point that the **SCO\_4** concept is not a classic fixed mirror solar collector (FMSC) but a **quasi-FMSC**; the mirrors are rotated following the position of sun, but the receiver is at a fixed focal point. The mirrors and the corresponding mechanical system are housed inside

a glass covered fixed box, similar to that of a flat-plate collector. The mirror module is installed in a fixed position. From this perspective the concept can be regarded as a quasi-fixed-mirror solar collector (quasi-FMSC).

If the implementation of the SCO\_4 concept is selected, the work allocation among the industrial partners must be redistributed. Up to now, it was agreed that Heliokon supplies the tracking unit for a receiver or a multi-channel variant, respectively. CALPAK is responsible for the reflector unit and supporting structure. For the SCO-4 concept, Heliokon would provide the tracked reflector unit with structural design and CALPAK could be responsible for the design of a receiver.

Furthermore, the German and Hellenic authorities that co-finance the project, should be consulted about the proposed changes.

It is interesting to optimize both variants of the system, with respect to the seasonal performance factor (SPF). So far, only the first calculations have been made to determine the solar fraction related aperture area; a system optimization with additional data is still pending. Besides the control parameters the component parameters are just a first estimation.

More detailed analysis of both concepts can be performed with the COMSOL software in the future. Currently the SIJ is examining the purchase of the COMSOL add-ons “Heat transfer” and “Optimization”. These add-ons allow the implementation of the heat transfer from the absorber surface to the fluid and combine the physics of raytracing and heat transfer. With this upgrade the complete solar collector system, from the ray to the fluid, can be simulated, taking into account realistic values of the material properties, the surface properties of the reflectors and the various error assumptions. The optimization tool allows to perform waste parameter variation and detect absolute minima or absolute maxima.

Moreover, once the final design is selected, the construction can be implemented with a higher level of detail. Therefore, additional component parts like the fixation elements, bellows and gaps between arrays sought, can be integrated in the model, since those components affect the performance of the collector.

## Introduction

At the kickoff meeting on 24<sup>th</sup> /25<sup>th</sup> Sept. 2018, the project partners agreed to investigate a minimum number of fixed mirror solar collectors (FMSC) concepts, as shown in Figure 1.

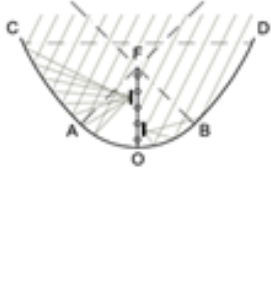
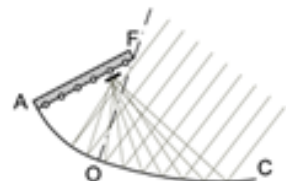
Concept	Type of reflector		
SCO-1 Single tube/tracking	symmetric	Asymmetric Option: secondary reflector	Parabolic shape or any other
SCO-2 Multiple tube	Symmetric 	Asymmetric Option: secondary reflector Specification of the number of tubes for the set-up 	
SCO-3 FPC and VTC	"Booster" reflector Theoretical examination of concepts SCO-3 FPC & SCO-3 VTC		

Figure 1: Overview concepts of fixed mirror solar collectors (FMSC) from 181023\_Protocol\_KickOff\_final.

Description of the concepts:

- Concept SCO\_1: A single receiver tube is biaxially tracked, in order to collect as much energy as possible. The basic mirror/reflector shapes are the one's introduced by Tripanagnostopoulos. Two options will be examined, a symmetric version and an asymmetric one. The size of the aperture area might vary as well. In addition, any other basic shape of reflectors might be chosen, in order to meet the defined collector criteria.
- Concept SCO\_2: A set of receivers are placed within the basic form according to Tripanagnostopoulos. Since the various receivers are exposed to a different solar irradiance distribution at a certain incident angle modifier (IAM), they can be operated separately. Hence, a tracking mechanism is not necessary.
- Option: A secondary reflector can be used in order to enhance the energy yield of a collector. Since a fixed mirror solar collector does not produce a narrow focal line, the secondary reflector can be used to collect more sun rays.
- Since the identification of the best concept is an extensive process that takes into account a multiplicity of parameters, any other concept (SCO\_X) may be derived during the course of the project.
- Concept SCO\_3: A conventional flat plate collector (FPC) and a conventional vacuum tube collector (VTC) combined with a flat mirror (booster reflector) will be examined. This simple approach will be used as the baseline configuration for the evaluation of the concepts. The collector (SCO\_1, SCO\_2 or SCO\_X) that will be constructed within the ScoSco project, should be able to clearly outperform SCO\_3.

## Initial Criteria

In order to identify a performing collector design, various criteria were defined. Some of the criteria are directly taken out of the project proposal [1, 2], others are derived from information at the kickoff meeting [3] or from practical considerations [4]. The criteria are listed below.

Criteria (every criterion is to be treated as a **knock-out** criterion!)

- [1] Design point of collector (50 % efficiency @250°C average fluid temperature, 800 W/m<sup>2</sup> DNI, and 30 °C ambient temperature) [project proposal]
- [2] Annual energy yield at Patras  $\geq 700$  kWh/m<sup>2</sup>a [defined in project proposal] of a collector with matched flow and given temperatures (inlet: 100 °C, outlet: 150 °C) [defined at kickoff meeting]
- [3] Energy supply for a “double”-effect absorption chiller [Application described by Calpak at kickoff meeting; solar fraction ~ 80%]

$$SF = \frac{\dot{Q}_{solar}}{\dot{Q}_{solar} + \dot{Q}_{aux}}$$

- [4] Pro and Cons, area consumption, resource efficiency, availability of materials and components, LCA, costs and any other practical considerations.

The evaluation of the criteria is marked at the following overview of concepts, Table 2.

Table 2 was developed on the basis of the overview of the kickoff meeting and was extended by another concept. In addition, the responsible project partners are listed as well as the evaluation of the listed criteria.

**Red**  $\approx$  miss, **Green**  $\approx$  comply with the criteria, **black**  $\approx$  not evaluated yet.

## Manufacturing errors – defect of fabrication

In order to evaluate a performing collector design, the errors of materials, shapes as well as natural deviations must be accurately considered.

Promising concepts out of the bundle of concepts presented in Figure 1, are going to be further evaluated and analyzed with respect to different errors. Table 1 summarizes the assumed errors of the different components and materials. Since in literature one may find several different names and representations of sources of error, the following nomenclature has been proposed by the SIJ. Further secondary classification into several different sources of error could prove to be useful during the production process later. The error values provided in Table 1 are taken from the document 190416\_Minutes\_Webconf\_final.pdf.

Table 1: Error assumptions for the various concepts

Specularity error	$\square_{sp}$	$\pm 1$ mrad	Increase of beam divergence after reflection, e.g. measured by pointing a laser with a very small beam divergence on the reflecting surface and measuring the intensity distribution on a screen hit by the reflected beam. It is a property of the mirror material.
Slope error	$\square_{sl}$	$\pm 2.7$ mrad	If the reflector is not in perfect alignment with the basic shape.
Shape error	$\square_{sh}$	$\pm 3$ mrad	Average deviation of the mirror normal direction (shape) from its ideal curvature.
Alignment error	$\square_{al}$	$\pm 9$ mrad	Error of the overall alignment of the (fixed) reflector unit.
Tracking error	$\square_{tr}$	$\pm 0$ mrad (for fixed mirror)	Error due to stepwise tracking and/or wrong tracking

The total error may be calculated as  $\sigma_{tot} = \sqrt{\sum_i \sigma_i^2}$ .

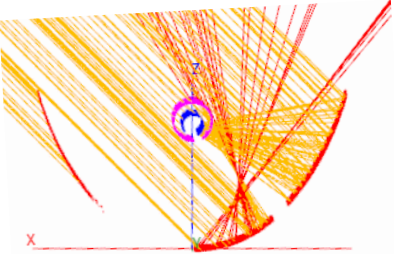
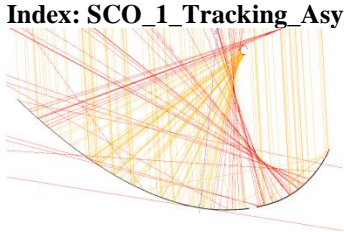
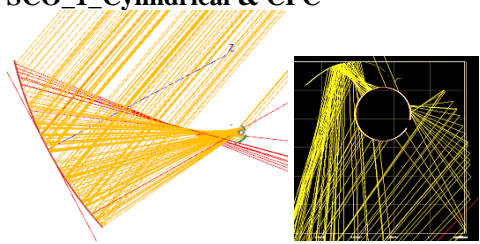
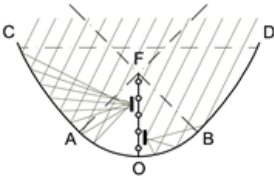
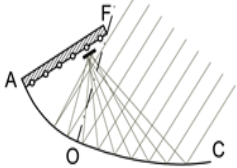
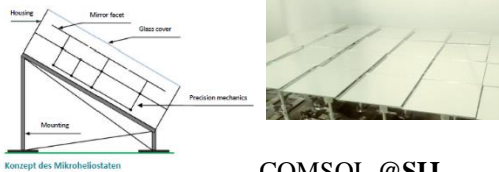
It is assumed that these errors follow a Gaussian (normal) distribution. e. g. with the data from Table 1 we obtain  $\sigma_{tot} \approx 10$  mrad for a single reflector system.

For concepts with a secondary reflector or a moving receiver a tracking error of  $\square_{tr} = \pm 3.5$  mrad is suggested by the SIJ. This corresponds to the positioning error ( $\square_x, \square_y$ ) of a tracked receiver.

Sun divergence:  $\pm 4.65$  mrad, with uniform circular distribution.

Properties of the active surfaces are specified as follows, according to the document 190416\_Minutes\_Webconf\_final.pdf: Mirror reflectivity  $\square = 0.9$ , absorber absorptivity  $\square = 0.95$ , glass transmissivity  $\square = 0.92$ . For simplicity, it is assumed that the mirror and absorber are opaque ( $\square = 0$ ), the glass has no absorption ( $\square = 0$ ), and no angular dependence of these properties is considered.



Overview Concepts	Table 2: Type of concentrator configuration and evaluated criteria				
<b>SCO-1</b> Single tube tracking	symmetric Index: SCO_1_Tracking_Sym  Software SolTrace @SIJ	1 asymmetric Option: secondary reflector 2 Index: SCO_1_Tracking_Asym  SolTrace @SIJ	1 <sup>1</sup> 2 3 4	Parabolic design or other basic design Index: SCO_1_XY • SCO_1_Cylindrical & CPC  SolTrace / Comsol @SIJ	1 2 3 4
<b>SCO-2</b> Multiple tube absorber	symmetric Index: SCO_2_Multi_Sym  SolTrace / Tonatiuh @UPAT COMSOL @SIJ not done yet	1 asymmetric Option: secondary reflector 2 Specification of the number of tubes. 3  4 Index: SCO_2_Multi_Asym SolTrace / Tonatiuh @UPAT	1 2 3 4		
<b>SCO-3</b> FPC and VTC	“Booster” reflector Theoretical examination of concepts with state-of-the-art collectors @UPAT				
<b>SCO_4</b> Microhelix	 COMSOL @SIJ				

<sup>1</sup> Criteria are only reached at single operation point for an asymmetric mirror with 2 times the nominal aperture area.

## Receiver-Concentrator Combinations

The thermal performance of a receiver-concentrator combination depends on the optical as well as on the thermal properties of its components.

A simple efficiency equation is used to describe the collector performance:

$$\eta = \eta_o - F'_c \cdot U_L \frac{(T_m - T_U)}{G_{DNI}},$$

with

$$\eta_o: \text{“optical efficiency”}, \eta_o = F'_c \cdot (\alpha\tau)_{eff}, \text{ and } (\alpha\tau)_{eff} = \alpha\tau \cdot \frac{1}{K} + \left(1 - \frac{1}{K}\right) \cdot \alpha\tau\rho,$$

where K is the ratio of aperture width and receiver diameter.

This equation describes the case of a concentrator with tubular receiver, where the geometric concentration ratio c (aperture area/absorber area) is given by  $c = K/\square$ . The first term in the equation of  $(\square\square)_{eff}$  is due to the fraction of sunlight that may hit the receiver tube directly, the second term describes the concentrated part.

$F'_c$ : collector efficiency factor, derived from the switch from absorber temperature to average fluid temperature in the collector efficiency equation. It can be expressed as  $F'_c = 1/(1+c*U_L/U_{af})$ , where  $U_{af}$  is the heat transfer coefficient between absorber and collector fluid (expressed with respect to absorber area).

$U_L$ : The overall heat loss coefficient, determined with respect to the collector aperture area. It usually depends on the temperature difference between the collector fluid  $T_m$  and the ambient air,  $T_U$ . It may be derived from the linear and quadratic heat loss coefficients of the absorber tube, ( $a_1$  and  $a_2$ ) as  $U_L = (a_1 + a_2 * (T_m - T_U))/c$ .<sup>1</sup>

$G_{DNI}$ : beam solar irradiance.

In order to evaluate the performance of receiver-concentrator combinations, a simple spreadsheet was created that determines the minimum required concentration ratio that would be necessary to achieve 50 % collector efficiency at an average fluid temperature of 250 °C, based on 2 parameters, the optical efficiency  $\eta_o$  and the term  $F'_c * a_1$  (see Figure 2). To reduce the parameter variation range, it was assumed that the coefficient  $a_2$  is related to  $a_1$  via the equation  $a_2 = a_1/175K$ .

The required concentration c was calculated as

$$c = \frac{F'_c \cdot (a_1 + a_2 \cdot (T_m - T_U)) \cdot (T_m - T_U)}{G_{DNI} \cdot (\eta_o - \eta_{real})}$$

using  $T_m = 250$  °C,  $T_U = 30$  °C,  $G_{DNI} = 800$  W/m<sup>2</sup>, and  $\eta_{real} = 50$  %.

<sup>1</sup> It should be noted that this is a simplified equation that can be used as an approximation for moderate temperatures but does not allow extrapolation to very high temperatures, for which a more detailed model must be applied that explicitly considers the T<sup>4</sup> law of radiative heat transfer.

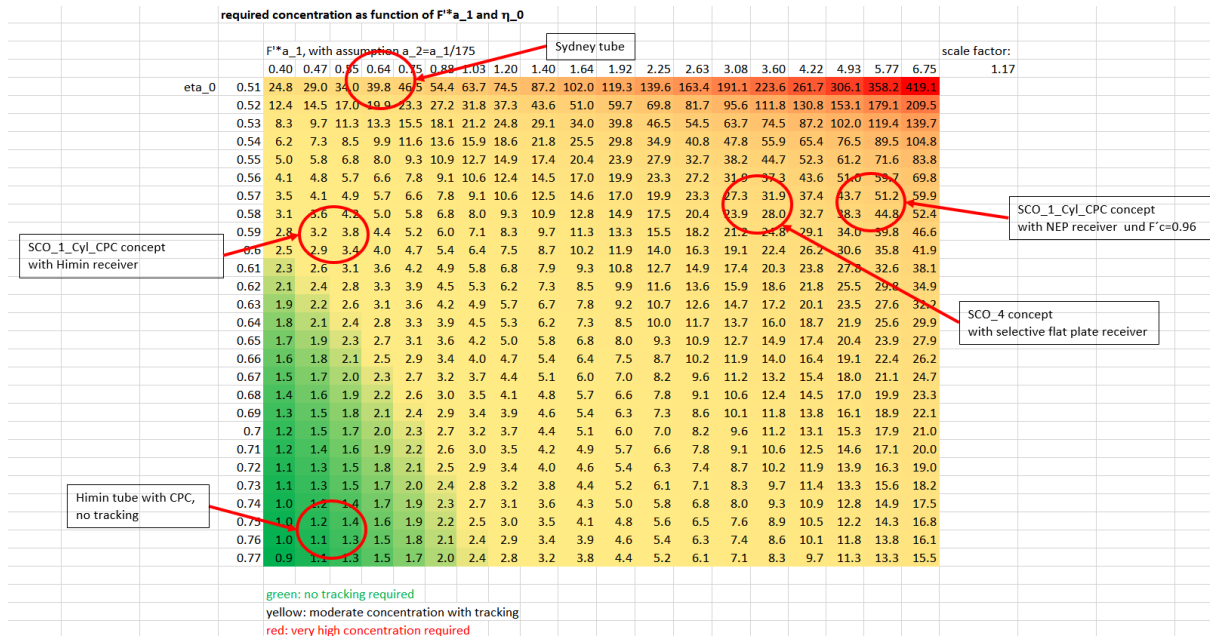


Figure 2: Graphical representation of several receiver-concentrator combinations (obtained with the spreadsheet file "190503\_scosco\_coll\_equation.xlsx").

It can be observed that on the market there are mainly two types of receivers: vacuum tubes (with  $F'_c a_1 < 0.8 \text{ W}/(\text{m}^2\text{K})$ ) and non-evacuated receivers (with  $F'_c a_1 > 3 \text{ W}/(\text{m}^2\text{K})$ ).

If quality vacuum receivers are used (e.g. the Himin tube), the required thermal performance (criterion [1]) can be reached with a concentration  $c < 1.5$ , which can be achieved with a fixed CPC reflector. No tracking is required in this case, neither for the concentrator nor for the receiver.

Cheaper "Sydney tube" receivers are characterized by low thermal loss coefficients and a relatively low  $\square_o$  (see "Sydney tube" in Figure 2), which results from the relatively bad heat exchange between the absorber and collector fluid,  $U_{af}$  being typically<sup>2</sup> in the order of  $5 \text{ W}/(\text{m}^2\text{K})$ . With  $\square_o = 0.51$ , a very high concentration ratio is required to obtain an overall collector efficiency of 0.5. This situation is related to extremely high absorber temperatures. If the desired collector efficiency is reduced to 30 %, then the required concentration ratio drops to about 1.9, which again leads to a situation where no tracking is necessary, neither for the concentrator nor for receiver.

When non-evacuated receivers are used, the concentration ratio must be high, if high efficiencies at high fluid temperatures are required.

According to the general behavior and preliminary results from the Figure above, the SIJ decided to examine the concept SCO\_1\_CYL\_CPC and SCO\_4 more in detail.

According to the manufacturer's specifications, vacuum tubes are tested up to  $275 \text{ }^\circ\text{C}$ . The initially selected concentration factor of 12 leads to temperatures much higher than the tested one while an average fluid temperature of  $250 \text{ }^\circ\text{C}$  would result to collector efficiency  $< 0.1$ . In order to achieve higher efficiency, we reduced  $T_m$  to  $150 \text{ }^\circ\text{C}$ . The simulations revealed that intercept factors should be  $\sim 0.6$  and working fluid temperature  $T_m < 150 \text{ }^\circ\text{C}$ . The results using the aforementioned values  $\gamma = 0,6$  and  $T_m = 150 \text{ }^\circ\text{C}$  are shown in Figure 6.

<sup>2</sup> Ma, Liangdong, et al. "Thermal performance analysis of the glass evacuated tube solar collector with U-tube." *Building and Environment* 45.9 (2010): 1959-1967

For safety purposes, the system should operate on  $T_{\text{abs}} < 240 \text{ }^\circ\text{C}$ , which results to a collector efficiency

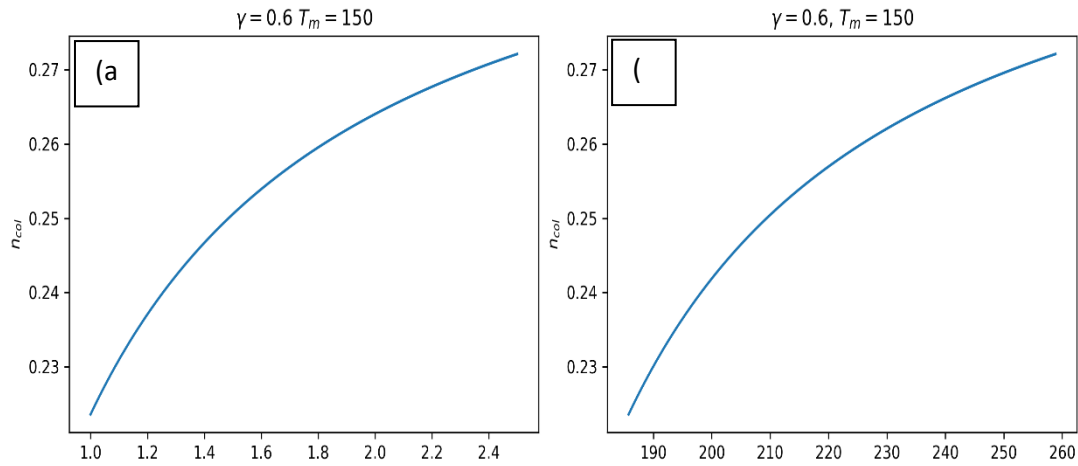


Figure 3 Collector efficiency as a function of the (a) geometric concentration ratio and (b)  $T_{\text{abs}}$  for  $\gamma = 0.6$  and  $T_m = 150 \text{ }^\circ\text{C}$ .

of  $\eta_{\text{col}} = 0.265$  and  $C_{\text{geo}} = 2.2$ .

Available materials as presented in the bibliography

For  $G = 800 \text{ W/m}^2$  and  $T_a = 20 \text{ }^\circ\text{C}$

Collector type	$\eta_0$ for $T_m - T_a = 150 \text{ K}$
High vacuum flat plate collector (MIT-Power v3.11)	0.46
CPC - Vacuum tube collector (Aqua Plasma)	0.48
Standard - vacuum tube collector (XL 15/26)	0.37
XL 19/49 P	0.49

For  $G = 800 \text{ W/m}^2$  and  $T_a = 20 \text{ }^\circ\text{C}$

Collector type	$T_m - T_a \text{ (K) for } \eta_0 = 30\%$
High vacuum flat plate collector (MIT-Power v3.11)	193
CPC - Vacuum tube collector (Aqua Plasma)	235
Standard - vacuum tube collector (XL 15/26)	170
XL 19/49 P	235

## Weather data

The weather data are provided by UPAT at a one-minute time step.

Annual energy yield depends on the location/region selection, thus selecting a weather data that can reach high global irradiation level is especially crucial for installation of concentrating solar collector system. The Project Static Concentrating Solar Collector (ScoSco) is focusing on the annual energy yield for the location in Southern Greece. The average annual horizontal solar energy in entire Greece is ranged between 1450 kWh/m<sup>2</sup>a to 1800 kWh/m<sup>2</sup>a. This indicates higher potential to harness the expected solar energy yield, which later needs to be verified with the simulated weather data.

Two weather data were selected for comparisons, namely Andravida (37°N) and Patras (or Patra) (38.2°N) in southern Greece.

The weather data for Andravida were retrieved from Meteonorm and cover a 365-day period. The weather data for Patras or Patra result from the automatic weather station of the Laboratory of Atmospheric Physics of the University of Patras (UPAT) and cover a 366-day period. It was chosen because of higher resolution, that for 2016 the most data have been available and that it seems to be quite an average year. The weather data was however simulated only for 365 days to make a better comparison with the weather data from Andravida. It is to be taken into account, 365 days is the simulation time and not the actual clock time. All weather data are in the format of .MAT file for the simulation with CARNOT toolbox.

To validate the value of global radiation with the estimated value for direct radiation on horizontal surface in Greece, a simple simulation model is developed in MATLAB. The simulation time is one year (0-365 days) with the input data from the weather file. The collector is mounted at a default position (tilted at 30° facing the South).

The value of the annual solar radiation on the direct surface of the collector measured at the default collector orientation is 1480 kWh/(m<sup>2</sup>a) for the weather data file Patras and 1354 kWh/(m<sup>2</sup>a) for Andravida. The annual solar radiation for Patras is higher than Andravida but it still lies within the range mentioned above.

## Energy yield calculation

Figure 3 shows the complete model of the solar collector system for the calculation of annual energy yield with the MATLAB Simulink Carnot toolbox.

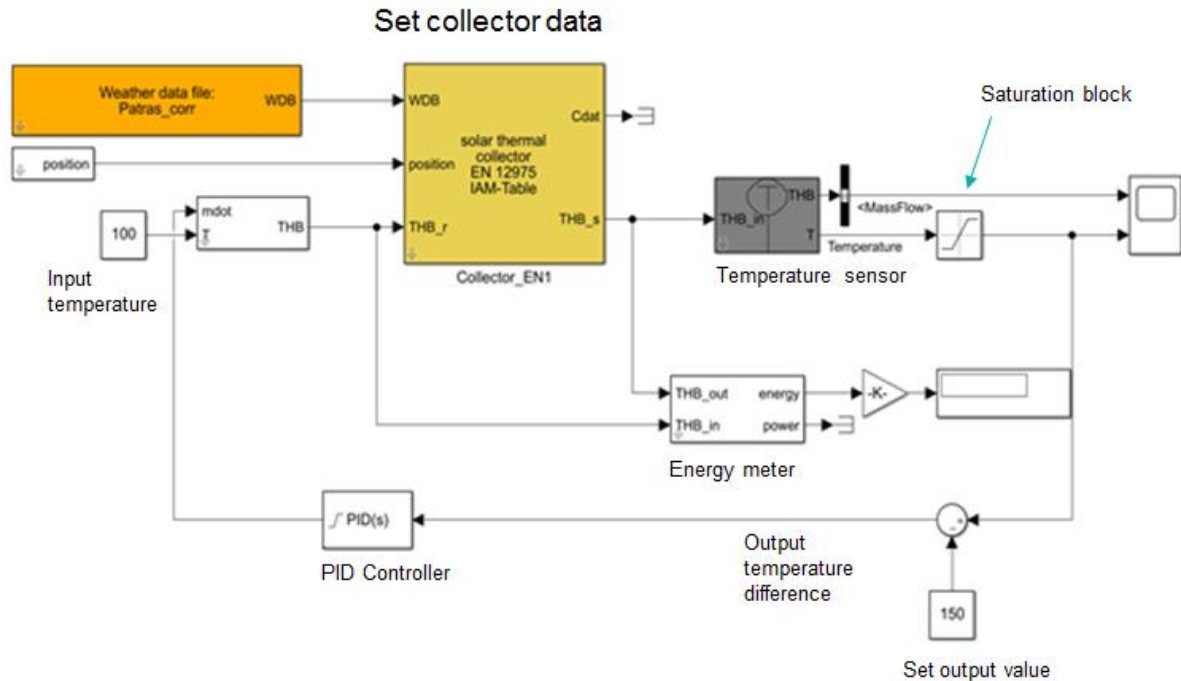


Figure 4: Complete model of the simulation for annual energy yield calculation.

A sensor is connected to the solar collector to measure the mass flow of the heat transfer fluid and the output temperature. The sum block calculates the temperature difference between the set point value (150°C) and the actual value of the outlet temperature of the solar collector measured by the sensor. Since there are fluctuations in solar radiation throughout the day, the temperature difference is fed into the PID Controller to control the mass flow of the heat transfer fluid inside of the collector and keeping the inlet temperature of the solar collector at a constant of 100 °C.

The input and output of the THB of the solar collector is connected to a block called Energy Meter. The Energy Meter block calculates the annual solar yield of the system in  $J$  by measuring the temperature of the inlet and outlet of the solar collector and the volumetric flow rate of the heat transfer medium.

The value for annual energy yield is normally written in the unit  $\frac{kWh}{m^2 a}$  in many literatures. The function of the gain block is to convert the energy in  $J$  to  $\frac{kWh}{m^2 a}$ . The area of the collector is variable, but for first estimations it was set to  $2.5 m^2$ .

The annual energy yield for different concepts, such as the default FMSC's, early assumption of the static concentrating solar collector and the four proposed design of the solar collectors are to be calculated.

## Complete system simulation

In order to simulate a possible later application of the design concepts a complete system simulation was set up. It includes the Yazaki WFC-SC5 absorption chiller with a cooling tower as a subsystem, two buffer tanks, the collector model, the weather data, an assumed cooling demand for the building, circulation pumps and the control units for the overall regulation. Energy meters are used to calculate the energy supply for the relevant subsystems.

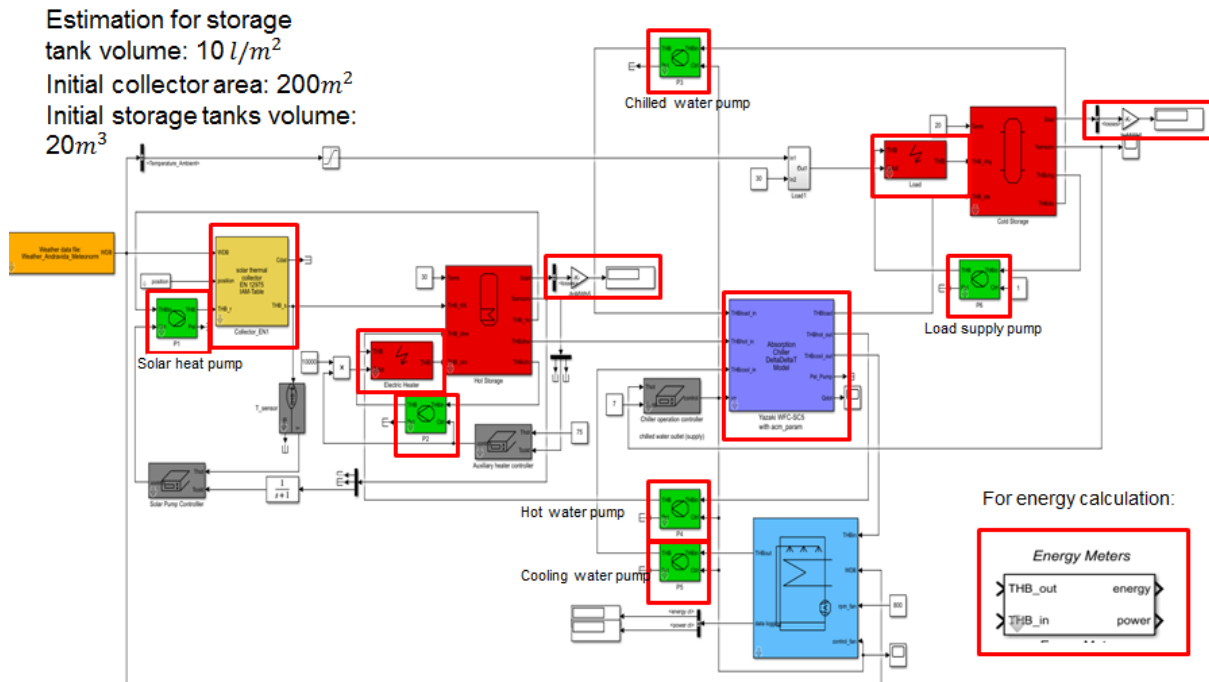


Figure 5: Complete system model of the simulation for solar fraction, SPF calculation and further optimization

At the time of authoring this report, an important number of assumptions are made because real data are not yet available e.g. storage tank specifications, heat exchanger design and pump specifications.

The control units required to simulate the whole solar cooling system are listed in Table 3. The definition of the control parameters is based on free assumptions, as no other data exists at this time.

Table 3: Controller settings based on temperature difference method and their control purpose.

Controllers	Switch on temperature difference, $\Delta T_{on}/^{\circ}C$	Switch off temperature difference, $\Delta T_{off}/^{\circ}C$	Maximum temperature, $T_{max}/^{\circ}C$	Control Purpose
Solar pump	1.5	3	130	-Pump water through to cool off the solar collector.
Auxiliary Heater	0	-5	85	-Switch on/off the auxiliary heater.
Chiller Operation	5	-4.5	50	-Control the operation of $P_3$ , $P_4$ and $P_5$ .  -Switch on/off the fan of cooling tower.

The volumetric flow of the fluid in the specific solar cooling subsystem is controlled by five circulation pumps as shown in Table 4. The power of the pump is assumed to be of  $25 W$  for a mass flow of  $1 m^3 / h$  or  $0.28 kg / s$ . The mass flow of the water and the power rating of the pumps are listed in Table 4.

Table 4: Power and flow rate of the pumps in the solar cooling system

Circulation pumps	Flow rate/ $kg / s$	Power/ $W$
Solar collector loop, $P_1$	1.1	98
Auxiliary heater loop, $P_2$	0.5	45
Chilled water for chiller, $P_3$	0.76	68
Hot water for chiller, $P_4$	1.2	108
Cold water for chiller, $P_5$	2.58	230
Demand supply loop, $P_6$	0.3	27

The simulation will be performed with the control method and parameters described above. Since the solar collector is used for cooling purposes, the operation time of the chiller is set from day 120 to 300 (May-October) based on the abovementioned ambient temperature and load calculation.

The control method used in this study for the operation of solar assisted cooling, can be characterized as a cold guided mode. This mode supplies cooling power only for a defined cooling load and with the needed driving heat for the operation of the chiller. As the load profile for the cooling demand is **not**



**yet available as an English version**, the cooling demand of the building is calculated as a function of the ambient temperature by using the following equation:

$$\dot{Q}_e = 17kW + (T_{amb} - 30^\circ C) \cdot 1,7kW$$

## Concepts

Within this chapter the individual concepts and their setup are presented.

### Concept SCO\_1\_Tracking\_SYM

As a variant the fixed symmetric reflector proposed by Trypanagnostopoulos is simulated with a single biaxial tracked receiver. The design of the base reflector shape is shown in the figure bellow. The middle bottom part of the reflector is a sector of a circle, on the right and left side a parabolic reflector, shifted by  $45^\circ$ , is added respectively. The cutting of the parabolic shape is done in accordance to the proposed aperture area of the publication.

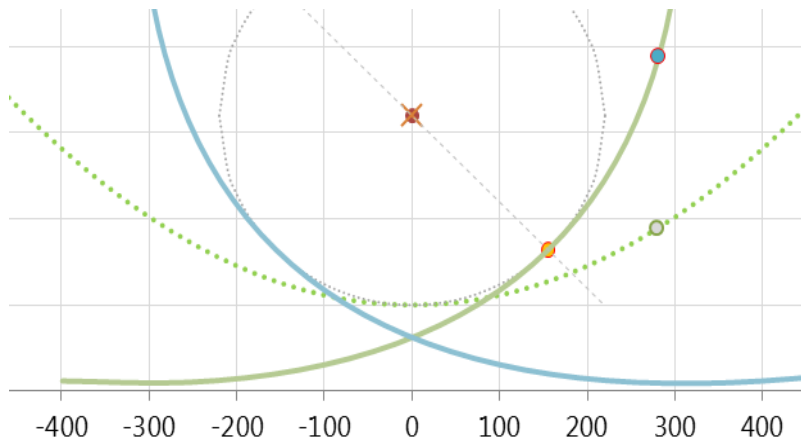


Figure 6: Design of basic reflector shape (axis in mm)

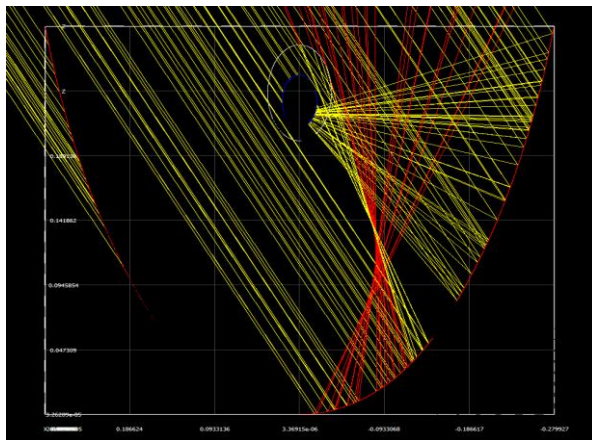


Figure 7: Basic reflector shape at SolTrace raytracing simulation with visualization of two focal points

Y. Tripanagnostopoulos and P. Yianoulis, "CPC solar collectors with multichannel absorber," *Solar Energy Vol.58 No.1-3*, pp. pp. 49-61, 1996

The main idea of the SCO\_1\_Tracking\_SYM as well as the concentrator geometry is described in the seminal paper (Tripanagnostopoulos and Yianoulis, 1996) of the SCoSCo project proposal.

In order to evaluate the ray-tracing software, UPat attempted to reproduce the work of Tripanagnostopoulos and Yiannoulis. The results could not be reproduced using SolTrace, due to a software bug; however the results using Tonatiuh were in good agreement with the previous work. Therefore, UPat switched to Tonatiuh software for the optical study of SCO\_1 concept.

## Concept SCO\_1\_Tracking\_ASYM

As a variant of the basic shape proposed by Trypanagnostopoulos an asymmetric approach with a biaxial tracked receiver is evaluated. The design is explained in the publication by Trypanagnostopoulos and an example is shown in the figure below. Moreover, the shape is transferred to a SolTrace simulation via a csv file and a spline interpolation. Eventually raytracing simulation could be carried out.

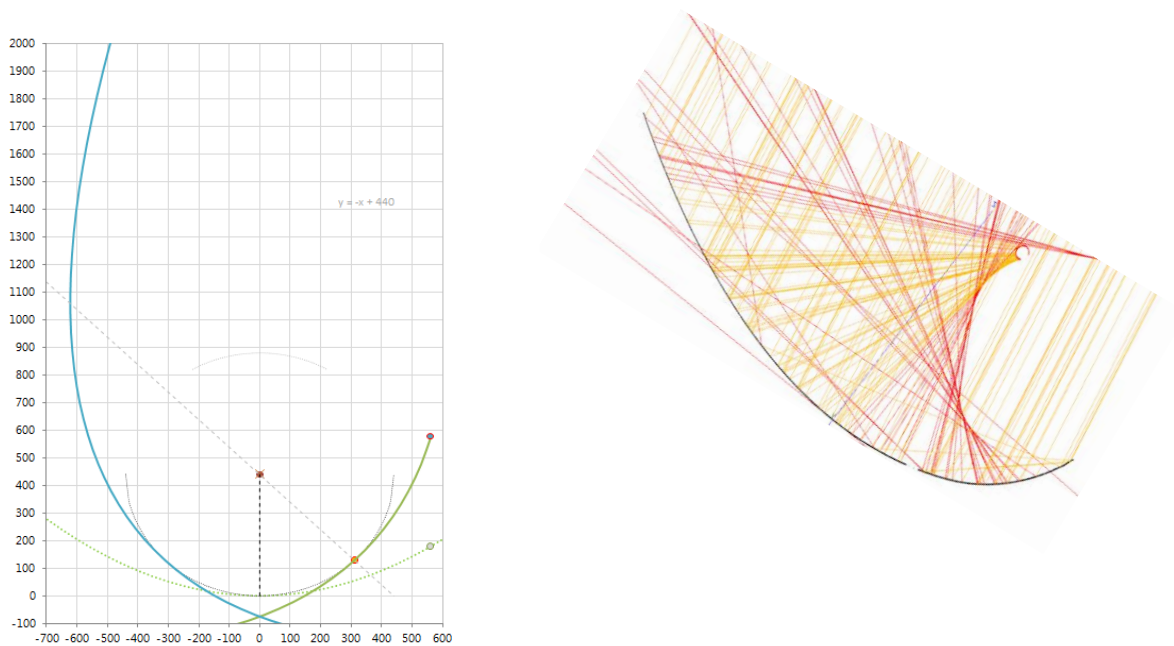


Figure 8: Design of asymmetric shape (axis in mm) and visualization in SolTrace

## Concept SCO\_1\_CYL\_CPC

### Preliminary examinations

The first idea of the SCO\_1\_CYL\_CPC system was inspired from the Duke collector, since it is an operating system in combination with a chiller – the exact combination that is required for the ScoSco project.

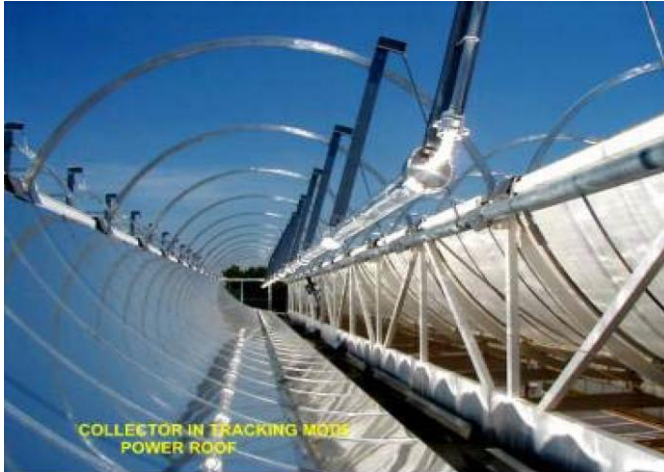


Figure 9: Duke power roof solar collector.

Gee, Cohen and Greenwood, Duke Solar Power Roof, Proceedings of ISEC 2003, 2003 International Solar Energy Conference, Hawaii, USA, ISEC2003-44035

After conducting some basic preliminary raytracing simulations in SolTrace on different shapes and dimensions, a first draft of the SCO\_1\_CYL\_CPC was created. In the following figure the design is drafted.

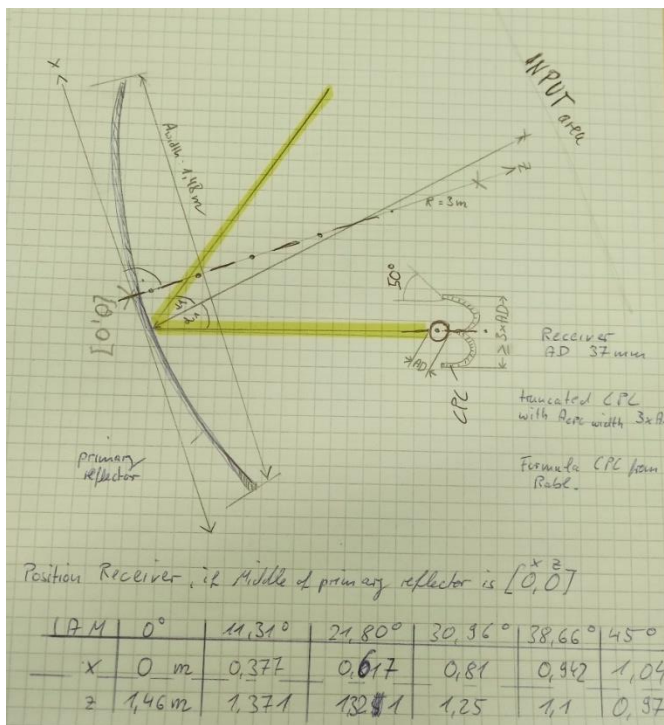


Figure 10: Sketch of the first basic design parameters.

As a first step, an estimation of the necessary aperture size of the used CPC aperture area was conducted. The following graph shows the influence of the CPC aperture area on the transversal IAM. The acceptance angle of the CPC was set to  $50^\circ$  in order to collect rays from a relatively broad area.

$C_{geo}$  refers to the concentration ratio of aperture width divided through the outer diameter of the receiver tube.

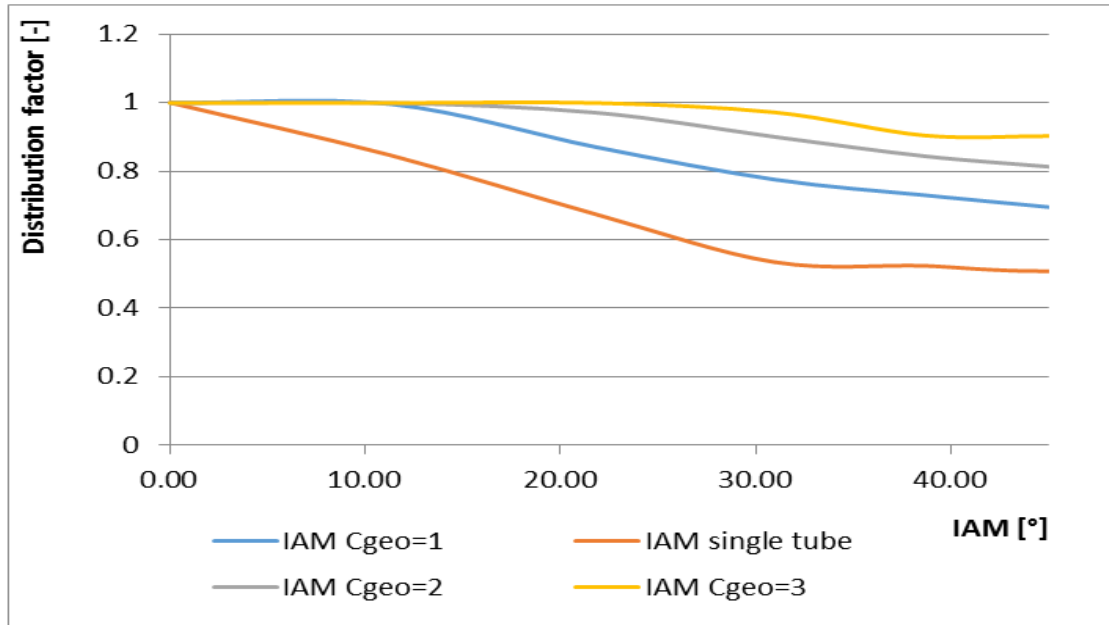


Figure 11: Parameter variation of the concentration ratio of a CPC with  $50^\circ$  acceptance angle.

In order to obtain high IAM factors for a broad range of angles, the  $C_{geo} = 3$  assumption was considered for the subsequent simulations.

The data set of the following table was used for a COMSOL Raytracing simulation for the transversal IAM. First, simulations in order to detect the transversal IAM without errors (evaluation of the pure geometry) were performed. The optimization rule applied during the simulation was to obtain the highest possible intercept factor for a given setup at various IAM.

Table 5: Incident angle modifier transversal with self-shadowing caused by the secondary reflector.

Angle [°]	0.00	11.31	21.80	30.96	38.66	45.00	90
Trans IAM factor [-]	0.88	0.86	0.84	0.70	0.68	0.69	0.025

For the longitudinal IAM a parameter variation was performed with respect to a different length of the collector arrays. A 1.5 m, 6 m and a 12 m long collector array was considered, neglecting any fixation elements, bellows and gaps between arrays.

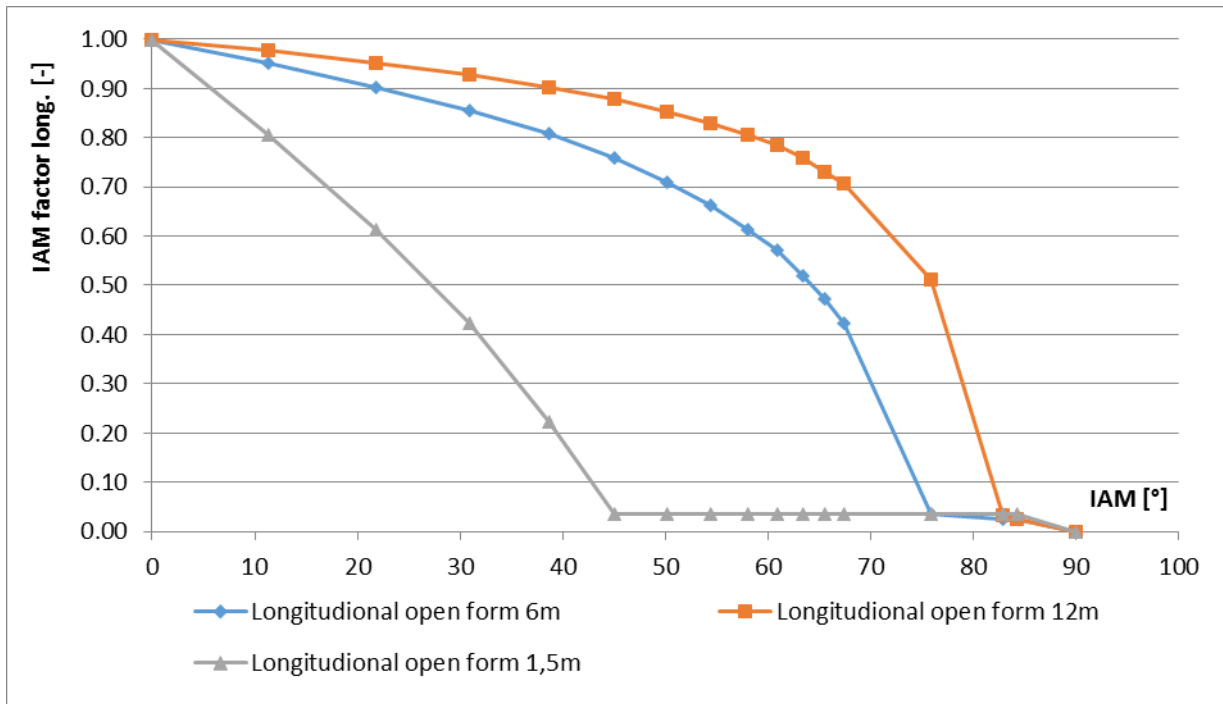


Figure 12: Parameter variation length of the solar collector array.

Apparently, the end losses are reduced when the collector array gets longer.

For the subsequent energy yield calculations of the preliminary concept, the 12 m long collector array is considered. Later, during the simulations with material properties and error assumptions only the 6 m long collector array was considered. Since the collector should be able to be integrated into buildings, it is going to be installed on roof tops. Consequently, a 12 m long array seems to be appropriate, taking into account the available space on the roof of industrial buildings. In addition to that, the 12 m long arrays lead to a better performance of the linear focus approach.

Table 6: Incident angle modifier longitudinal 12 m long array and 6m long array for linear focus approach.

Angle [°]	0.00	11.31	21.80	30.96	38.66	45.00	90
Long 6m IAM factor [-]	1.00	0.95	0.90	0.86	0.81	0.76	0
Long 12m IAM factor [-]	1.00	0.98	0.95	0.93	0.90	0.88	0

Since the material and surface properties haven't been defined at an early stage of the project, educated assumptions on basis of the data available for competitive products have been used. Therefore, a parameter variation for the collector efficiency factor, transmittance, absorptance and reflectivity was considered. With the simulated collector zero loss efficiency and the assumed heat loss coefficients, an energy yield calculation was performed for a set of data. The  $c_p$  value was estimated in accordance to a test report for a PTC with similar dimensions.

Table 7: Parameter variation zero loss efficiency.

	standard	Opti 1	Opti 2	Opti 3
F`	0.97	0.97	0.97	0.99
tau	0.902	0.902	0.96	0.96
alpha	0.905	0.905	0.97	0.97
reflector 1	0.9	0.95	0.95	0.95
Intercept 1	0.95	0.95	0.97	0.97
reflector 2	0.9	0.95	0.95	0.95
Intercept 2	0.95	0.95	0.97	0.97
Optical efficiency	0.57884073	0.64494291	0.76701769	0.78283249

Table 8: Results of preliminary assessment.

opt.eff.	c1	c2	c5	Annual yield
[-]	[W/(m <sup>2</sup> K)]	[W/(m <sup>2</sup> K <sup>2</sup> )]	[J/(Km <sup>2</sup> )]	[kWh/m <sup>2</sup> a]
0.6449	0.2	0.001	675	716.11
0.6449	0.1	0.0005	675	761.89
0.7670	0.2	0.001	675	870.78
0.7670	0.1	0.0005	675	916.44
0.7828	0.2	0.001	675	890.56
0.7828	0.1	0.0005	675	936.44

The 700 kWh/m<sup>2</sup>a benchmark can be reached with a couple of parameter variations and the corresponding heat loss coefficients. Since at an early state of the project, no heat loss coefficients have been accurately known, this parameter is modified during the annual yield calculations.

With 65% of zero loss efficiency and heat loss coefficients equal or better than 0.2 W/(m<sup>2</sup>K) and 0.001 W/(m<sup>2</sup>K<sup>2</sup>), criterion 2 is reached. These first promising results lead to the decision to investigate this concept more in detail.

### **SCO\_1\_CYC\_CPC with a real receiver (Himin receiver) and with material and slope errors**

According to an agreement between the partners during a teleconference [28.03.2019], the following errors have been defined: (see also chapter: Manufacturing errors – defect of fabrication)

Table 1: Suggested error assumptions

Specularity error	$\sigma_{sp}$	$\pm 1$ mrad
Slope error	$\sigma_{sl}$	$\pm 2.7$ mrad
Shape error	$\sigma_{sh}$	$\pm 3$ mrad
Alignment error	$\sigma_{al}$	$\pm 9$ mrad
Tracking error	$\sigma_{tr}$	$\pm 0$ mrad (for fixed mirror)

The total error may be calculated as  $\sigma_{tot} = \sqrt{\sum_i \sigma_i^2}$ .

For the CPC-receiver unit a tracking error of  $\pm 3.5$  mrad is suggested by the SIJ.

Figure 13: Excerpt from minutes 190423\_Minutes\_Webconf\_final.docx.

Moreover, the following surface properties have been defined during the teleconference:

A common data set of realistic optical properties shall be used for the calculation of IAM:

**Mirror reflectivity  $\rho = 0.9$ , absorber absorptivity  $\alpha = 0.95$ , glass transmissivity  $\tau = 0.92$ . For simplicity, it is assumed that the mirror and absorber are opaque ( $\tau = 0$ ), the glass has no absorption ( $\alpha = 0$ ) and no angular dependence of these properties is considered.**

**Optical errors shall be defined and used in the forthcoming simulations.** A suggestion can be found in Table 1 above.

Figure 14: Excerpt from minutes 190423\_Minutes\_Webconf\_final.docx.



The above parameter values were introduced in COMSOL. Table 9 shows the boundary conditions together with other parameters.

Table 9: Boundary conditions and rules in COMSOL.

Name	Ausdruck	Wert	Beschreibung
R_REC	0.0185 [m]	0.0185 m	Receiver Radius
R_Glas	0.0235 [m]	0.0235 m	Radius Glashüllrohr
R_CY	3 [m]	3 m	Radius cylinder section
Ap_W	1.48 [m]	1.48 m	Aperture area
alpha	50 [deg]	0.87266 rad	acceptance angle CPC
C_CPC	3	3	Concentration ratio geom.
Ap_W_CPC	$C\_CPC * 2 * R\_REC$	0.111 m	Aperture width CPC
DNI	1000 [W/m <sup>2</sup> ]	1000 W/m <sup>2</sup>	Direct normal irradiance
theta	0 [deg]	0 rad	IAM trans
Refl_Pri	0.9	0.9	Reflectivity primary reflector
Y_0	3 [m]	3 m	Fixpunkt Y
X_0	0 [m]	0 m	Nullpunkt X
x_dr	$X_0 * \cos(\theta) - Y_0 * \sin(\theta)$	0 m	Rotation x
y_dr	$X_0 * \sin(\theta) + Y_0 * \cos(\theta)$	3 m	Rotation y
d_x	$R\_REC * \sin(\theta)$	0 m	Move_CPC
d_y	$R\_REC * \cos(\theta)$	0.0185 m	Move_CPC
N	4000	4000	Number Rays
Refl_CPC	0.9	0.9	Reflectivity CPC
Track_dx	0.01 [m]	0.01 m	Movement of focus x
Track_dy	0.01 [m]	0.01 m	Movement of focus y
Track_Y	1.46 [m]	1.46 m	Position of Receiver Y
Track_X	0.0 [m]	0 m	Position of Receiver X
Versatz_C...	$\sqrt{(R\_CY^2 - (Ap\_W/2)^2)} * (-1) + R\_CY$ [m]	0.092699	Versatz der Ray-Line
sunDiskA...	4.65 [mrad]	0.00465 rad	Divergenz sun 4.65mrad
error_pri...	$\sqrt{\text{specError}^2 + 4 * \text{slopeError}^2 + 4 * \text{shapeError}^2 + \dots}$	0.019752 rad	Primary mirror error
specError	1 [mrad]	0.001 rad	Specularity error primary mirror
slopeError	2.7 [mrad]	0.0027 rad	Slope error primary mirror
shapeError	3 [mrad]	0.003 rad	Shape error primary mirror
alignError	9 [mrad]	0.009 rad	align error primary mirror
trackingEr...	0 [mrad]	0 rad	tracking error primary mirror
theta_long	0 [mrad]	0 rad	longitudinal deviation
error_seco...	$\sqrt{\text{specError}^2 + 4 * \text{slopeError}^2 + 4 * \text{shapeError}^2 + \dots}$	0.020956 rad	Secondary mirror error
specError2	1 [mrad]	0.001 rad	Specularity error secondary mirror
slopeError2	2.7 [mrad]	0.0027 rad	Slope error secondary mirror
shapeError2	3 [mrad]	0.003 rad	Shape error secondary mirror
alignError2	9 [mrad]	0.009 rad	align error secondary mirror
trackingEr...	3.5 [mrad]	0.0035 rad	tracking error secondary mirror
Trans_gl	0.92	0.92	transmission glas envelope

Notes: No. of rays [N] was increased to 100000 after a series of preliminary test runs.

Since the CPC enables several hits per ray, the material properties are included in the evaluation with the respective errors. Figures 12 and 13 illustrate the setup of the system in COMSOL. Figure 13 provides a close-up of the CPC and the various rays can be seen. Some are impinging directly on the receiver directly, some need 2 or more reflections to do so and some don't reach the receiver at all.

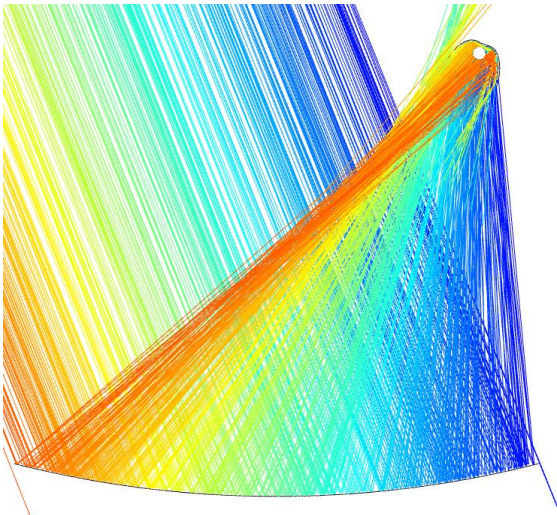


Figure 15: 2D Setup in COMSOL for raytracing simulations

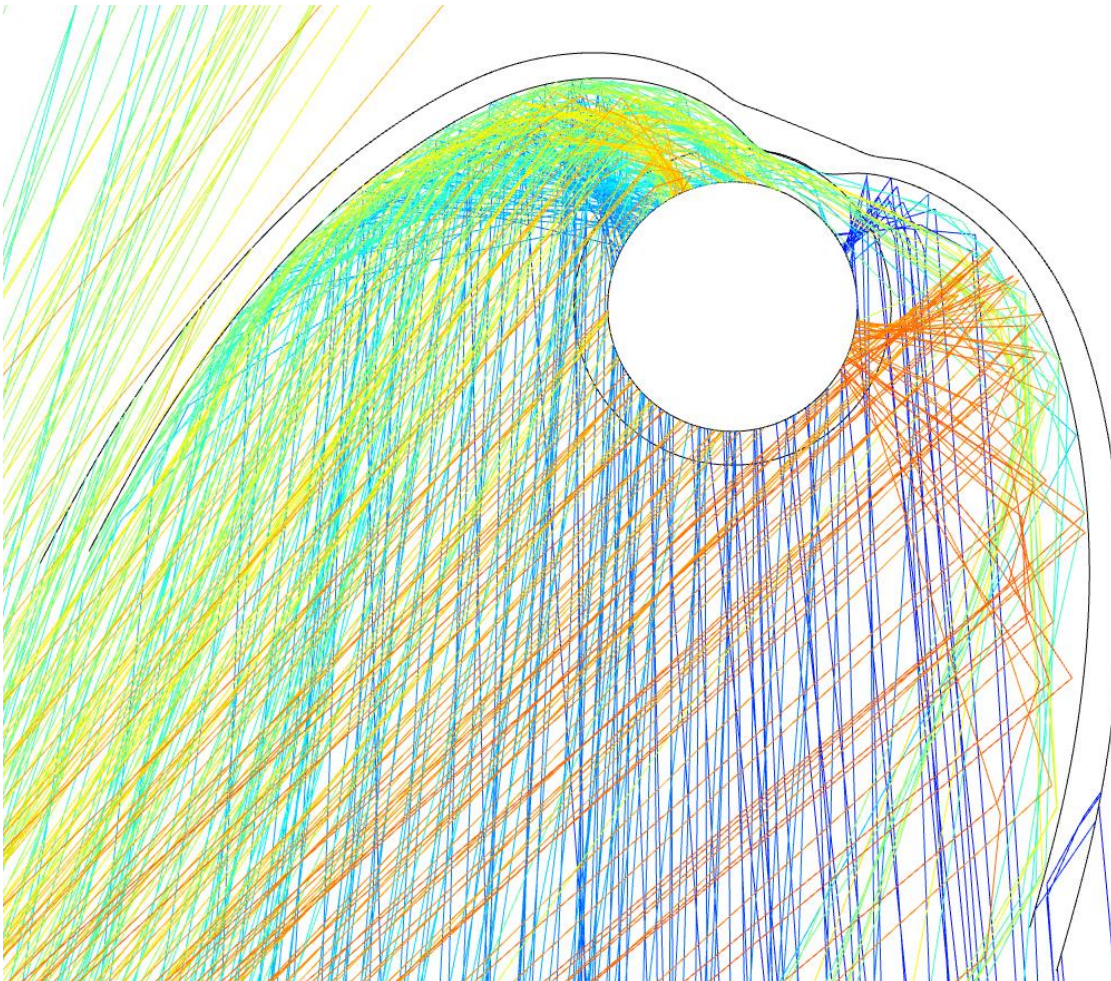


Figure 16: CPC with visualization of the ray tracing

In general, the following equation is valid:

$$\eta_0 = F_c \cdot \left[ \left( \alpha \frac{1}{K} + \left( 1 - \frac{1}{K} \right) \alpha \tau \gamma_1 \rho_1 C_{L1} \gamma_2 \rho_2 C_{L2} \right) IAM_{(L,T)} \right]$$

where  $C_L$  (cleanliness factor is neglected);  $F_c$  is not yet established;  $\alpha \frac{1}{K}$  is going to be 0 for most incidence angles, caused by shadowing of the receiver with the CPC.

Consequently the following relation occurs for the results of the COMSOL simulation:

$$\frac{\eta_0}{F_c} = \left[ \left( \left( 1 - \frac{1}{K} \right) \alpha \tau \gamma_1 \rho_1 \gamma_2 \rho_2 \rho_x \right) IAM_{(L,T)} \right]$$

In accordance with the raytracing results some ray spells are subjected to one reflection, some are subjected to two and some to several. In order to get accurate values for the performance evaluation a raytracing simulation with material properties is imperative. The optimization rule for various simulations was to collect as much power on the receiver tube as possible, while the optimization rule during the preliminary tests was to obtain the highest possible intercept factor.

Detailed calculation of  $F_c$  can be performed at a later stage of the project, using the COMSOL options “heat transfer” and “optimization”.

### Concept SCO\_4\_Micro-mirror concentrator concept

The solar concentrator consists of an array of mirror facets that are preconfigured to form a focal point at approximately 1.5 m. During tracking all mirrors are moved simultaneously in a coupled mode by 2 motors in two axes, in order to maintain the system in focus with the moving sun. The Micro-mirror concentrator concept or the so-called Microhelix concept is designed by Heliokon.

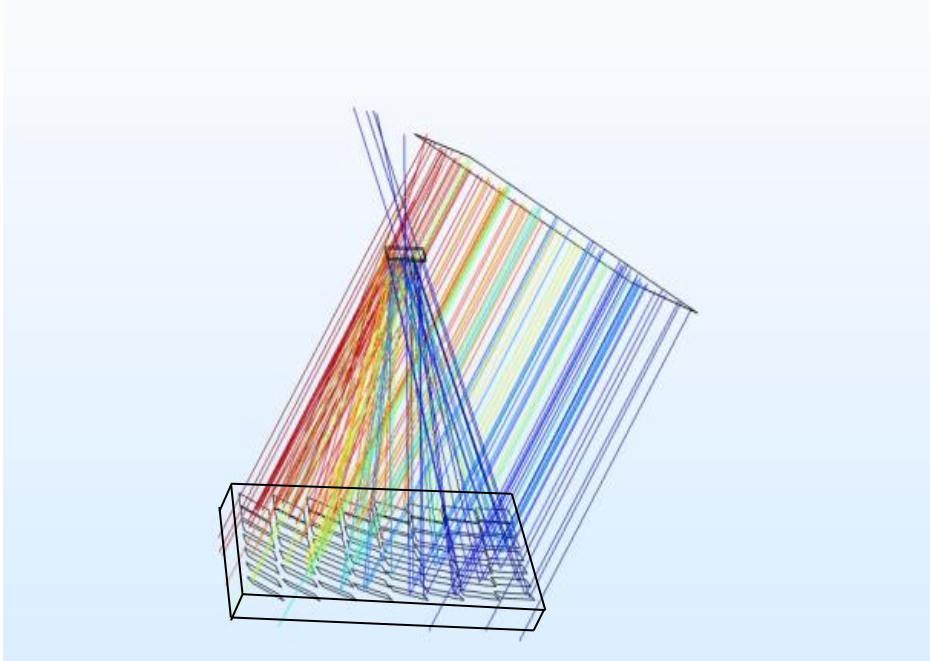


Figure 17: View of a mirror module and receiver in raytracing software.

The mirrors and the corresponding mechanical system are housed inside a glass covered casing, like that of a flat-plate collector. The mirror module will be installed in a fixed position. Therefore, this concept can be regarded as fixed-mirror solar concentrator (FMSC).

The receiver can be a relatively small flat-plate collector, optimized for high-flux solar irradiance and higher temperatures (e.g. AR-coated iron-free glass cover, thicker absorber sheet, closer fluid channels, high-temperature materials and insulation).

This concept presents the following advantages:

- The point-focusing feature allows high concentration rates of ~50 even with relatively large optical and tracking errors.
- Instead of the receiver tube, a small non-evacuated flat-plate receiver can be used (which will have to be optimized for high flux densities) and may be produced by Calpak.
- The German companies Hilger and Heliokon have already some experience with such mirror modules and could provide a prototype. A prototype developed for CSP applications was designed by the German company Hilger (see Fig. 2).
- It is an innovative concept that has not yet been examined or published elsewhere.

## Design study

The industrial partners carried out a design study based on the preparatory work for the micro heliostat. The possibility of adjusting the individual facets to generate a module focus was examined. In addition, a roof mounting system and a first version of a receiver holder were constructed. As a result of the design study it can be stated that the realization of a small mirror concentrator is possible by means of micro heliostat technology.



*Figure 18: Concept of the micro-mirror concentrator*

## Brief description of the micro heliostat system

The background to the considerations in the development of micro heliostats lies in the fact that the production costs for heliostats can be significantly reduced by developing a mirror system suitable for mass production. The micro heliostat was developed as an immovable heliostat segment with a large number of internal micro mirrors that track the sun via three small actuators.

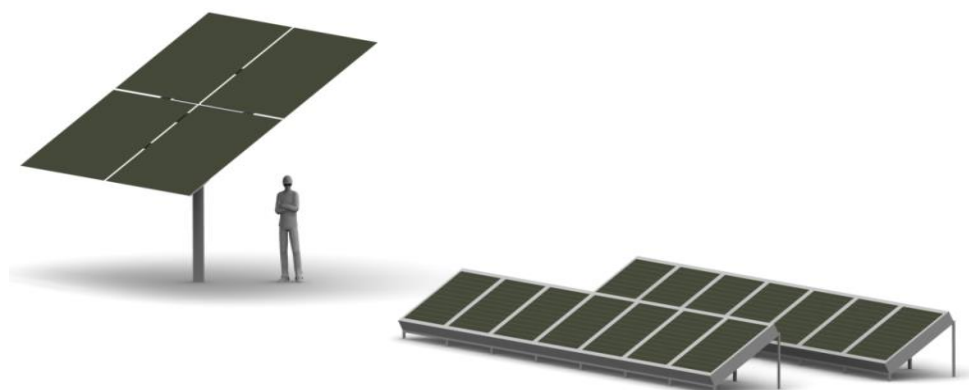


*Figure 19: Classic heliostat vs. microheliostat, 35 m<sup>2</sup> mirror surface each*

The large number of identical and manageably small individual components allows the use of mass production processes in the production and assembly of microheliostats. Mass production is justified to the extent that, for example, for a 100 MW<sub>el</sub> power plant block with a 10 h storage at an annual irradiation

of 2600 kWh/m<sup>2</sup> near the 40th degree of latitude, about 480,000 micro heliostats (2.5 m<sup>2</sup> per heliostat) with a total of 24,000,000 mirror facets, joints and other individual parts are required.

In addition, the mechanical structure of the heliostat offers a high potential for material savings. Cost reductions of up to 5 % can be achieved with efficient designs. By reducing material consumption, it is also possible to avoid the risk of a sharp increase in costs in the future due to rising material prices.

There is also a high cost reduction potential of 10 % in the area of the drives. Drives in the form of low-cost linear actuators have proven to be particularly economical. The drive system is mounted in its centre of gravity. Together with the fact that the mirror facets are not exposed to wind load, a very low drive energy is required.



*Figure 4: View of a prototype mirror module with nearly parallel mirrors*

The maximum drive power is approx. 3 W. Due to the low drive power, the control system can be produced very cost-effectively. For this it is necessary to adapt the control exactly to the requirements of the microheliostat. The controller has a power requirement of approx. 1 W. Together with the drive power of 3 W a peak power of 4 W results. Due to the low power requirement, the microheliostats are suitable for the use of autonomous radio-based control systems.

A greater cost reduction of up to 5 % can be achieved in the field of heliostat controls by tailor-made hardware components. Standard industrial controllers are currently used in heliostats. These are not adapted to the requirements of the heliostats, are usually oversized and therefore too expensive. Customized heliostat controllers are required in order to significantly reduce costs.

In addition to the above-mentioned potential for reducing investment costs, microheliostats offer a number of advantages that increase the safety and efficiency of heliostat fields in operation by solving the following technical problems of heliostat fields:

The heliostats are subject to a very high load due to the weather. High wind loads often lead to damage to the reflector units and thus to high maintenance costs. In addition, the maximum operating wind speed is around 15 m/s. As a result, the heliostats are moved to their safety position from this wind speed onwards in order to avoid possible damage. This reduces the annual yield of the power plant. In the case of microheliostats, the reflectors or mirror facets are mounted in a glazed box. Thus, they can be operated at higher wind speeds of up to 50 m/s. This in turn leads to an increase in the total operating time of the heliostat field. The housing and the glass cover also protect the individual reflectors, the drive and the mechanics of the heliostats, so that the frequency of failures, repair and maintenance work is reduced.

## Raytracing

A raytracing model was created in the COMSOL software. It allows the specification of the mirror number and dimensions and their gap width. All (rectangular and flat) mirror facets are arranged such that their centres are positioned on a regular grid on a flat plane. The size and position of the receiver can be modified. It is always facing the centre of the mirror array. Its position can only be modified in form of a rotation around the mirror array y axis.

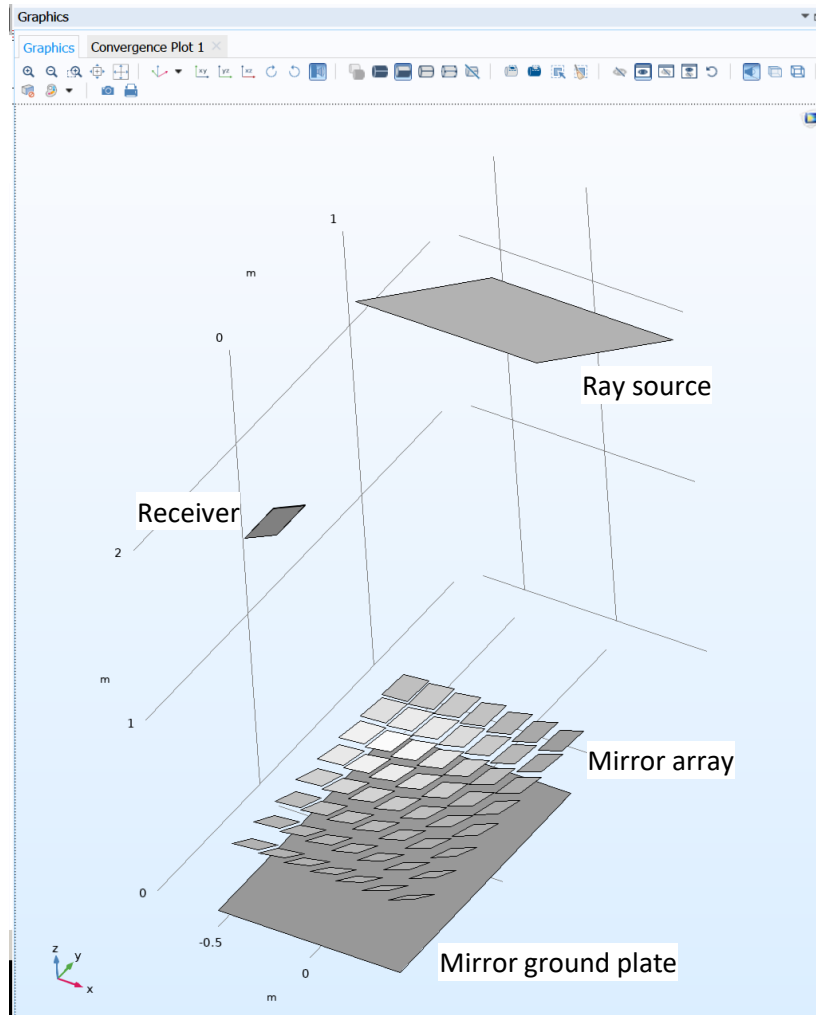


Figure 20: View of the raytracing elements of the micro-mirror system.

The alignment of the mirrors is defined by the method “create\_FMA” in which all mirror facets are adjusted to reflect incoming light from each mirror facet centre to the receiver centre if the incidence angle is normal to the array plane (see appendix A for the code of this alignment). The adjustment angles are different for each mirror facet. This 2-axis rotation is carried out in two steps, first a rotation around the y axis pivoted at the facet centre, second a rotation around the x axis pivoted at the facet centre. The order matters in two aspects: firstly, the angular adjustments have to be calculated differently if the order of rotations is reversed, secondly, it affects the facet orientation (in the sense of its rotation around its facet normal).

Similar considerations have to be done with respect to the tracking angles. They are directly related to the arrangement of the cardanic bearings of the mirror facets, which consist of an outer (fixed) bearing and an inner one fixed to the rotating outer one. The COMSOL model assumes an inner bearing that allows rotation around the y axis and an outer (fixed) bearing with x-axis rotation (see appendix B for the code of this alignment). The tracking angles are the same for each mirror facet.

The optical errors of the tracking, alignment and mirror surface quality are combined in one parameter “opticalError” which is used to create a random cone of reflected rays with normal distribution. The sigma value of this distribution is set to “opticalError”. The angular ray distribution of the sun disk is also implemented on the mirror surfaces and combined with the optical error calculation. In order to implement this, the equations of the surface reflection at the element “wall\_1” had to be modified accordingly (see Appendix B).



## Results

In the following chapter the simulation results from the concepts are delivered.

### Results SCO\_1\_Tracking\_SYM

Parabolic

Geometry

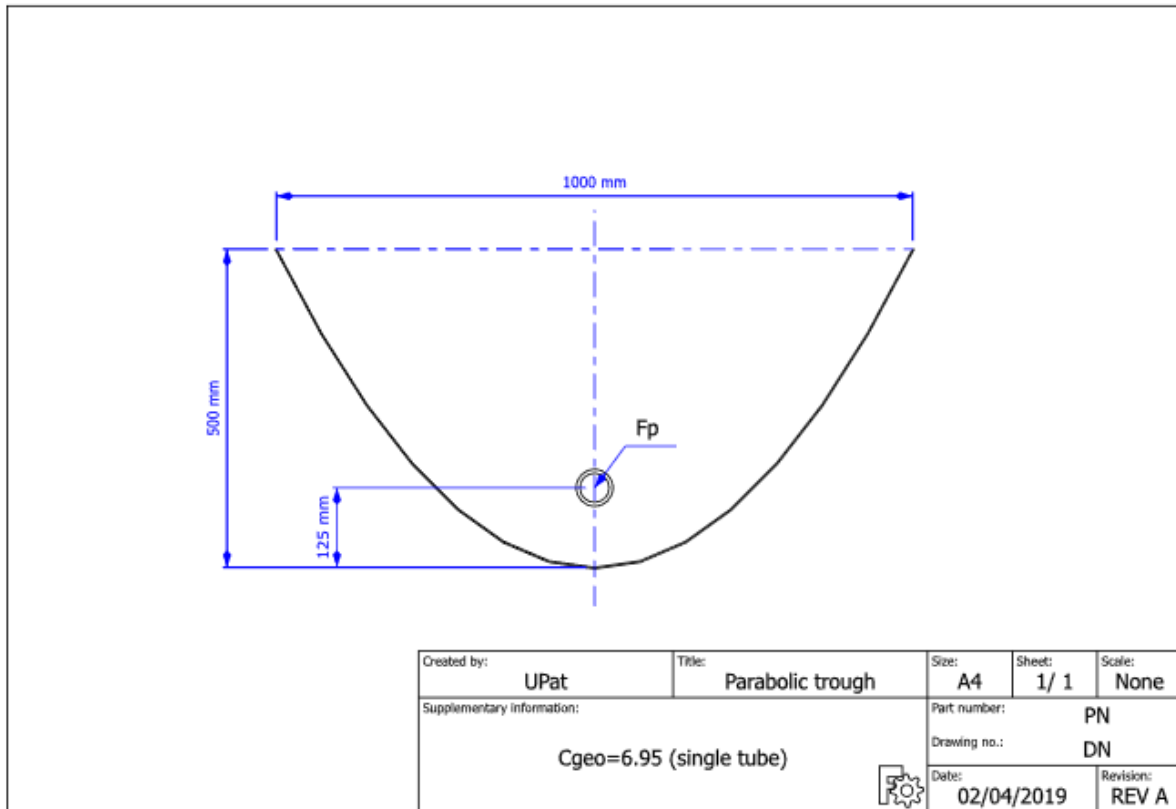


Figure 21 SCO\_1 parabolic - cross section

<i>Ltotal</i>	1.5	<i>m</i>
<i>Aaper</i>	0.456	<i>m2</i>
<i>Aabs</i>	0.26376	<i>m2</i>
<i>Cgeo</i>	1.72	-

Table SCO\_1 parabolic - geometry specifications

#### Transversal tracing

The system is properly orientated so that the aperture plane vector belongs to the azimuth plane and points at  $180^\circ$ . This way, the intercept factor at normal incidence is  $\gamma_{NI} = \gamma(180^\circ)$ .

#### Linear absorber path

The absorber is positioned along the axis of symmetry ( $y$ ), where 0 is at the bottom of the reflector. Ray-trace results are exported for each  $y$  and solar azimuth  $\theta_{az}$ .

#### Trace variables

- $0.03 \text{ m} < y < 0.3 \text{ m}$ ,  $step = 0.0001 \text{ m}$
- $135^\circ < \theta_{az} < 225^\circ$ ,  $step = 1^\circ$

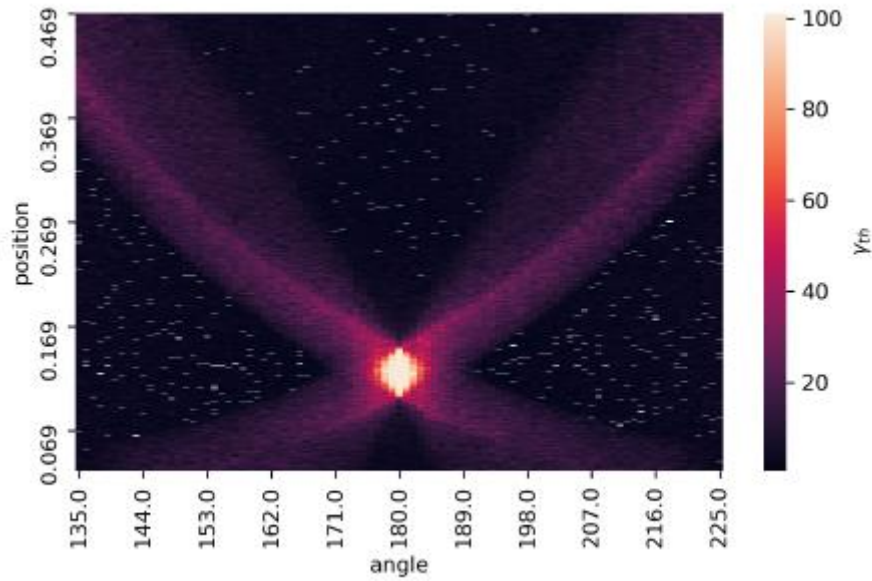


Figure 22  $\gamma_{th} = f(y, \theta_{az})$  heatmap

Comments

- Max  $\gamma_{th} = 100\%$
- Linear path can be approximated through linear regression between maximum intercept factor points for each angle.
- Lots of missing values, probably due to a software bug. Further investigation required.

Linear regression

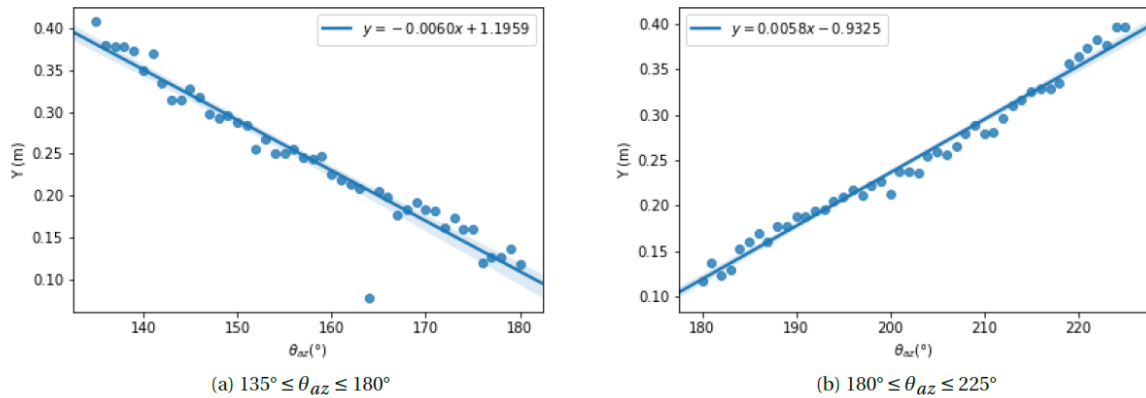


Figure 23 Linear fit,  $y=f(\theta_{az})$

$135^\circ \leq \theta_{az} \leq 180^\circ$			
Parameter	Value	SE	P-value
Intercept	1.1959	0.0402023	8.88313e-31
Slope	-0.00603663	0.00025435	1.03452e-26
$180^\circ < \theta_{az} \leq 225^\circ$			
Parameter	Value	SE	P-value
Intercept	-0.932538	0.0235866	5.08364e-36
Slope	0.00584453	0.000116227	1.61837e-40

Table 10 Regression parameters. SE: Standard Error.

The linear regression parameters are satisfactory. It should be noted that the results are not symmetric for the two sections. The extracted equations for the absorber's motion are:

$$y = -0.006(\pm 0.002) \times x + 1.2(\pm 0.3), (r = 0.97, n = 47, p < 1.03452e-26), 135^\circ \leq \theta_{az} \leq 180^\circ$$

$$y = 0.0058(\pm 0.0008) \times x - 0.9 (\pm 0.2), (r = 0.97, n = 46, p < 1.61837e-40), 180^\circ < \theta_{az} \leq 225^\circ$$

### Equation test

The system was traced again with  $0.1^\circ$  increment, this time with the absorber position determined by Eq. 1, in order to test the extracted equation. The  $\gamma_{th}=f(\theta_{az})$  plot is shown below.

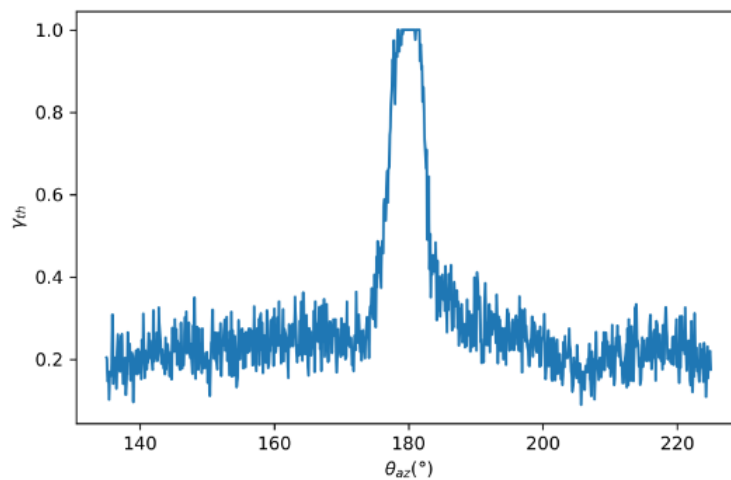


Figure 24 Equation test –  $\gamma_{th} = f(\theta_{az})$ .

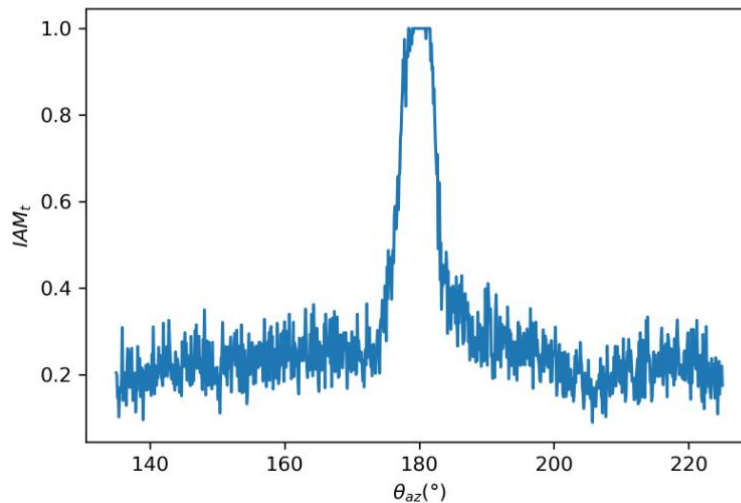


Figure 25 Equation test –  $IAM_t = f(\theta_{az})$ .

### Comments

The SCO\_1 parabolic shape results to low  $\gamma_{th}$  values of about 0.2 along most of the y axis length, and a peak of  $\gamma_{th} = 1$  at the parabola's focal point. Therefore, this concept is not considered as suitable for a linear tracking system.

Cylindrical  
Geometry

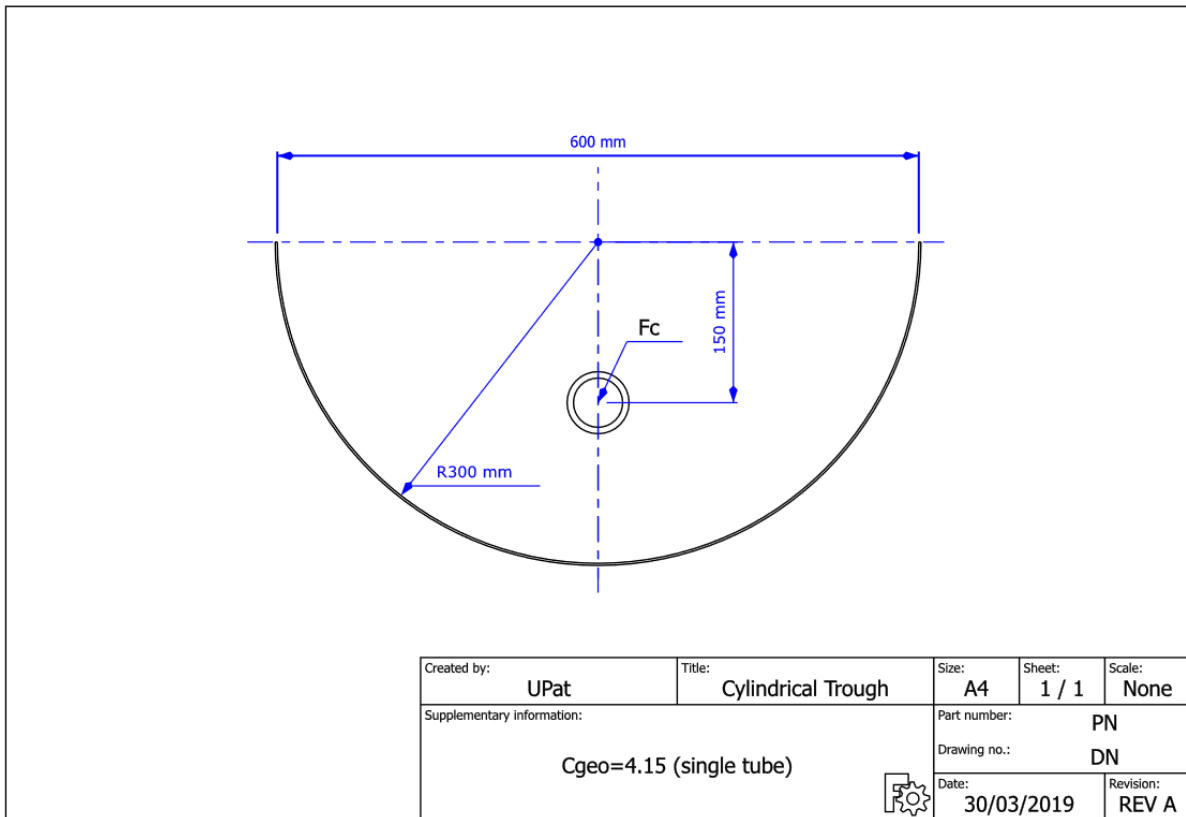


Figure 26 SCO\_1 cylindrical - cross section.

Transversal tracing

The system is properly orientated so that the aperture plane vector belongs to the azimuth plane and points at  $180^\circ$ . This way, the intercept factor at normal incidence is  $\gamma_{NI} = \gamma(180^\circ)$ .

Linear absorber path

The absorber is positioned along the axis of symmetry ( $y$ ), where 0 is at the bottom of the reflector. Ray-trace results are exported for each  $y$  and solar azimuth  $\theta_{az}$ .

Trace variables

- $0.03 \text{ m} < y < 0.27\text{m}$ , step = 0.0001 m
- $135^\circ < \theta_{az} < 225^\circ$ , step =  $1^\circ$

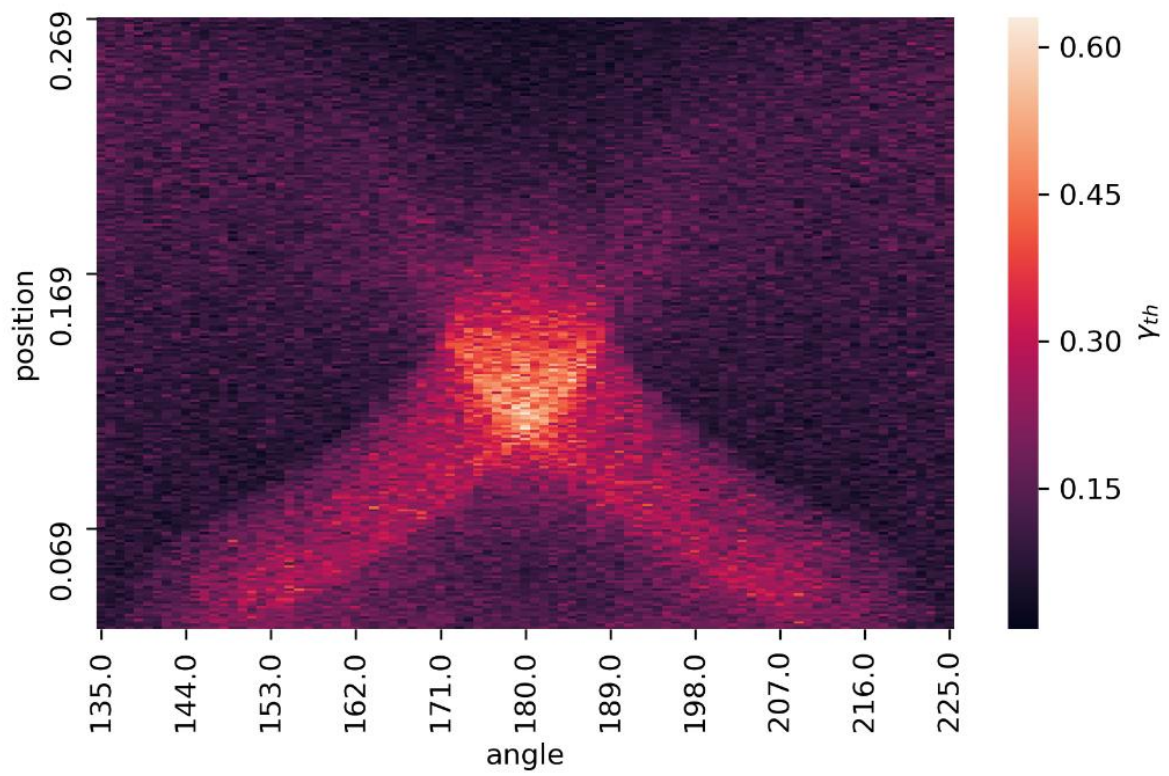


Figure 27  $\gamma_{th} = f(y, \theta_{az})$  heat map.

#### Comments

- Max  $\gamma_{th} = 60\%$
- Linear path cannot be approximated through linear regression.

CPC

Geometry

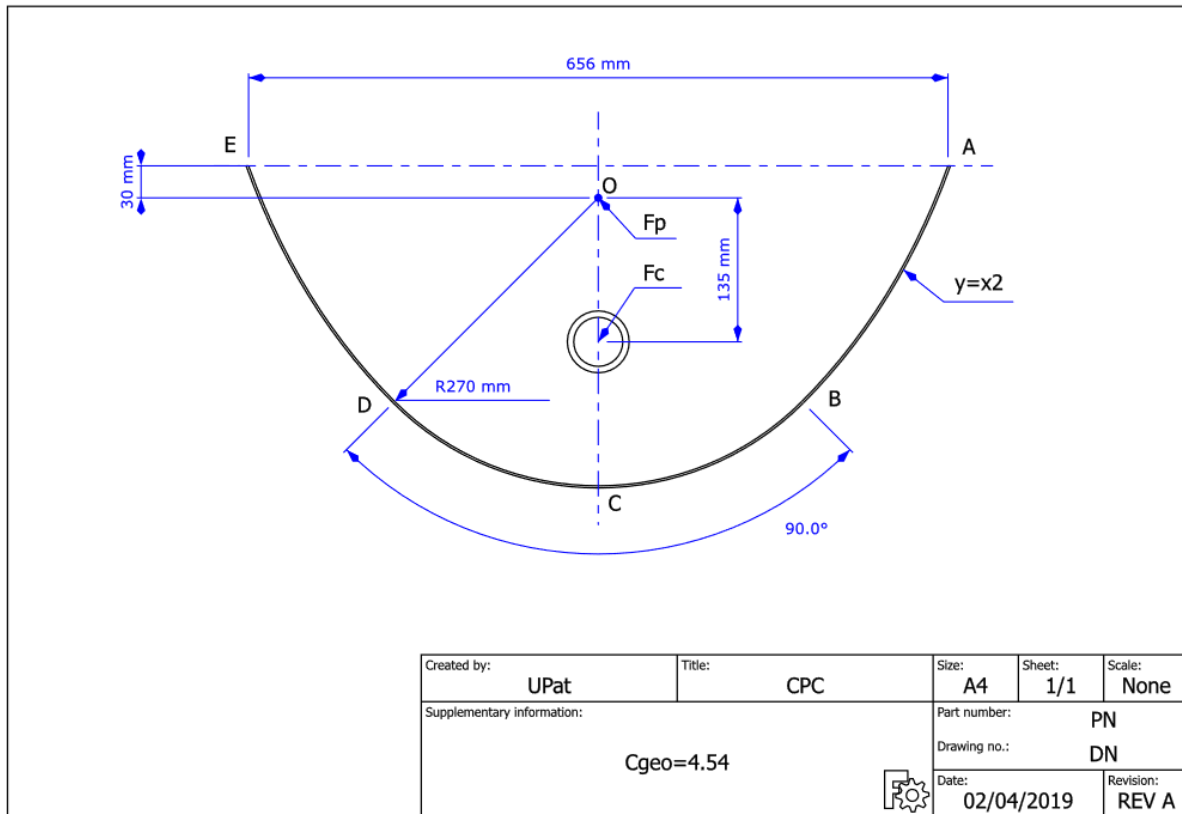


Figure 28 SCO\_1 CPC - cross section

The reflector geometry consists of a 90° circular sector BCD and two parabolic parts AB and ED ( $y=x^2$ ) rotated by 45°. The focal points of the circular and parabolic parts are  $F_c$  and  $F_p$  respectively.

Transversal tracing

The system is properly orientated so that the aperture plane vector belongs to the azimuth plane and points at 180°. This way, the intercept factor at normal incidence is  $\gamma_{NI} = \gamma(180^\circ)$ .

Linear absorber path

The absorber is positioned along the OC axis ( $y$ ), where  $C(0,0)$ . Trace results are exported for each  $y$  and solar azimuth  $\theta_{az}$ .

Trace variables

- $0.03 \text{ m} < y < 0.3 \text{ m}$ , step = 0.001 m
- $135^\circ < \theta_{az} < 225^\circ$ , step = 1°

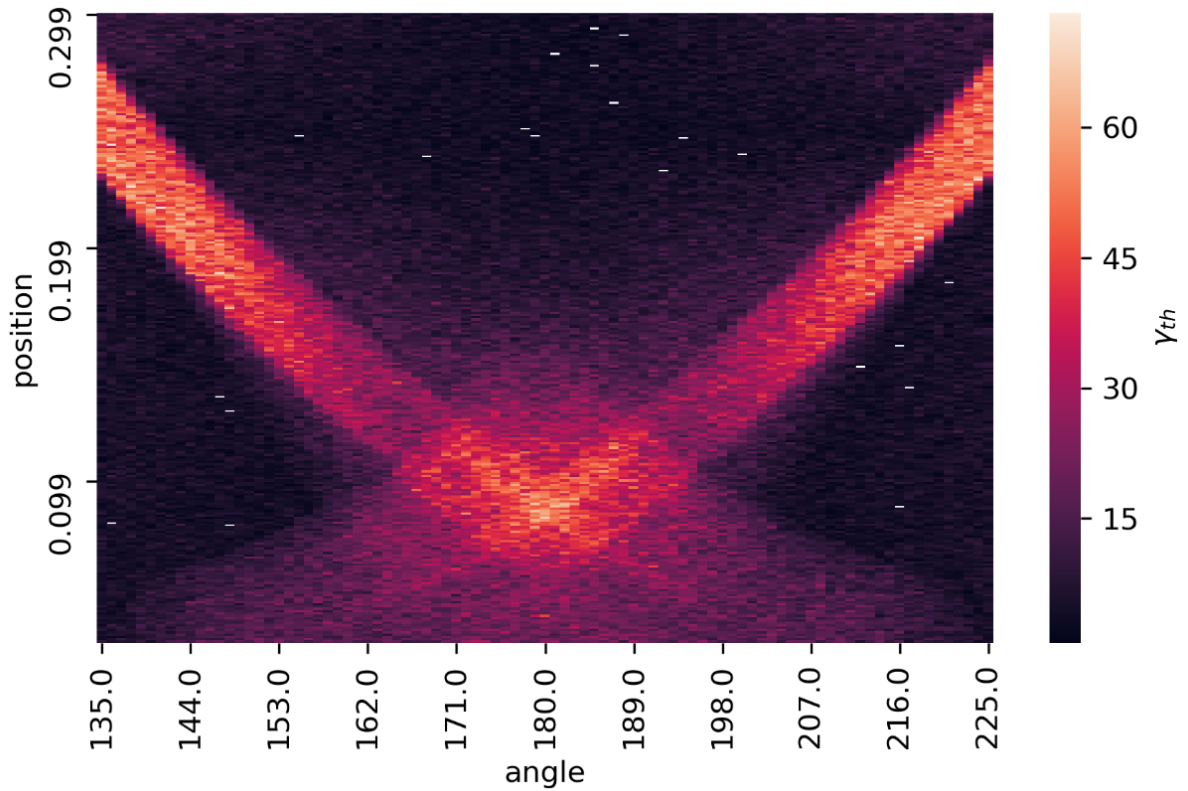


Figure 29  $\gamma_{th} = f(y, \theta_{az})$  heatmap

Comments

- Max  $\gamma_{th} = 70\%$
- Linear path can be approximated through linear regression between maximum intercept factor points for each angle.
- Areas with  $\gamma_{th} = 30\%$  are observed at  $165^\circ$

Linear regression

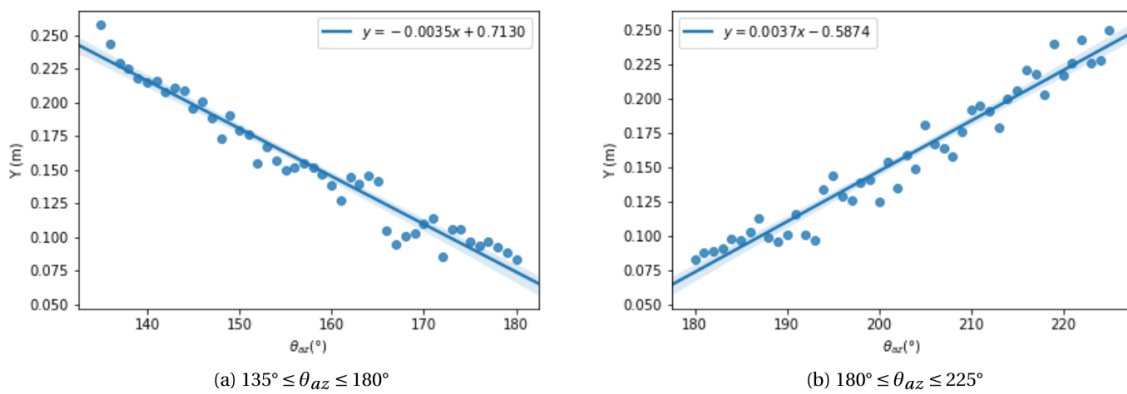


Figure 30 Linear fit,  $y = f(\theta_{az})$

$135^\circ \leq \theta_{az} \leq 180^\circ$			
Parameter	Value	SE	p-value

Intercept	0.71	0.02	2.48279e-35
Slope	-0.0036	0.0001	6.44052e-31
$180^\circ < \theta_{az} \leq 225^\circ$			
Parameter	Value	SE	p-value
Intercept	-0.59	0.03	4.4069e-26
Slope	0.0037	0.0001	2.36575e-30

Figure 31 Regression parameters. SE: Standard Error.

The linear regression parameters are satisfactory. It should be noted that the results are not symmetric for the two sections. The extracted equations for the absorber's motion are:

$$y = -0.0035(\pm 0.0008) \times x + 0.71(\pm 0.05), (r = 0.96, n = 47, p < 6.44052e-31), 135^\circ \leq \theta_{az} \leq 180^\circ$$

$$y = 0.0036(\pm 0.0009) \times x - 0.6(\pm 0.2), (r = 0.95, n = 46, p < 2.36575e-30), 180^\circ < \theta_{az} \leq 225^\circ$$

#### Equation test

The system was traced again with  $0.1^\circ$  increment, this time with the absorber position determined by Eq. 1, in order to test the extracted equation.

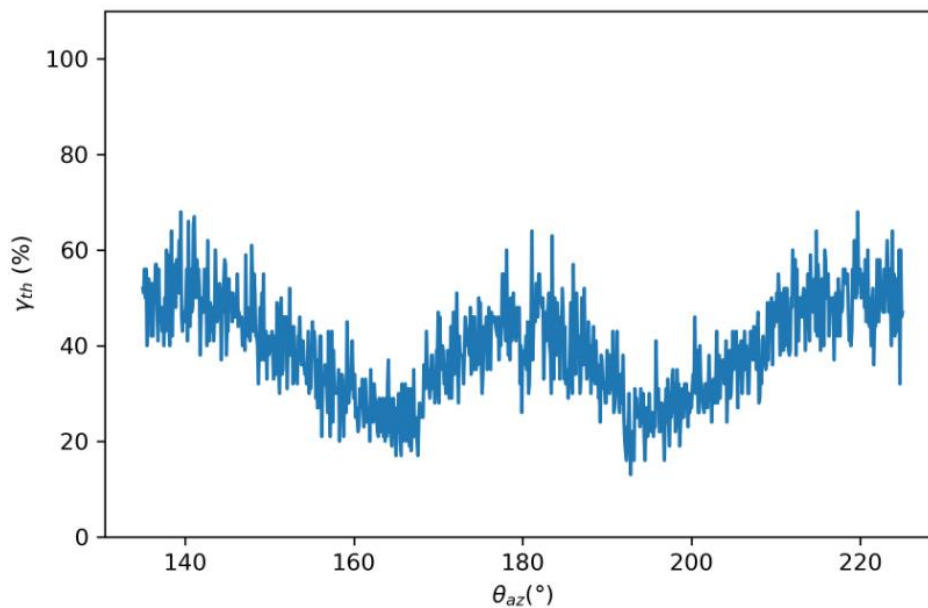


Figure 32 Equation test –  $\gamma_{th} = f(\theta_{az})$ .

#### Comments

- $\gamma_{th}$  fluctuates between 20% and 60% for a linear absorber path. Non-linear path should be investigated to achieve as stable  $\gamma_{th}$  as possible.

#### Non-linear absorber path

The absorber is traced along the x and y axis. Trace results are exported for each x,y and  $\theta_{az}$ .

#### Trace variables

- $-0.10 \text{ m} < x \leq 0 \text{ m}$ , step = 0.001 m
- $0.03 \text{ m} < y < 0.3 \text{ m}$ , step = 0.001 m
- $135^\circ < \theta_{az} < 180^\circ$ , step =  $1^\circ$



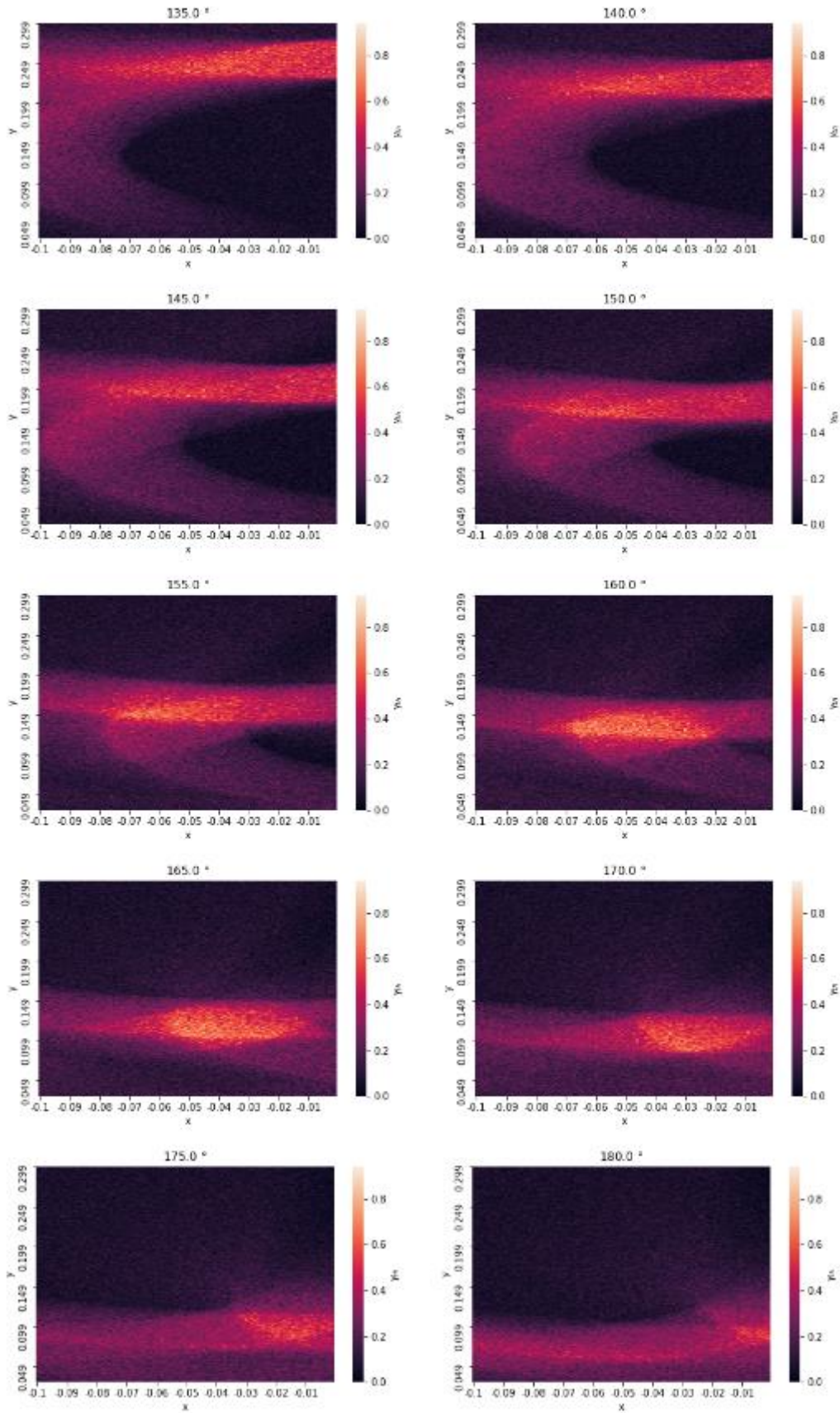


Figure 33  $\gamma_{th} = f(x,y)$  for each  $\theta_{az}$  – heat maps.

Absorber positions can be filtered according to  $\gamma_{th}$  values. As an example, absorber positions where  $\gamma_{th} > 0.6$  are shown below.

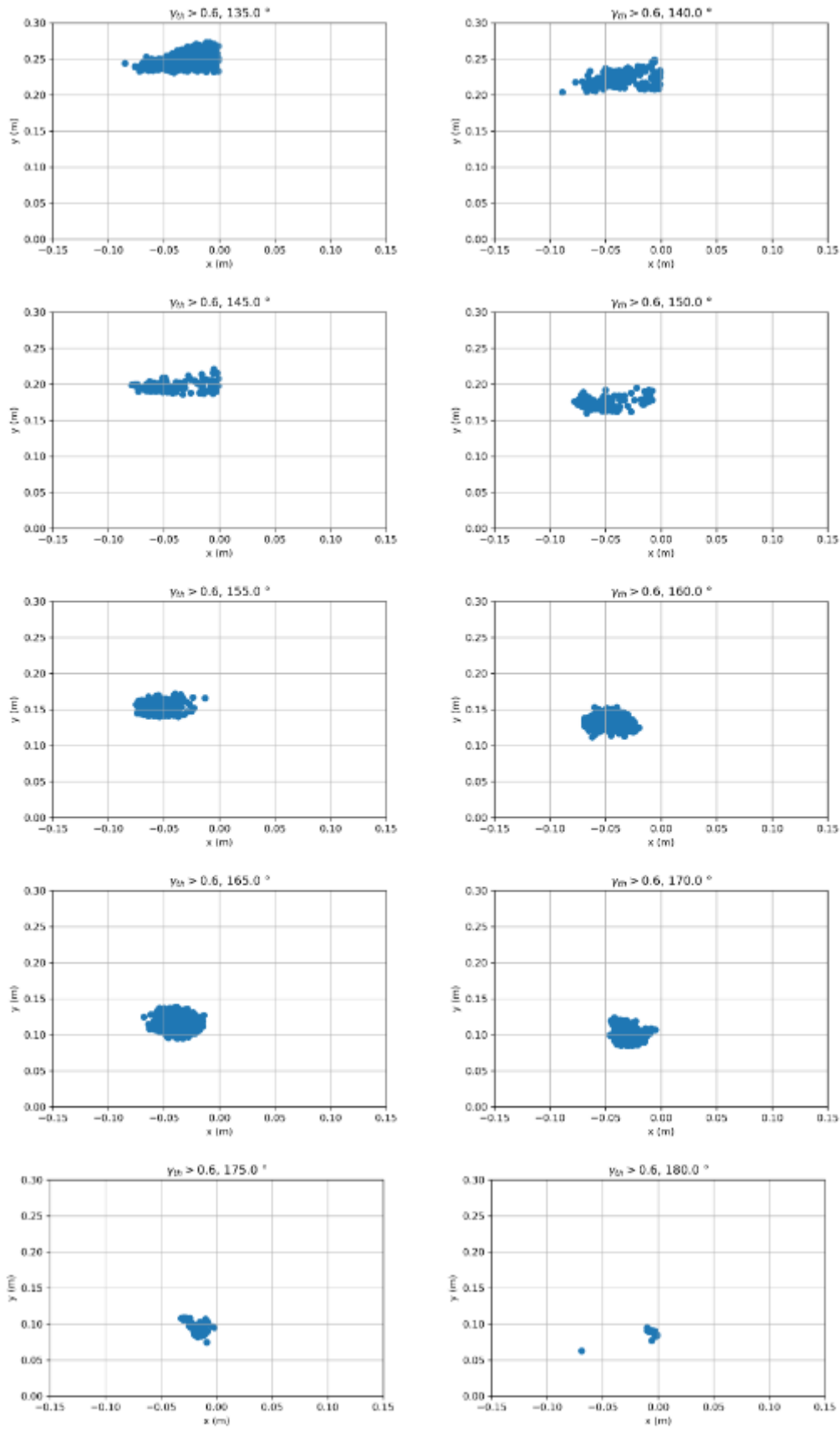


Figure 34 Absorber positions -  $\gamma_{th} > 0.6$  for each  $\theta_{az}$ .

The mean of the best absorber coordinates, according to the  $\gamma_{th}$  threshold applied, are shown below.

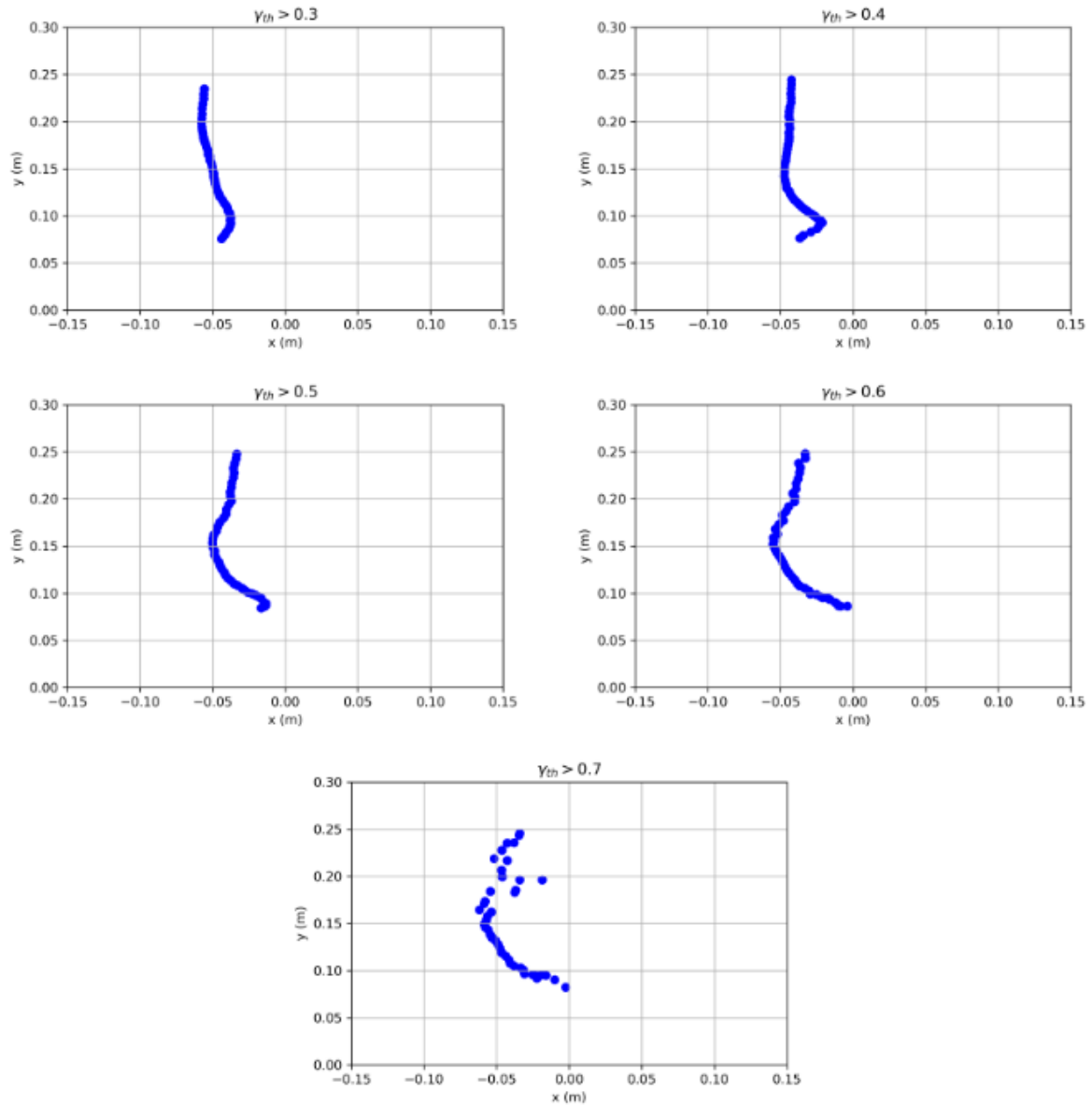


Figure 35 Mean absorber positions - various  $\gamma_{th}$  thresholds for all  $\theta_{az}$ .

The number of data points produced at 0.001 m x 0.001 m x 1° are shown below.

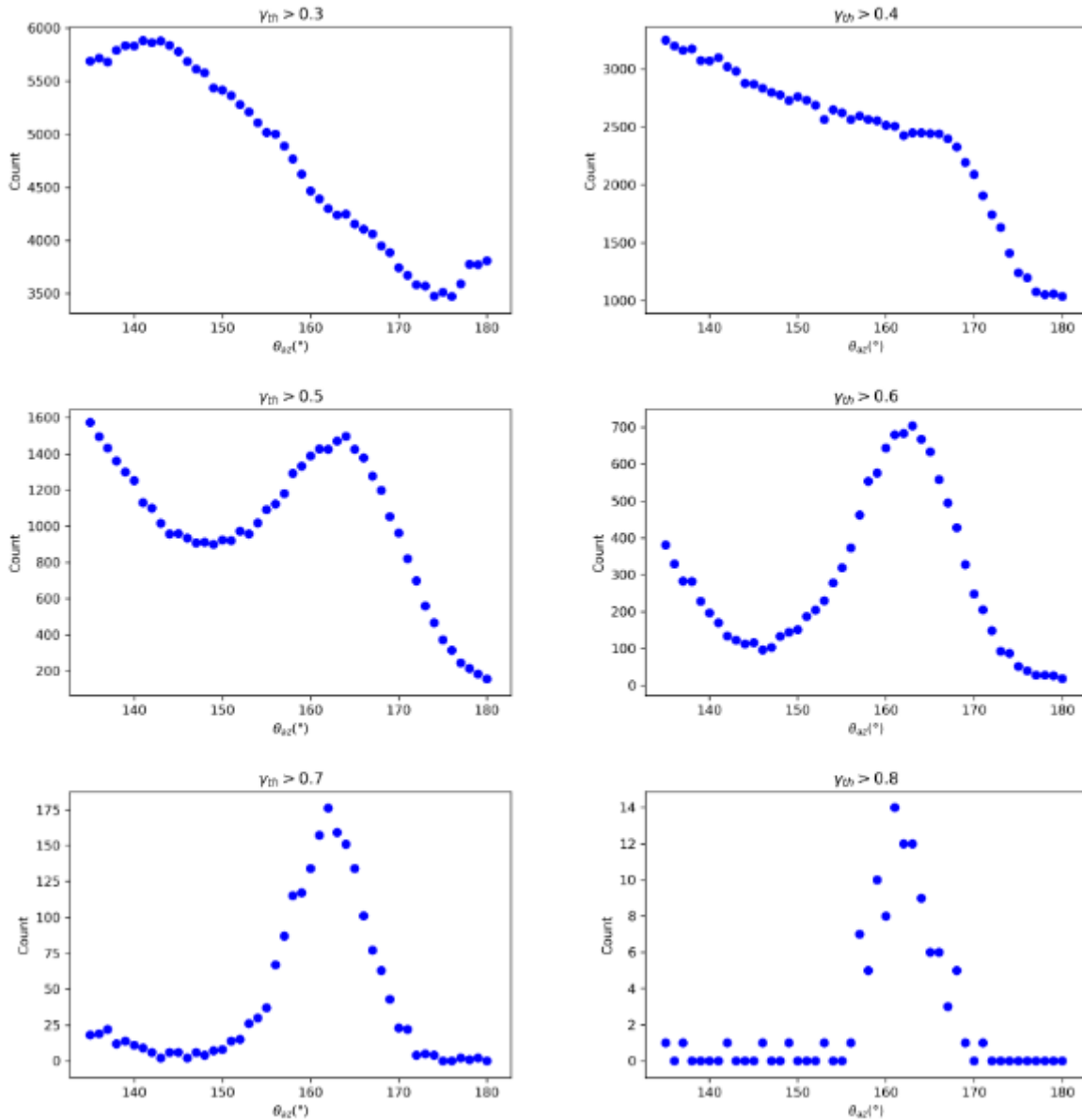


Figure 36 Data points for various  $\gamma_{th}$  for all  $\theta_{az}$ .

#### Comments

The number of data points over 0.7 and 0.8 are not sufficient to provide reliable results, therefore a maximum  $\gamma_{th} = 0.6$  will be considered.

#### Comments on the software

Tonatiuh is a fast and reliable tool for a relatively small number of traces. However, a progress bar window is launched and closed at every trace, slowing down the whole process and using most of the computer's RAM, making the software prone to crashing. This is why the software had to run for 2 days and 17 hours to produce the 1,242,000 files for the results provided above. Additional efforts have been made to increase the overall trace speed, such as reducing the number of rays for each separate trace and running the software on the computer clusters available at our laboratory. Although the trace code, written in C++, utilizes CPU resources for a very little time, compared to the GUI window, we could not take advantage of the cluster's computing power. We concluded that when it comes to situations where a high number of traces is required, a different ray-tracing software should be used.

## Results SCO\_1\_Tracking\_SYM and ASYM @ SIJ

The concept was setup with the CALPAK receiver, since at the beginning of the project no other data had been available.

Obviously, the design criteria 1 couldn't be reached with this setup. Moreover, the intercept factor at direct IAM is rather low with 70%. Since the basic shape creates two focus lines it is not suitable and meaningful for a single biaxial tracked receiver. The design criteria 1 could just be reached for the asymmetric approach with two times the aperture width. Since the IAM at different angles is rather low the approach is not fulfilling the yearly yield criteria.

At the tables below the results for the concept with its sub-concepts is shown.

Obviously, none of the concept is suitable to reach the criteria. Even with an improved receiver and the Andravida weather dataset the basic shape collector can't fulfill the criteria. At this point, it is important to notice that the calculations did not even include the error assumptions.

Therefore, the basic form has not been taken into account for further consideration. In addition, the different resulting focal lines make no sense with a single biaxial tracked receiver.

Table 11: Summary concept SCO\_1 basic form (SCO\_1\_SYM\_37mm, SCO\_1\_2xSYM\_37mm and SCO\_1\_2xASYM\_37mm) with assumptions and first calculations for MATLAB Simulink simulations

1) SCO\_1\_SYM\_37mm

<b>Optical efficiency</b>	<b>49.88 %</b>
<i>derived from</i>	$\eta_0 = F[\alpha\tau\gamma\rho] \cdot IAM(\theta_T, \theta_L)$
$\alpha\tau$ - product of transmission and absorptance	$\alpha$ : 0.905 test value Calpak $\tau$ : 0.902 test value Calpak
F'- collector efficiency factor	0.97 (Sydney tube with fin and U-shaped tube)
$\gamma$ - Intercept factor	70 % (direct radiation IAM 0°/0°) from Soltrace raytracing
$\rho$ - reflection	$\rho$ : 90 % Alanod MICRO-SUN weather-proof reflective is only 90%
$\beta$ - spillage factor	1- $\gamma$ :30 % (direct radiation IAM 0°/0°)

Angle [°]	0.00	11.31	21.80	30.96	38.66	45.00	50.19	54.46	57.99	60.95	63.43	65.56	67.38	75.96	82.87	84.29	90.00
Trans [-]	1.000	1.080	1.097	0.939	0.901	0.873	0.884	0.889	0.929	0.931	0.890	0.841	0.785	0.603	0.422	0.374	0.094
Long [-]	1.00	0.99	0.97	0.96	0.95	0.94	0.93	0.91	0.90	0.88	0.87	0.86	0.84	0.74	0.50	0.40	0.00

2) SCO\_1\_2xSYM\_37mm

<b>Optical efficiency</b>	<b>32.69 %</b>
<i>derived from data and assumptions</i>	See equation above
$\alpha\tau$ - product of transmission and absorptance	$\alpha$ : 0.905 test value Calpak $\tau$ : 0.902 test value Calpak
$\gamma$ - Intercept factor	46 % (direct radiation IAM 0°/0°) Soltrace raytracing
$\rho$ - reflection	$\rho$ : 90 % Alanod MICRO-SUN weather-proof reflective is only 90%
$\beta$ - spillage factor	1- $\gamma$ :54 % (direct radiation IAM 0°/0°)
F'- collector efficiency factor	0.97 (Sydney tube with fin and U-shaped tube)

Angle [°]	0.00	11.31	21.80	30.96	38.66	45.00	50.19	54.46	82.87	90.00
Trans [-]	1.000	1.176	1.184	1.136	1.221	1.226	1.227	1.196	0.511	0.226

Angle [°]	0.00	11.31	21.80	30.96	38.66	45.00	50.19	54.46	57.99	60.95	75.96	90.00
Long [-]	1.000	0.975	0.950	0.927	0.901	0.876	0.853	0.829	0.804	0.779	0.513	0.000

3) SCO\_1\_2xASYM\_37mm

<b>Optical efficiency</b>	<b>56.73 %</b>
<i>derived from data and assumptions</i>	See equation above
$\alpha\tau$ - product of transmission and absorptance	$\alpha$ : 0.905 test value Calpak $\tau$ : 0.902 test value Calpak
$\gamma$ - Intercept factor	79.6 % (direct radiation IAM 0°/0°) Soltrace raytracing
$\rho$ - reflection	$\rho$ : 90 % Alanod MICRO-SUN weather-proof reflective is only 90%
$\beta$ - spillage factor	1- $\gamma$ :20.4 % (direct radiation IAM 0°/0°)
F' - collector efficiency factor	0.97 (Sydney tube with fin and U-shaped tube)

Angle [°]	-90.00	-83.66	-81.12	-72.65	-57.99	-38.66	-21.80	-11.31	0.00	11.31	21.80	38.66	67.38
Trans [-]	0.031	0.880	0.901	0.789	0.590	0.569	1.000	0.659	0.540	0.499	0.442	0.530	0.031

Asymmetrische Verteilung !

Angle [°]	0.00	11.31	21.80	30.96	38.66	45.00	63.43	75.96	82.87	90.00
Long [-]	1.000	0.929	0.860	0.790	0.720	0.650	0.327	0.043	0.043	0.000

Table 12: Summary Evaluation SCO\_1\_base\_shape *without error assumptions*

Variante	Criteria 1 Design point ≥50% @250°C	Criteria 2 Yearly yield with Calpak Receiver a <sub>1</sub> 0.844 W/m <sup>2</sup> K a <sub>2</sub> 0.004 W/m <sup>2</sup> K <sup>2</sup> @Patras ≥700 kWh/m <sup>2</sup> a	Criteria 3 System performance solar fraction 80%	Criteria 4 Any other criteria
SCO_1_1xSym_37mm	NO	NO 397 kWh/m <sup>2</sup> a	not done	
SCO_1_2xSym_37mm	NO	NO 219 kWh/m <sup>2</sup> a	not done	
SCO_1_2xAsym_37mm	OK at a single IAM	NO 83 kWh/m <sup>2</sup> a	not done	
		with improved Receiver a <sub>1</sub> 0.1 W/m <sup>2</sup> K a <sub>2</sub> 0.0005 W/m <sup>2</sup> K <sup>2</sup> @Patras ≥700 kWh/m <sup>2</sup> a		
SCO_1_1xSym_37mm	NO	NO 674 kWh/m <sup>2</sup> a	not done	
SCO_1_2xSym_37mm	NO	NO 476 kWh/m <sup>2</sup> a	not done	
SCO_1_2xAsym_37mm	OK at a single IAM	NO 277 kWh/m <sup>2</sup> a	not done	

## Results SCO\_1\_CYL\_CPC

The following simulation of concept SCO\_1\_CYL\_CPC had been running with COMSOL according to the initial defined parameters:

Table 13: Result with initial parameter setup SCO\_1\_CYC\_CPC optical efficiency, IAM trans & energy yield.

Variant/ Parameter change	Opt.eff [-]	IAM <sub>t</sub> factor [-] @ 0°	IAM <sub>t</sub> [-] @ 11.31°	IAM <sub>t</sub> [-] @ 21.80°	IAM <sub>t</sub> [-] @ 30.96°	IAM <sub>t</sub> [-] @ 38.66°	IAM <sub>t</sub> [-] @ 45°	Yearly Yield [kWh/m <sup>2</sup> a]
1. Err. ~10mrd/refl	0.4518	0.992	0.952	0.975	0.947	0.937	0.992	not completed

For the longitudinal IAM the dataset of a 6m long collector row is considered.

Apparently, the optical efficiency for the chosen setup is below 50%, so it is impossible to reach the design point based on criterion 1. Therefore, an energy yield calculation was not performed. The reason for the rather small efficiency is partly caused by the several hits of rays at the CPC, which means a lot of optical losses since every hit subtracting 10% of energy. (e.g.: 5 hits of a ray on the reflector are equal to an optical efficiency of  $0.9^5=0.59$ ).

Another reason is the rather high optical error. The specularity and slope error have been derived from publications [Ulmer, Heiz; Lüpfert, Slope error measurements of Parabolic Troughs using the reflected Image of the absorber tube, 2014, DOI: 10.1115/1.3035811], the other errors are based on basis of conservative assumptions. The assumption of the tracking error of the receiver is derived from recent measurements at a tracking system at the SIJ.

### Optical properties of example materials

	Glass mirror	Polymer film	Aluminum 1	Aluminum 2
$P_{SWH}$	0.939	0.922	0.903	0.868
$P_{SWD}$	0.939	0.874	0.830	0.835
$\alpha_{sdec}$	<< 0.3 mrad	0.9 mrad	1.2 mrad	0.8 mrad

Figure 37: Excerpt from specularity error for different materials [Ulmer, Heiz; Lüpfert].

However, the approach to use conservative assumption seems to be pessimistic, since a lot of rays are not hitting the receiver, even though the focal point is just ~1.5 m away. The behavior of the setup is shown in the following Figure 35.



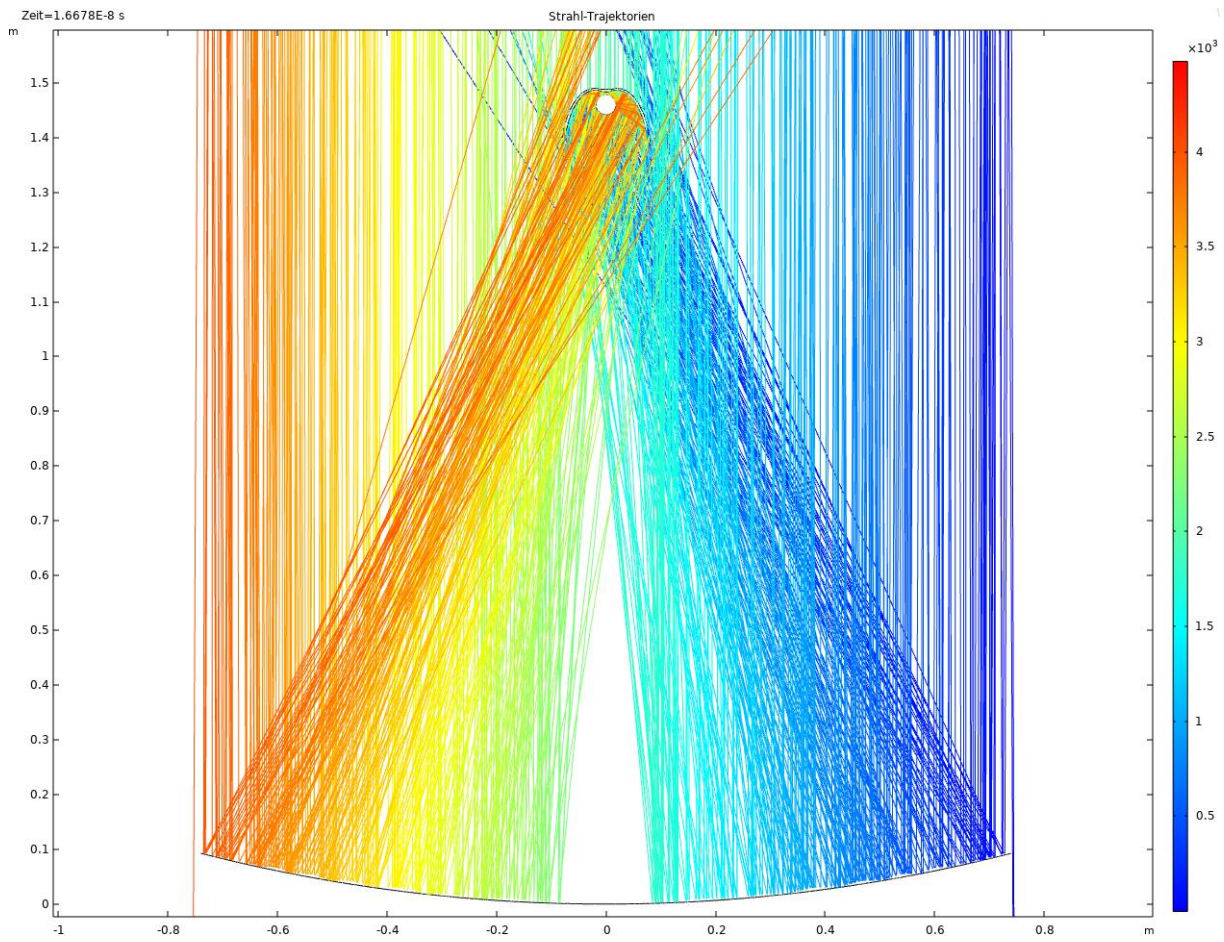


Figure 38: Raytracing with errors (>10mrad/Refl) and defined surface properties for SCO-1\_CYL\_CPC.

Hence, a more optimistic approach was selected, and some error values were modified in accordance to the following Table 11. This assumption is supported by experience from measurement campaigns of PTC's with similar dimensions.

Table 14: Improved error assumptions (higher quality of construction).

Parameter			
Name	Ausdruck	Wert	Beschreibung
Versatz_C...	$\sqrt{R_{CY}^2 - (...}$	0.092699	Versatz der Ray-Line
sunDiskA...	Nicht-konsistente Einheit	rad	Divergenz sun 4.65mrad
error_pri...	$\sqrt{\text{specError}^2 + ...}$	0.0070824 rad	Primary mirror error
specError	1 [mrad]	0.001 rad	Specularity error primary...
slopeError	2.7 [mrad]	0.0027 rad	Slope error primary mirror
shapeError	1 [mrad]	0.001 rad	Shape error primary mirror
alignError	2 [mrad]	0.002 rad	align error primary mirror
trackingEr...	0 [mrad]	0 rad	tracking error primary mi...
theta_long	0 [mrad]	0 rad	longitudinal deviation
error_seco...	$\sqrt{\text{specError}^2 + ...}$	0.0099579 rad	Secondary mirror error
specError2	1 [mrad]	0.001 rad	Specularity error seconda...
slopeError2	2.7 [mrad]	0.0027 rad	Slope error secondary mi...
shapeError2	1 [mrad]	0.001 rad	Shape error secondary mi...
alignError2	2 [mrad]	0.002 rad	align error secondary mir...
trackingEr...	3.5 [mrad]	0.0035 rad	tracking error secondary...

With the new setup another simulation was carried out and the collector data were then used for the energy yield calculations. The complete matrix with different variations is shown in Table 12. In order to evaluate and analyze other improvements on the collector designs, several additional simulations with the reduced errors and higher values for the reflectivity, transmission and tracking have been carried out.

Table 15: Results SCO\_1\_CYC\_CPC optical efficiency,  $IAM_{trans}$  & energy yield.

Variant/ Parameter change	Opt.eff [-]	$IAM_t$ factor [-] @ 0°	$IAM_t$ [-] @ 11.31°	$IAM_t$ [-] @ 21.80°	$IAM_t$ [-] @ 30.96°	$IAM_t$ [-] @ 38.66°	$IAM_t$ [-] @ 45°	Yearly Yield [kWh/m <sup>2</sup> a]
1. Err. ~10mrd/refl	0.45180	1.0	0.952	0.975	0.947	0.937	0.992	not done
2. Red.err; refl=90	0.63643	1.0	0.963	0.825	0.817	0.766	0.754	631
3. Red.err; refl=95	0.68524	1.0	0.972	0.858	0.844	0.794	0.784	703
4. Red.err; refl=95, Tau97, a96	0.73664	1.0	0.972	0.857	0.842	0.793	0.782	760
5. Red.err; refl=95, Tau97, a96 circular pathway	0.71986	1.0	0.949	0.913	0.927	0.723	0.747	744

Notes on variants: 3. Necessary setup; 4. Possible “best of breed” setup, 5. Additional circular tracking motion setup.

As already discussed, the first variant is not sufficient to reach both performance criteria. The second variant contains all the previous defined parameter, only the error is reduced according to the improved error table. With this improvement the collector fulfills criterion 1 but is failing to reach criterion 2 by almost 10%.

In order to reach the second criterion, the concept needs further improvement. For this reason, reflectivity is changed from 90% to 95%. It is possible that such a material is available on the market and used at many PTC’s, but most probably a glass mirror must be used to guarantee a high degree of reliability. Notably, the specular error of the reflective surface is decreasing considerable ( $\ll 0.3$  mrad) with the use of a glass mirror. With the use of an improved reflector, criterion 2 is met.

When looking in the market of medium and high temperature solar collectors, the leading products have the following specifications:

- transmittance 97%, reflectance 95% and absorbance 96%.

Using those values together with the reduced error assumptions, an energy yield of 760 [kWh/m<sup>2</sup>a] can be reached under the weather conditions of Patras.

A last set of simulations was performed for this “best in class” or “best of breed” setup by using a circular tracking path instead of the optimal tracking pathway. A circular pathway is advantageous, because only one driver is necessary, instead of two or three, for the optimal tracking pathway. An example of a circular pathway track is shown in Figure 36. With the use of a counterweight the torsional moment is reduced, and the motor drive just needs to shift the receiver with the consideration of the law of lever and with respect to the wind speed.

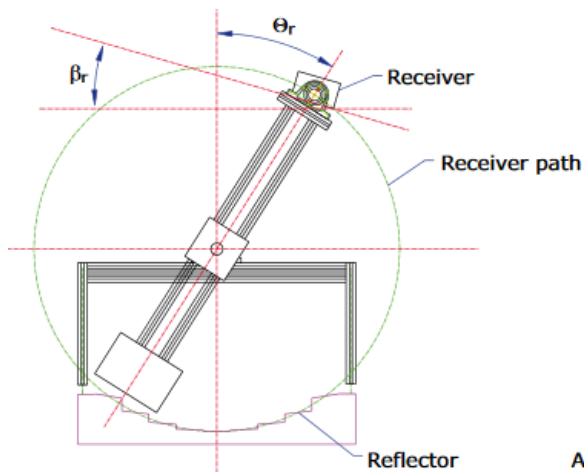


Figure 39: Sample of a circular tracking

Werner Weiss, "State of the art within Task 33/IV," in *IEA SHC Task 33*, Gleisdorf, Austria, 2008.

In Figure 37 the optimal tracking path is drawn as well as the circular pathway. In addition, a couple of simulations have been performed in order to specify a confidence level around the optimum tracking path, where still a maximum intercept factor is reached. Until now this simulation has only been performed for a version without errors and surface parameters. Obtaining the maximum intercept factor was applied as the optimization rule. The optimum was found by applying a gradient method to find the absolute optimum.

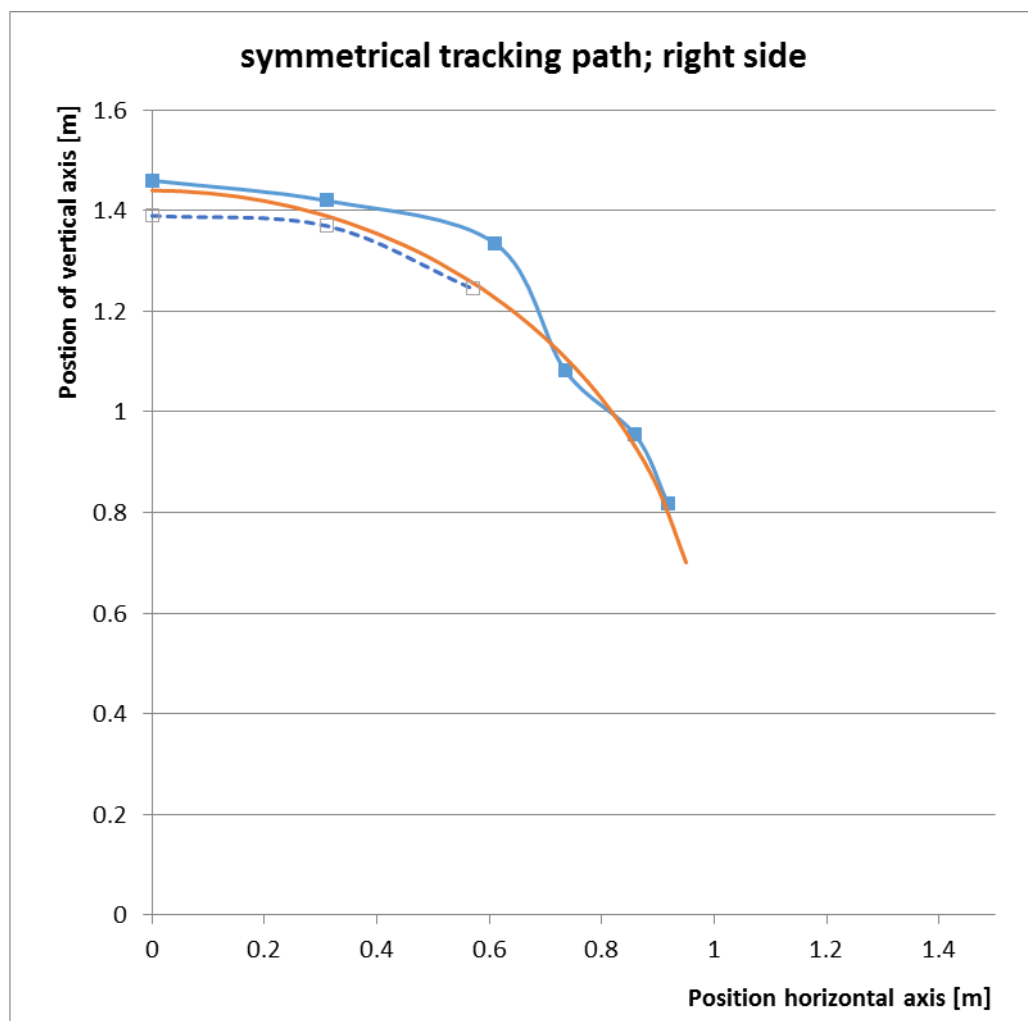


Figure 40: Optimal tracking pathway (blue), confident interval (dashed blue line) and circular pathway (orange).

Further simulations with consideration of the error assumptions and the surface properties may lead to slightly better results for the variants, because the energy flux is then optimized instead of the intercept factor.

The energy yield calculation for Patras, shows that criterion 2 cannot be reached with the assumptions for the absorptance, transmittance, reflectance values and errors as agreed during the Telco meeting of 28.03.2019. Therefore, in the first step, the defined errors of the materials and shapes had been revised and eventually improved. Since the previous errors are mainly based on conservative assumptions, the reduction of errors to an overall error less than 7 mrad per reflector unit has been assumed. The tracking error of the receiver was set to 3.5 mrad. Even with the consideration of the improved construction, criterion 2 could not be met. In order to reach the criteria in the first place more parameters of the model setup had been freed. When the reflectivity of the primary and secondary reflector is set to 95%, a value typically reached by a glass mirror, the benchmark of criterion 2 is going to be fulfilled. If the parameters of the used materials is further improved, like it is stated for the Schott receiver and therefore technical proofed, the energy yield is reaching a point about ~8.5% above the benchmark.

Moreover, a circular tracking is meaningful since it may decrease the investment costs and the performance of the collector remains at a relatively high level at the same time.

In order to enhance the yearly yield longer collector arrays are efficient, but for on-roof installation rows > 6 m may be too long.

For the version SCO1\_Cyl\_CPC both, the properties of the used reflector and the error of the surfaces and shapes, must be improved (e.g. reflectance of the prime and the secondary from 90% -> 95%). Since the assumptions for the errors are mainly based on conservative assumptions there might be space for improvements by means of an accurate and precise construction.

Table 16: Summary Evaluation SCO\_1\_CYL\_CPC.

Variant	Criterion 1 Design point ≥50% @250°C	Criterion 2 Yearly yield with Himin Receiver a <sub>1</sub> 0.5 W/m <sup>2</sup> K a <sub>2</sub> 0.00358 W/m <sup>2</sup> K <sup>2</sup> @Patras ≥700 kWh/m <sup>2</sup> a	Criterion 3 *) System performance solar fraction 80% **)	Criterion 4 Any other criteria
0. without error, preliminary studies	OK	OK	not done	Costs receiver Tracking in two directions with additional rotation High requirements on materials and construction Manufacturing of reflectors
1. Err. ~10mrd/refl	NO	NO	not done	
2. Red.err 7mrad; refl=90	OK	NO 631 kWh/m <sup>2</sup> a	not done	
3. Red.err; 7mrad refl=95	OK	OK 703 kWh/m <sup>2</sup> a	94 m <sup>2</sup>	
4. Red.err7mrad; refl=95, Tau97, a96	OK	OK 760 kWh/m <sup>2</sup> a	87 m <sup>2</sup>	
5. Red.err 7mrad; refl=95, Tau97, a96, circular pathway	OK	OK 744 kWh/m <sup>2</sup> a	90 m <sup>2</sup>	

\*) Since the processing time with the Patras weather file is currently too long the Andravida data are used for the SF calculation.

\*\*\*) at this state of the project many of assumptions for the system components have been considered. In the future these values should be defined in accordance with some parameter optimization and/or real component specifications.

### Linear absorber path

The absorber is positioned along the axis of symmetry (y), where 0 is 0.5m from the main mirror. Ray-trace results are exported for each y and solar azimuth  $\theta_{az}$ .

#### Trace variables

- $-0.30 \text{ m} < y < 1.20\text{m}$ , step = 0.01 m
- $135^\circ < \theta_{az} < 225^\circ$ , step =  $1^\circ$

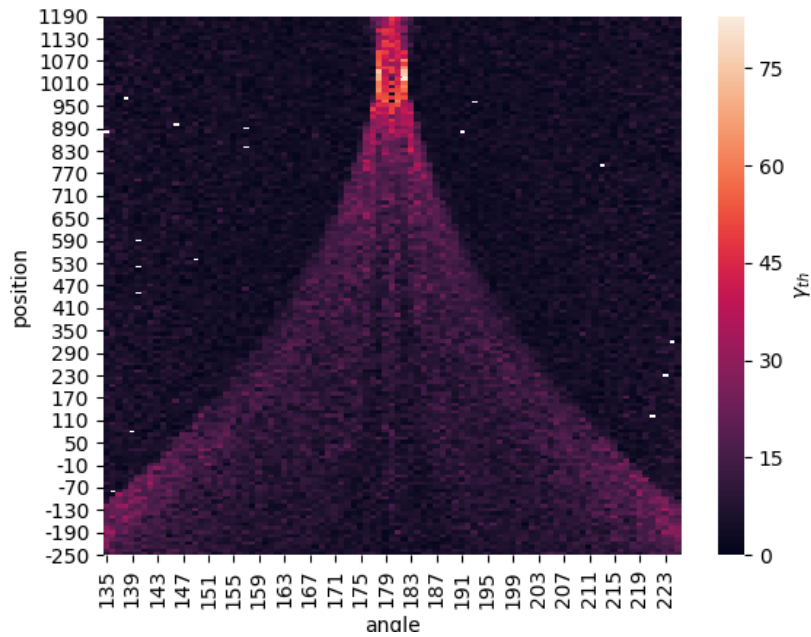


Figure 42 SCO1\_CYL\_CPC – heatmap

#### Comments

The maximum  $\gamma_{th}$  is observed at the cylinder's focal point and for normal incidence, as expected. However,  $\gamma_{th}$  is not expected to go over 30% on any other part of the y axis.

#### Linear Regression

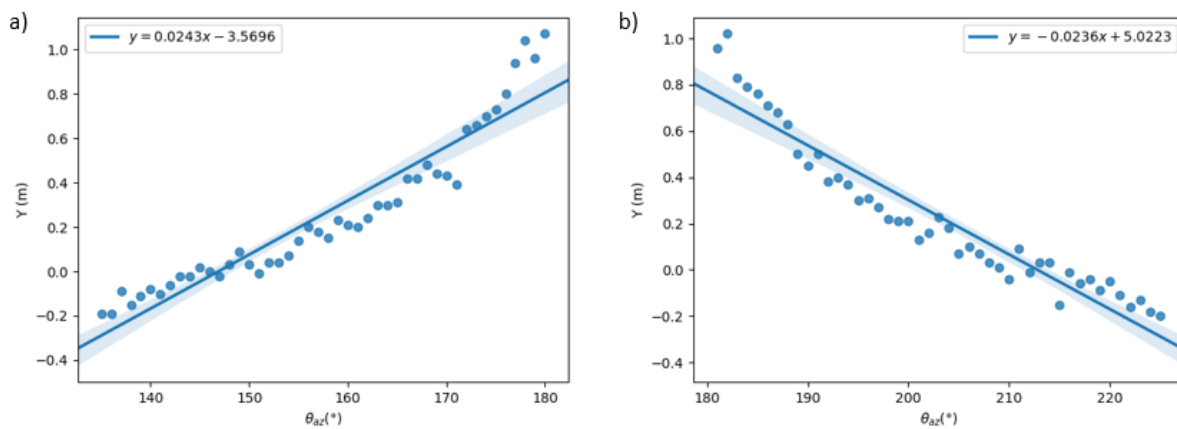


Figure 43 SCO1\_CYL\_CPC - linear regression. a)  $135^\circ \leq \theta_{az} \leq 180^\circ$ , b)  $180^\circ < \theta_{az} \leq 225^\circ$

$$135^\circ \leq \theta_{az} \leq 180^\circ$$

Parameter	Value	SE	StDev	P-value	R2	n
Intercept	-3.56957	0.195868	1.32844	4.00E-22	0.897329	46
Slope	0.024301	0.001239	0.008405	2.25E-23		
$180^\circ < \theta_{az} \leq 225^\circ$						
Parameter	Value	SE	StDev	P-value	R2	n
Intercept	5.02234	0.238686	1.60115	2.91E-24	0.90393	45
Slope	-0.0236	0.001173	0.007871	1.70E-23		

Table 17 SCO1\_CYL\_CPC- regression parameters SE: Standard Error, StDev: Standard Deviation, n: number of observations

The linear regression parameters are satisfactory. It should be noted that the results are not symmetric for the two sections. The extracted equations for the absorber’s motion are:

$$y = 0.024(\pm 0.001) \times x - 3(\pm 1), (r = 0.89, n = 46, p < 2.25e-23), 135^\circ \leq \theta_{az} \leq 180^\circ$$

$$y = -0.024(\pm 0.008) \times x + 5.0(\pm 0.2), (r = 0.90, n = 45, p < 1.70e-23), 180^\circ < \theta_{az} \leq 225^\circ$$

#### Equation test

The system was traced again with  $0.1^\circ$  increment, this time with the absorber position determined by Eq. 1, in order to test the extracted equation.

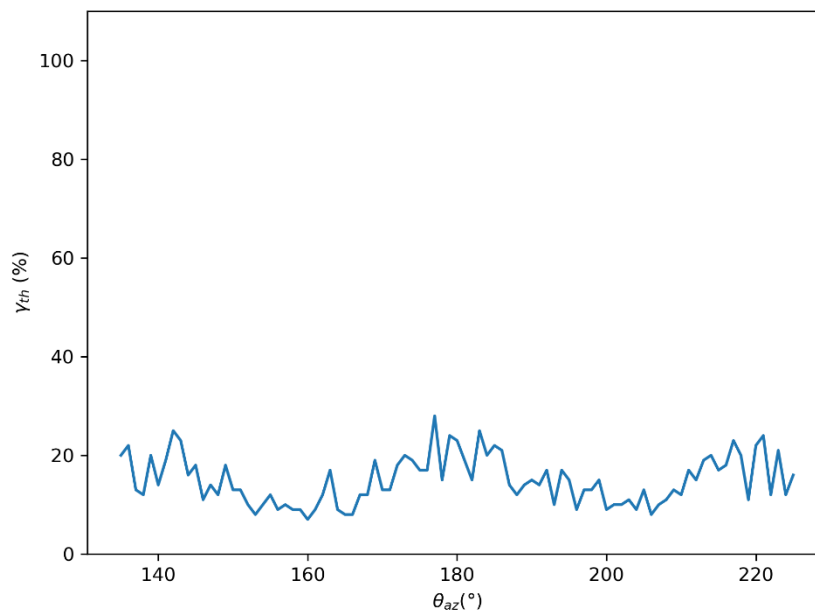


Figure 44 SCO1\_CYL\_CPC - equation test

#### Comments

The absorber’s equation of motion for a linear path results to an intercept factor of 20% from  $135^\circ$  to  $225^\circ$ , which is not considered satisfactory. A non-linear path should be further investigated.



## Results SCO\_2\_Multi\_SYM/ASYM

The SCO2 system implements a number of receiver tubes and operates by the control of the flow of the liquid according to the total reflected irradiance which arrives from the compound mirror. In that way, it maximizes the temperature that the liquid can reach. The general idea on **symmetric** SCO2 is to adjust the SCO1 CPC reflector shape, as seen in figure 24, to accommodate 3 or 4 tubes.

The latter consists of a compound parabolic mirror (1 circular part and 2 parabolic parts with 0.25 m radius and focal length respectively), optical analysis was conducted mainly for the transversal motion of the Sun with respect to the system's orientation.

As for the material properties both the concentrator and the tubes system were considered ideal. More specifically, regarding the receivers, Sydney evacuated tubes were used as an example.

Table 14: Specifications of concentrator and absorber tubes for the SCO2 system

Concentrator		Receiver	
Mirror reflectivity	1	Absorber tube outer diameter	0.047 m
Tube absorbance	1	Receiver outer diameter	0.058 m
Vacuum tube outer glass transmissivity	1		
Cover transmissivity	1		

The concentration ratio of the system is equal to 3.48 and has been derived from the following equation

$$Concentration\ ratio_{n\ receivers} = \frac{Area_{aperture}}{Area_{receiver}}$$

As a first approximation, no space is considered between the absorbers as seen in Figure 37.



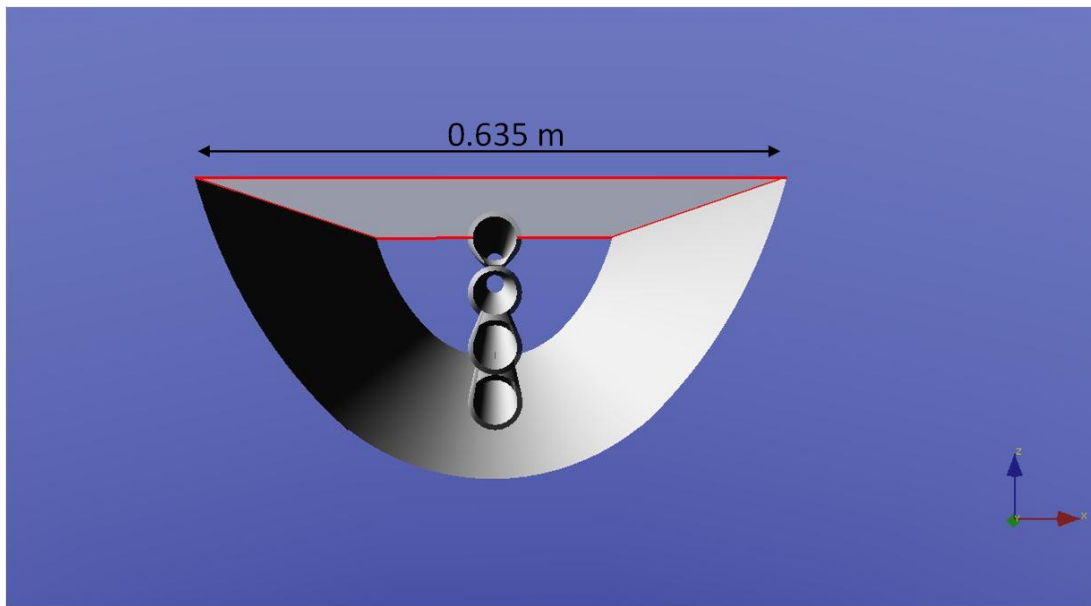


Figure 37: 4 absorbers – no space

The trace results are reported in Figure 38.

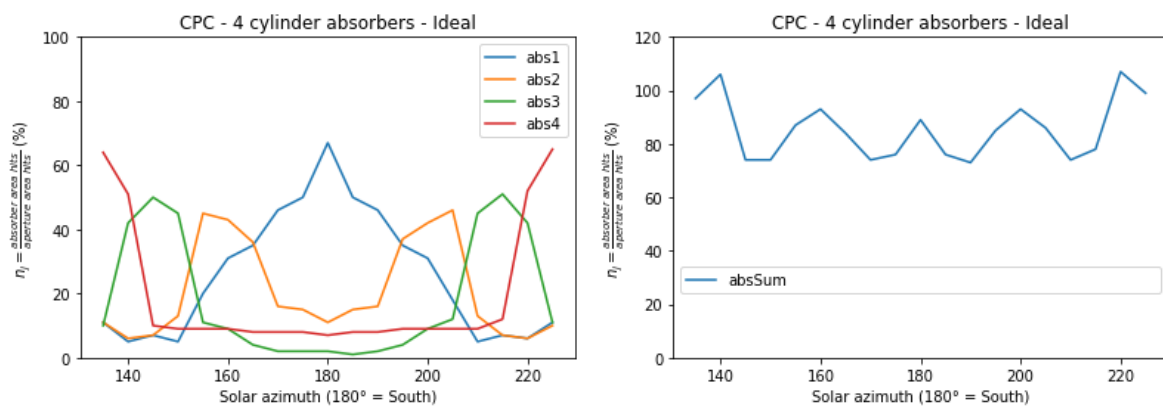


Figure 38: No space- ideal

The former scenario cannot be considered as realistic, so the absorbers were positioned along the y axis with 0.01275 m space between them.

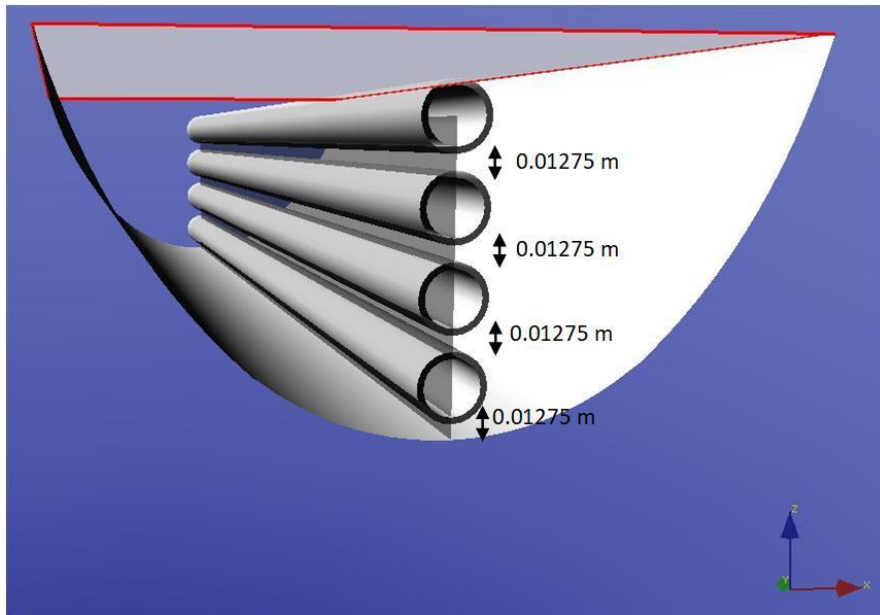


Figure 39: 4 absorbers – 0.01275 spacing

Next, a spacing of 0.005 m was implemented as it can be seen in Figure 40.

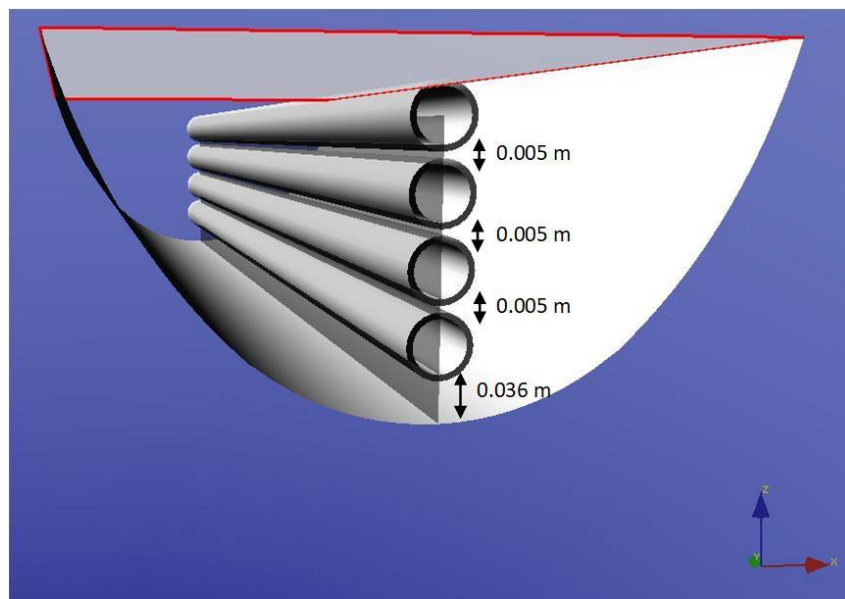


Figure 40: 4 absorbers – 0.005 m spacing.

The trace results are reported in Figure 41.

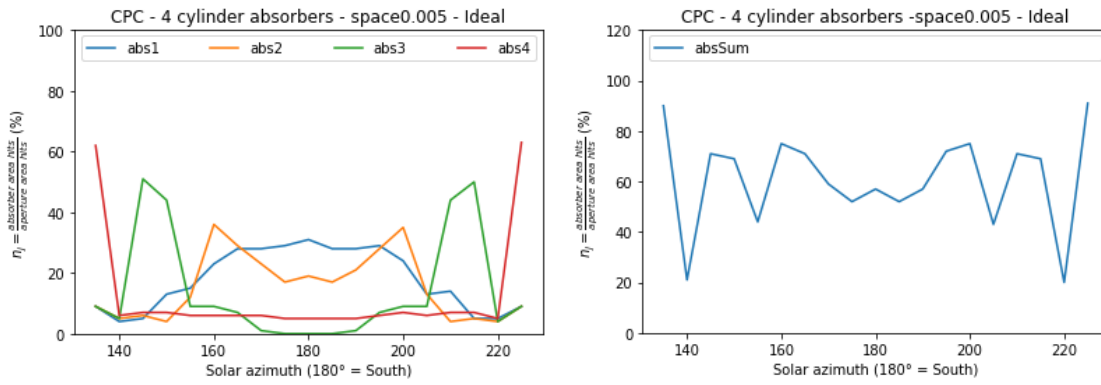


Figure 41: No space - ideal

Subsequently, a three-tube configuration has been introduced in order to test its optical performance. The system is presented in Figure 42.

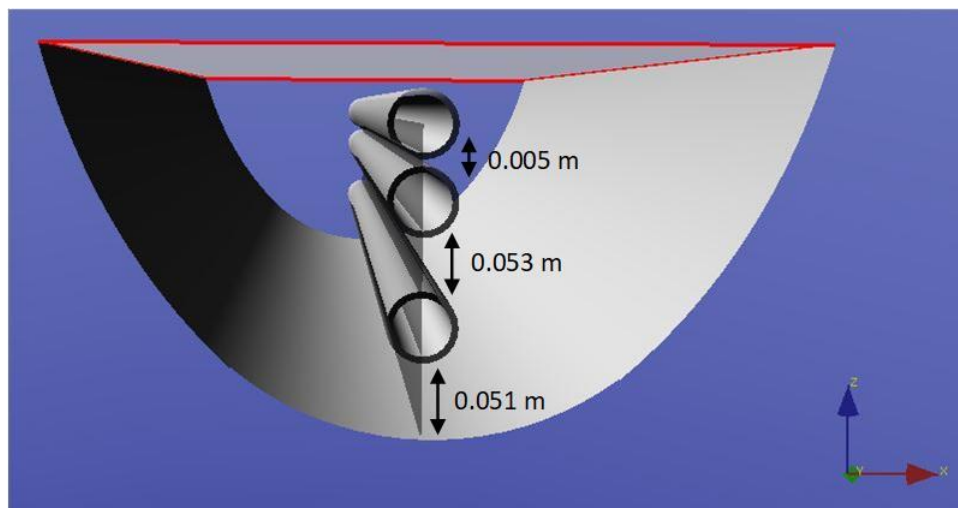


Figure 42: 3 absorbers configuration

And the results from the optical simulations are shown in Figure 43.

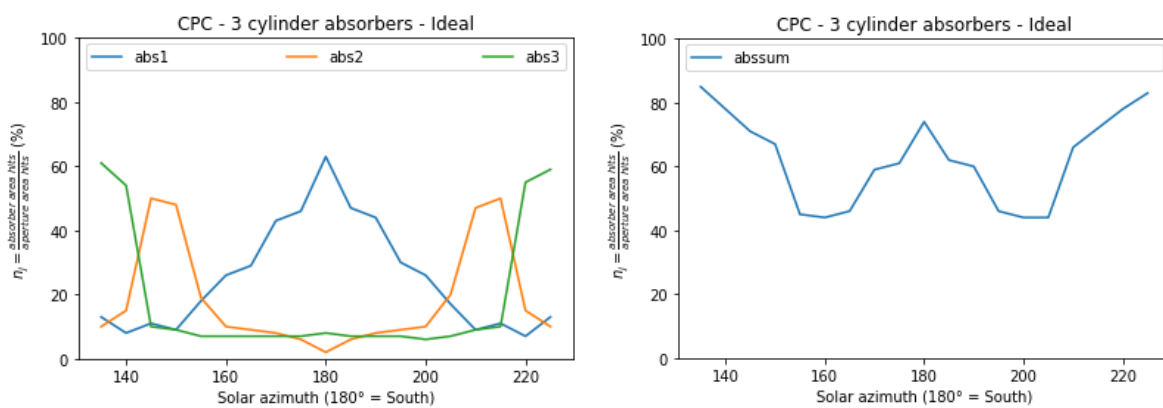


Figure 43: 3 absorbers

## Results SCO\_3\_FPC/VTC

If required, please add information from UPAT here

### SCO\_3F

In Fig. 41 appears a cross section of the SCO3F configuration. It consists of a flat absorber with width equal to 1.6 m and an equal mirror. The angle between the absorber and the horizontal plane is fixed to a value of  $37.98^\circ$ . Furthermore, in the following simulations the angle between the mirror and the horizontal plane, symbolized herein as “a”, has three distinct angle values namely,  $37.98^\circ$ ,  $25^\circ$  and  $12^\circ$ , the first angle being the latitude of Patras. In Fig. 42-47 the intercept factor values appear as a function of the angle.

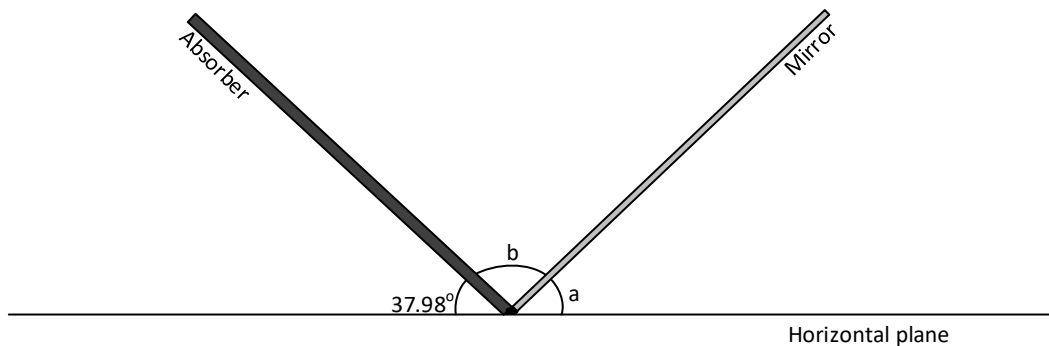


Figure 41: Cross section of the SCO\_3F configuration with a flat absorber and a flat booster mirror.

### SCO\_3F (Equal mirror)

Firstly, the value of the angle -a- was set equal to  $37.98^\circ$ .

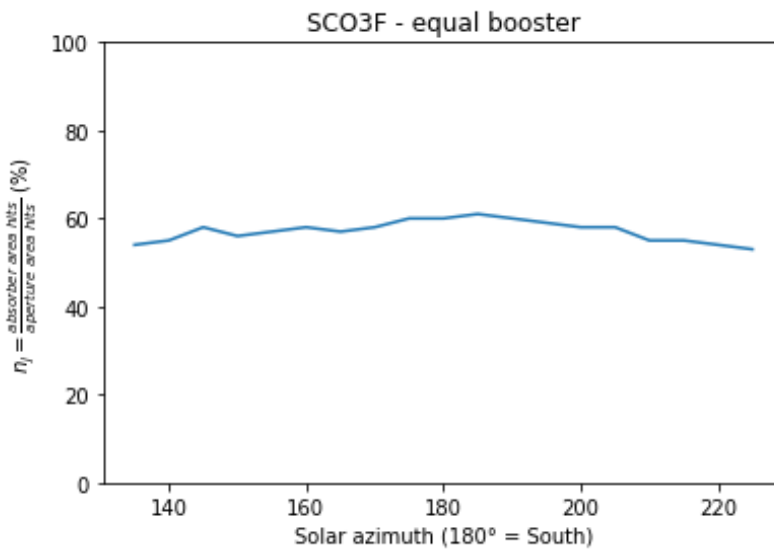


Figure 42: Transversal ray tracing. Daily variation ( $90^\circ$ ) of the solar insolation

## Results SCO\_4\_Micro-mirror concentrator concept

Simulations were carried out with the following set of parameters:

Table 17: Ray tracing parameters allowing a concentration ratio of  $c=30$ 

mirrorWidthX	0.14	m	Width of the mirror in X direction
mirrorWidthY	0.187	m	Width of the mirror in Y direction
gapX	0.0015	m	gap between mirrors in X direction
gapY	0.0015	m	gap between mirrors in Y direction
focalLength	1.5	m	Focal length of the mirror array and distance of receiver from array centre
height	0.25	m	height above the ground
numMirX	7		number of mirrors in X direction
numMirY	8		number of mirrors in Y direction
ref	1		mirror reflectivity
opticalError	5e-3		optical error normal random distribution
sundisk	4.65e-3		sun disk uniform random distribution
rec_width	0.2	m	receiver width
rec_length	0.25	m	receiver length
alpha	25	°	receiver tilt angle (rotation around y axis wrt array centre)

With 10,000 rays the IAM graph of Figure 43 was obtained. In this context, as there is no natural system axis, we are using the terms "transversal" indicating a rotation of the sun's direction in the (x-z) plane (axis of rotation = y axis) and "longitudinal" indicating a rotation in the (y-z) plane (axis of rotation = x axis).

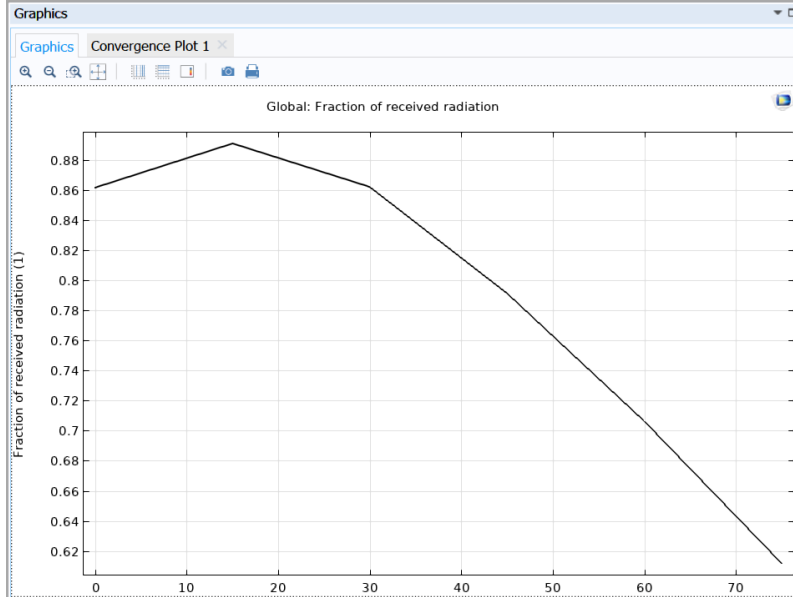


Figure 43: IAM function (fraction of deposited ray power on receiver with respect to total emitted ray power) at **longitudinal** angles  $0^\circ$  to  $75^\circ$ , 10,000 rays.

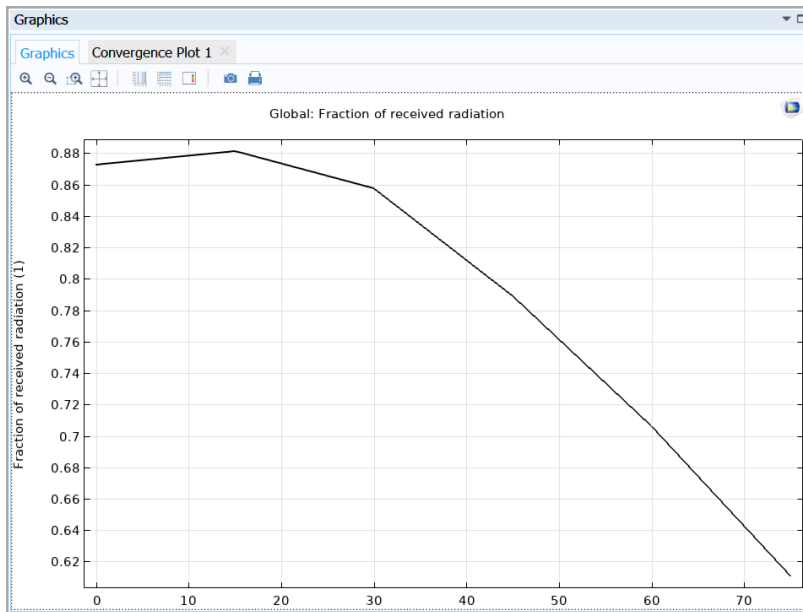


Figure 44: IAM function (fraction of deposited ray power on receiver with respect to total emitted ray power) at longitudinal angles  $0^\circ$  to  $75^\circ$ , 50,000 rays.

The intensity distribution on the receiver at  $0^\circ$  incidence is displayed in Figure 45.

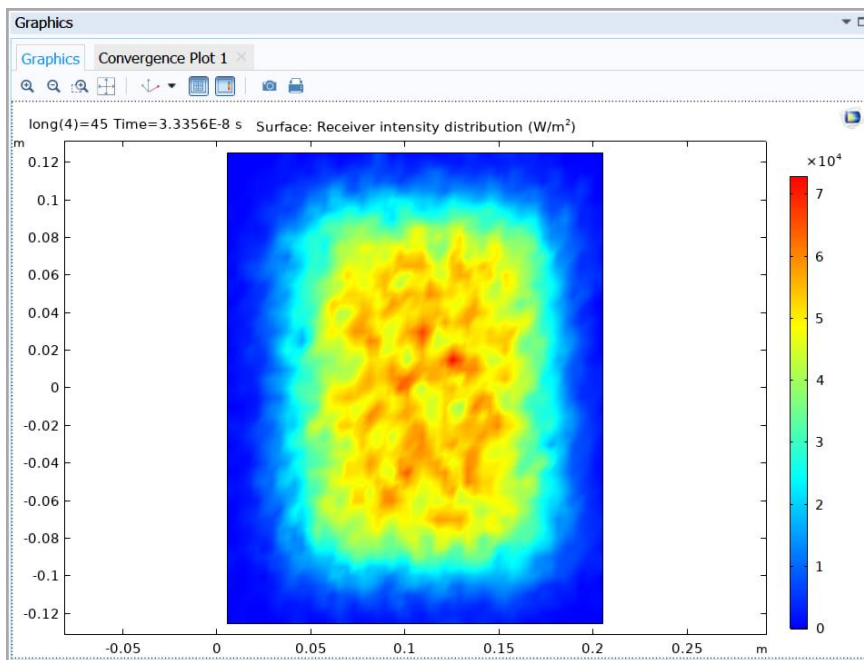


Figure 45: intensity distribution on the receiver surface at longitudinal solar incidence angle  $0^\circ$ , 50,000 rays

At longitudinal angle  $45^\circ$  the intensity distribution is rotated (Figure 46).

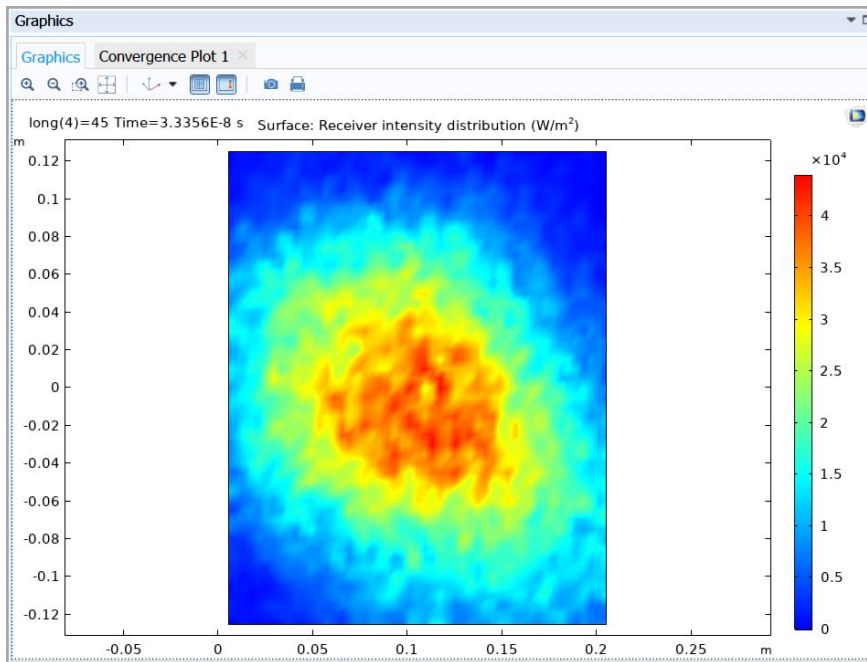


Figure 46: intensity distribution on the receiver surface at longitudinal solar incidence angle  $45^\circ$ , 50,000 rays.

When the transversal angle is modified, the IAM function of Figure 47 and Figure 48 is obtained. The asymmetry is due to shadowing effect of the receiver and its off-centre position.

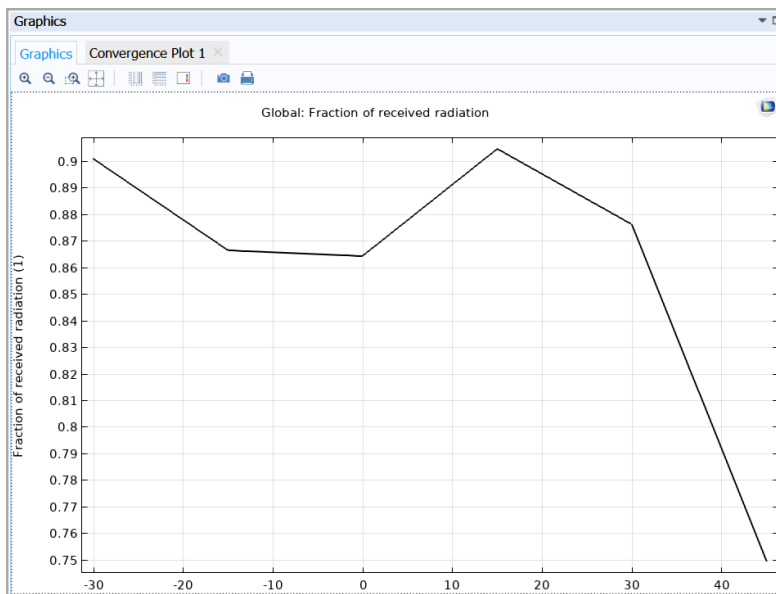


Figure 47: IAM function (fraction of deposited ray power on receiver with respect to total emitted ray power) at transversal angles  $-30^\circ$  to  $45^\circ$ , 10,000 rays.

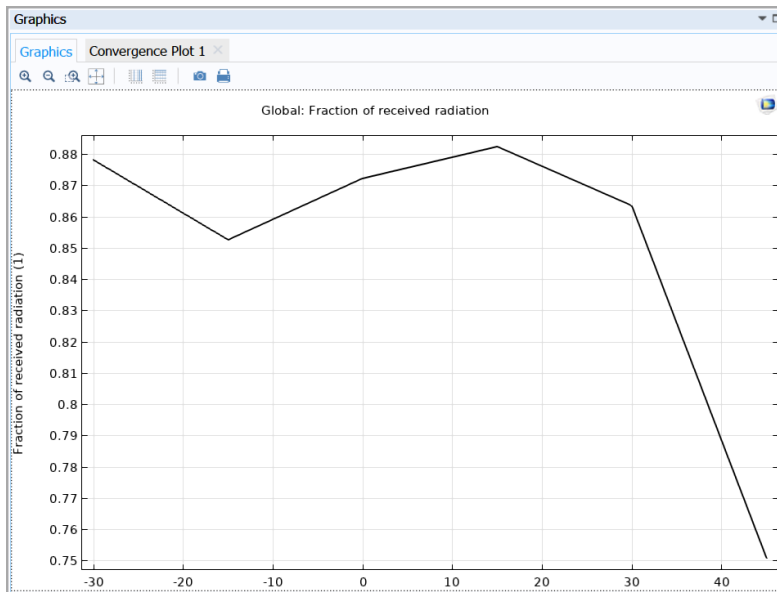


Figure 48: IAM function (fraction of the deposited ray power on the receiver with respect to the total emitted ray power) at transversal angles  $-30^\circ$  to  $45^\circ$ , 50,000 rays.

It is observed that the intensity centre on the receiver shifts slightly when the transversal angle deviates from  $0^\circ$ . Therefore, it can be assumed that the performance can even be slightly improved if an angular correction function is applied.

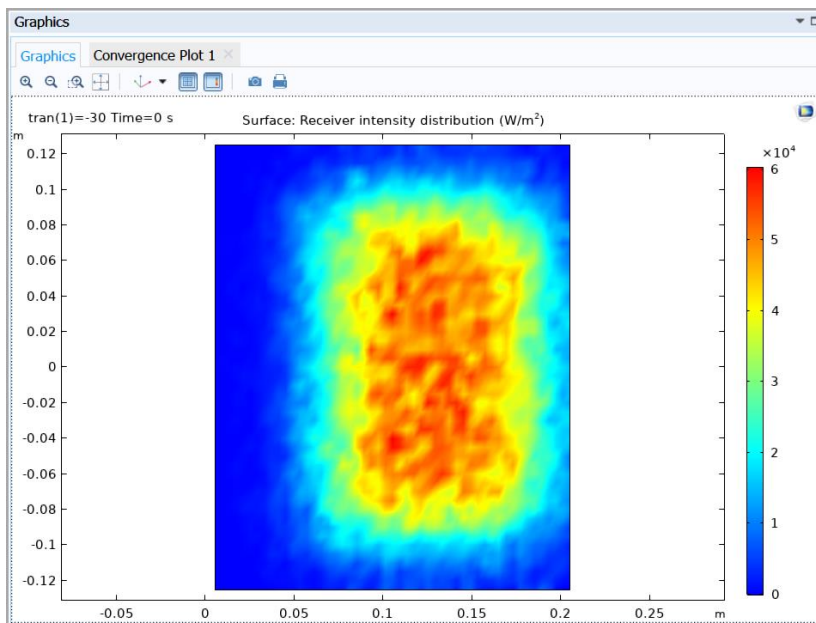


Figure 49: intensity distribution on the receiver surface at transversal solar incidence angle  $-30^\circ$ , 50,000 rays

The influence of the optical error on the intercept factor at  $0^\circ$  incidence (calculated with 20,000 rays) is shown in Table 18. With a focal length of 1.5 m, the gap between the facets (size as in Table 17) must be at least 1.3 mm to avoid facet collisions. The intercept results of simulations with 100,000 rays differ by  $< 0.2\%$  from those with 20,000 rays.



Table 18: Influence of optical errors on the intercept factor (20,000 rays)

Optical error	5 mrad	7 mrad	10 mrad	20 mrad	
Intercept*	86.9 %	84.0 %	77.1 %	50.5 %	Focal length = 2 m, gap = 1 mm
	86.5 %	85.1 %	81.3 %	61.4 %	Focal length = 1.5 m, gap = 1.3 mm

\* the intercept is calculated as the fraction of rays that hit the receiver based on all rays that hit the mirror array, gaps inclusive

The optical error has a significant influence on the performance. All efforts should be made to keep the errors below 7 mrad. Otherwise even the use of antireflective glazing will not be sufficient to meet the thermal requirements of this receiver-concentrator combination. Alternatively, smaller (and more) mirror facets in one array could improve the concentration ratio.

Table 19: Optical performance of various array configurations (20,000 rays) at 0° incidence angle with off-centre receiver

Case #	Receiver size	Mirror facets	Concentration factor	Focal length	Optical error	intercept
1	19 cm x 19 cm	14 cm x 14 cm 7 x 11	42.3	2 m	7 mrad	80.8 %
2	20 cm x 20 cm	14 cm x 14 cm 7 x 11	38.2	2 m	7 mrad	82.8 %
3	19 cm x 19 cm	14 cm x 14 cm 7 x 11	42.3	1.5 m	7 mrad	83.3 %
4	20 cm x 20 cm	14 cm x 14 cm 7 x 11	38.2	1.5 m	7 mrad	84.6 %
5	20 cm x 20 cm	14 cm x 14 cm 7 x 11	38.2	1.2 m	7 mrad	82.2 %
6	20 cm x 20 cm	14 cm x 14 cm 7 x 11	38.2	1.6 m	7 mrad	84.7 %
7	18 cm x 18 cm	10 cm x 10 cm 10 x 15	47.1	1.5 m	8 mrad	84.3 %
8	18 cm x 18 cm	10 cm x 10 cm 10 x 15	47.1	1.5 m	7 mrad	85.4 %
<b>9</b>	<b>18 cm x 18 cm</b>	<b>10 cm x 10 cm 10 x 15</b>	<b>47.1</b>	<b>1.6 m</b>	<b>7 mrad</b>	<b>85.9 %</b>
10	18 cm x 18 cm	10 cm x 10 cm 10 x 15	47.1	1.7 m	7 mrad	85.8 %

Among these cases the best overall performance can be achieved with a 10 x 15 mirror array of 10 cm x 10 cm facets, a focal length of 1.6 m and a receiver size of 0.18 m x 0.18 m. Still the optical errors should not exceed  $\pm 8$  mrad. The main advantage of using smaller facets is the potential for an increased concentration ratio with an intercept  $> 85$  %, which is required if plain glass ( $\eta = 92$  %) is used for the mirror array cover. The use of AR-coated glass ( $\eta = 95$  %) would reduce the minimum required intercept to 79 %.

It is interesting to observe that even without optical errors, the intercept is only about 88 %, because the gaps between the canted facets are much larger than the nominal gaps (as measured when all facets are oriented in one plane), and about 12 % of the incoming radiation is passing between the mirror facets to the mirror background (see Figure 50).

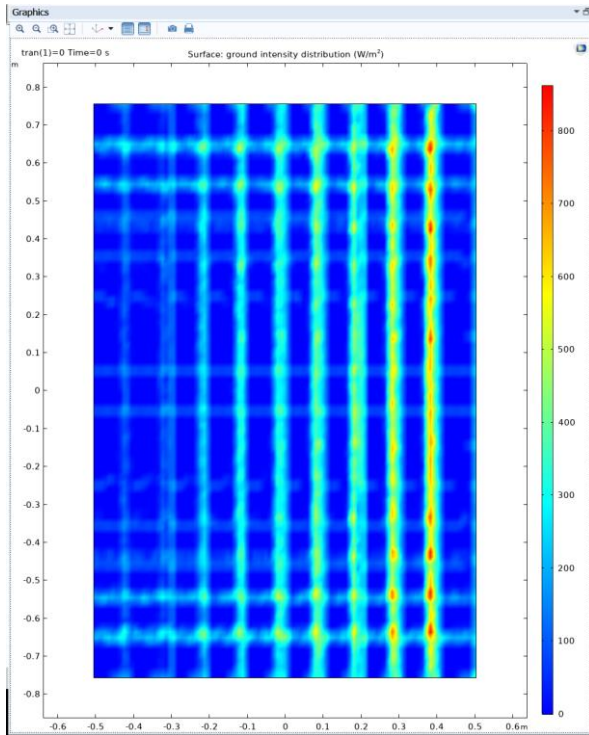


Figure 50: Intensity distribution on the mirror background (focal length 1.7 m, 300,000 rays)

The IAM curves:

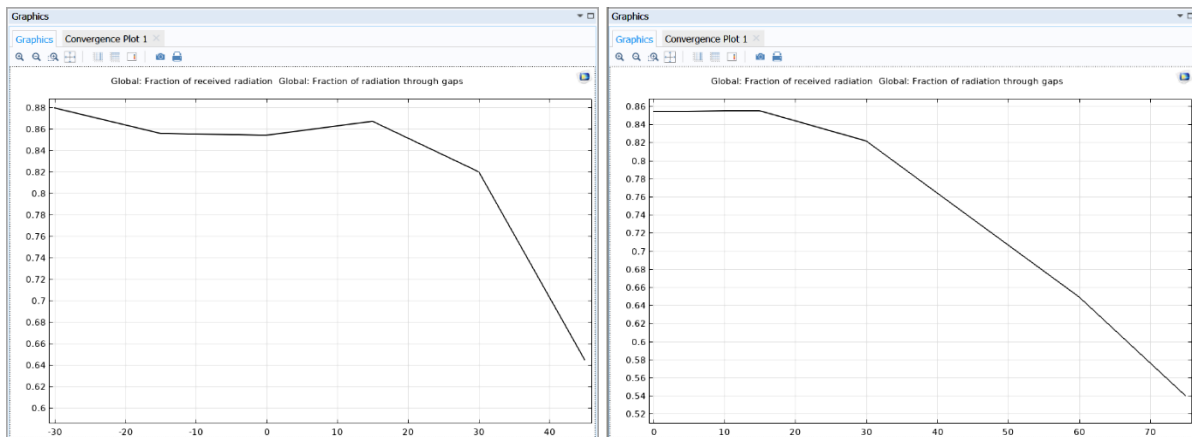


Figure 51: IAM curves of transversal (left) and longitudinal angles (right), parameters of case 9 in Table 19.

Table 20: IAM supporting values

transversal		longitudinal	
-30	0.880	0	0.88
-15	0.856	15	0.855
0	0.855	30	0.822
15	0.867	45	0.736
30	0.821	60	0.650
45	0.645	75	0.540

When the receiver is placed above the centre of the mirror array, better performance can be achieved despite the shadowing.

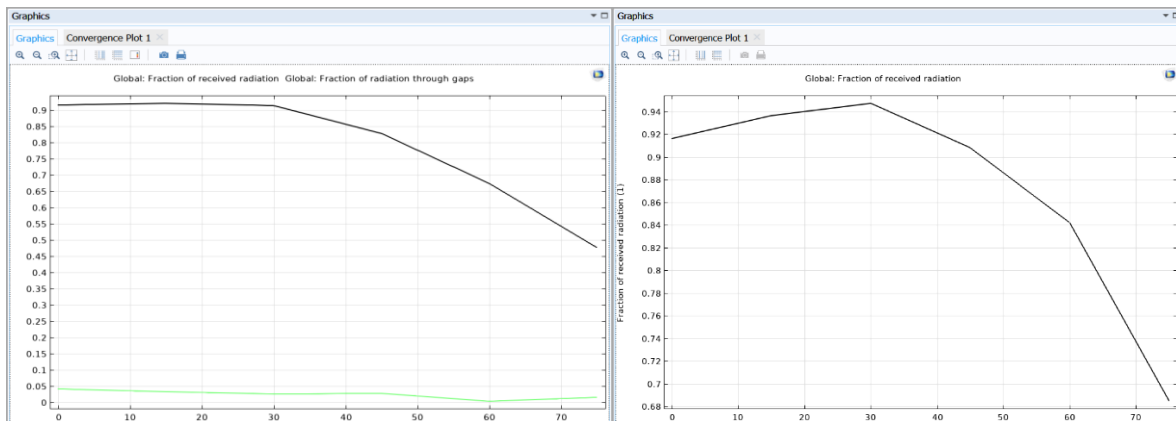


Figure 52: IAM curves of transversal (left) and longitudinal angles (right), parameters of case 9 in Table 19 but central receiver ( $\alpha=0$ ).

Table 21: IAM supporting values

transversal		longitudinal	
0	0.916	0	0.916
15	0.922	15	0.937
30	0.915	30	0.947
45	0.828	45	0.909
60	0.676	60	0.842
75	0.477	75	0.685

In this design even a box with 2 cm rim and 7 cm height can be added to the receiver and 10 mrad optical error can be assumed to achieve an intercept of 85.4 % (300,000 rays), if the focal length is set to 1.4 m. Changing the size and number of facets to 7x11 (14 cm) and increasing the receiver to 20 cm x 20 cm reduces the intercept to 83.3 %. This parameter set is referred to as case A.

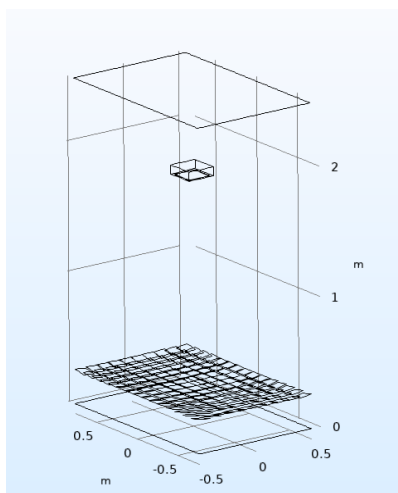


Figure 53: Visualisation of setup (10 x 15 mirrors) in COMSOL.

Table 22: Intercept data from COMSOL simulations of case A, left: transversal, right longitudinal variation of incidence angle (100,000 rays).

0.0000	0.83255	0.0000	0.83255
15.000	0.83864	15.000	0.84846
30.000	0.83976	30.000	0.87791
45.000	0.75742	45.000	0.87178
60.000	0.62348	60.000	0.79430
75.000	0.46338	75.000	0.66268

Table 23: Optical performance of various array configurations (20,000 rays) at 0° incidence angle with centred receiver including box

Case #	Receiver size	Mirror facets	Concentration factor	Focal length	Optical error	Intercept at 0° incidence
A	20 cm x 20 cm	14 cm x 14 cm 7 x 11	38.2	1.4 m	10 mrad	83.26 % (100,000 rays)
B	20 cm x 20 cm	14 cm x 14 cm 7 x 11	38.2	1.4 m	7 mrad	88.3 % (100,000 rays)
C	18 cm x 18 cm	10 cm x 10 cm 10 x 15	47.1	1.4 m	10 mrad	85.4 % (300,000 rays)
D	18 cm x 18 cm (no box)	10 cm x 10 cm 10 x 15	47.1	1.4 m	10 mrad	91.6 % (300,000 rays)

Data preparation for the thermal simulation

The values of Table 22 have to be divided by the intercept at incidence angle 0° (0.83255) to obtain the IAM data to be used in the CARNOT collector model, while the intercept at incidence angle 0° is considered in the calculation of  $\eta_o$  ( $F' \eta_o$  in the CARNOT nomenclature).

If the optical error is reduced from 10 mrad to 7 mrad (case B) the results of Table 24 are obtained.

Table 24: Intercept data from COMSOL simulations of case A1, left: transversal, right longitudinal variation of incidence angle (100,000 rays).

0.0000	0.88304	0.0000	0.88304
15.000	0.88704	15.000	0.89793
30.000	0.88598	30.000	0.92582
45.000	0.79546	45.000	0.91603
60.000	0.65271	60.000	0.83587
75.000	0.48191	75.000	0.69756

The most promising and relevant options were chosen and the particular dataset was simulated with the annual energy yield tool. The results have been:

Table 25: Results for the design point and annual energy yield calculation

Variant	Criterion 1 Design point ≥50% @250°C	Criterion 2 Yearly yield with <b>flat</b> Receiver $a_1$ 0.075 W/m <sup>2</sup> K $a_2$ 0.000426 W/m <sup>2</sup> K <sup>2</sup> , F'=1 @Patras ≥700 kWh/m <sup>2</sup> a	Intercept factor and zero loss efficiency
10 mrad version	No -48%	OK 718 kWh/m <sup>2</sup> a *	83.3 % / 53.7 %
7 mrad version	OK (51.5 %)	OK 759 kWh/m <sup>2</sup> a	88.3 % / 57.0 %

\*) **But design point not reached - unless C is going to be set to C=80**

Note on annual energy yield calculations:

- simulation data set  $\text{ETA}_0 = 0.5295$ ,  $a_1=3.5$  (W/m<sup>2</sup>K)/C [47]=0.074468,  $a_2=0.02$  (W/m<sup>2</sup>K<sup>2</sup>)/C [38.2]=0.000426 Intercept 81.3%: Annual Yield: **718 kWh/m<sup>2</sup>a**
- $\text{Eta}_0 = F' \cdot \text{Intercept} \cdot \tau_{\text{glas\_Box}}^2 \cdot \text{Refl\_Microhelix} \cdot \tau_{\text{receiver}} \cdot \alpha_{\text{receiver}}$
- $0.537 = 0.97 \cdot 0.833 \cdot 0.92^2 \cdot 0.9 \cdot 0.92 \cdot 0.95$
- simulation data set  $\text{ETA}_0 = 0.57$   $a_1$ ,  $a_2$  see above, Intercept 85%, Annual Yield: **759 kWh/m<sup>2</sup>a**

### Modification of the Incidence Angle to simplify the box construction

In addition, a series of simulations were done with Matlab/Simulink/Carnot to calculate the performance with different IAM functions, in which the IAM was set to zero above angles of incidence varying between 20° and 45° (transversal) and between 40° and 70° (longitudinal). In this way, the effect of restricting the angular range can be explored. For very flat angles of incidence the energy of the rays reflected by the mirrors do not have a big influence for the annual energy yield. Because of that fact the construction of the mirror box, especially the movement of the mirrors, can be simplified. Through the limited angle, the mounting pins can be constructed shorter and as a result of that the height and the width of the box is even smaller. Nevertheless, it is very important that the Energy Yield is bigger than 700 kWh/m<sup>2</sup>a, and in the following steps the incidence angle was varied to find out the optimum.

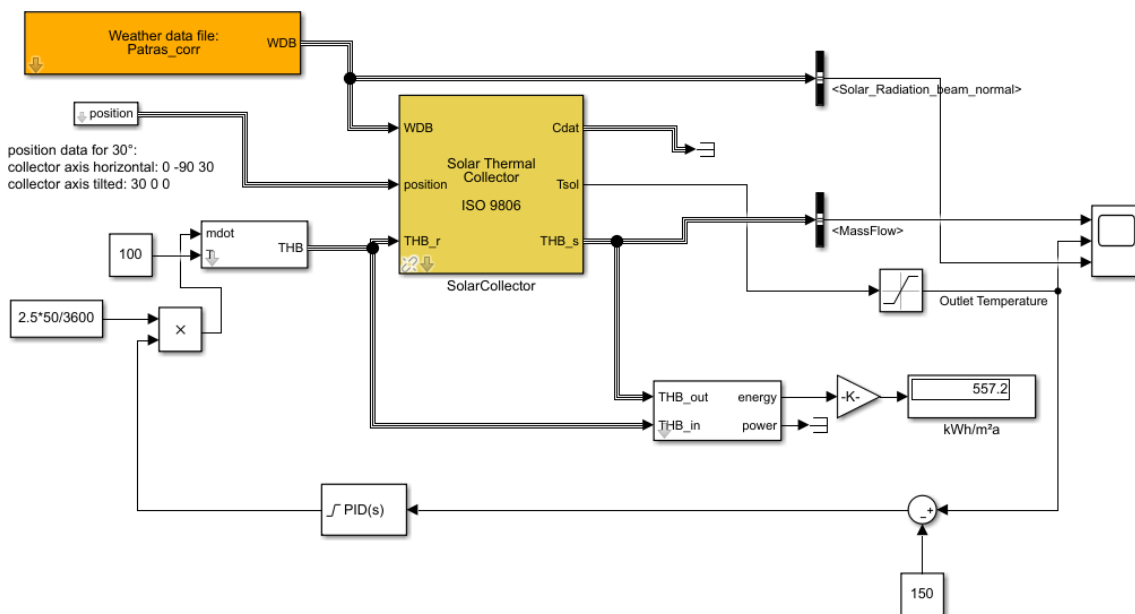


Figure 54:- Annual Energy Yield Simulation (Carnot Toolbox)

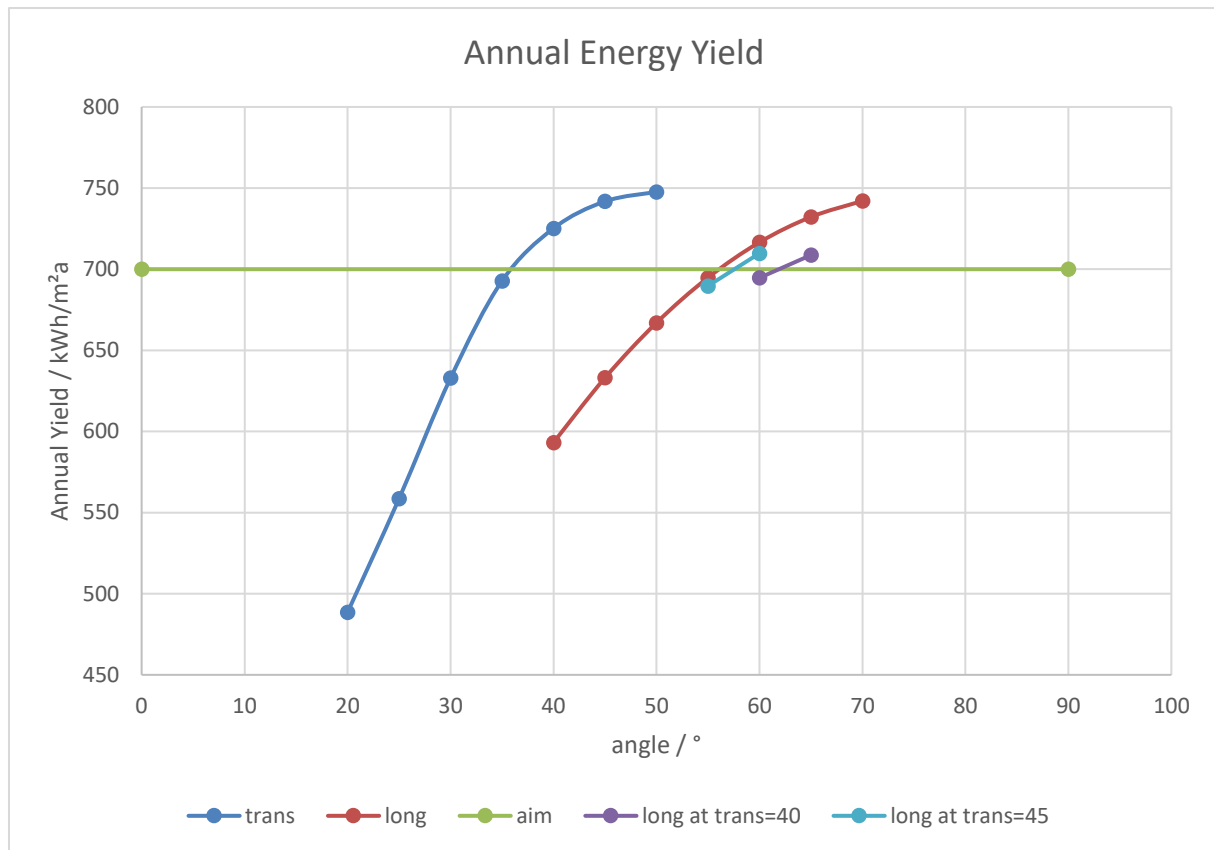


Table 26: Annual Energy Yield with variation of incidence angle (longitudinal and transversal) at which the IAM is set to zero

degree	A 10 mrad		annual energy yield / kWh/m²a			
	trans	long	trans	long	long at trans=40	long at trans=45
0	1.0000	1.0000				
5	1.0024	1.0064				
10	1.0049	1.0127				
15	1.0073	1.0191				
20	1.0078	1.0309	488.6			
25	1.0082	1.0427	558.6			
30	1.0087	1.0545	632.9			
35	0.9757	1.0520	692.8			
40	0.9427	1.0496	725.2	593.2		
45	0.9098	1.0471	741.8	633.1		
50	0.8561	1.0161	747.6	667.0		
55	0.8025	0.9851		694.8		689.7
60	0.7489	0.9541		716.6	694.7	709.8
65	0.6848	0.9014		732.2	708.7	
70	0.6207	0.8487		742.1		
75	0.5566	0.7960				
80	0.3711	0.5306				
85	0.1855	0.2653				
90	0	0				

The results of the simulation in Table 26 and [Error! Reference source not found.](#) show that it is possible to “cut-off” the incidence angle. With the full range of rays in longitudinal direction and the variation in transversal direction it appears that it is possible only to regard the rays with an incidence angle  $\pm 40^\circ$  with an annual energy yield of 741.8 kWh/m<sup>2</sup>a. For longitudinal direction, with the full range of transversal rays, it is possible to stop simulation at  $\pm 60^\circ$  with the annual energy yield of 716.6 kWh/m<sup>2</sup>a. The combination of both gives as a simplification optimum at transversal  $\pm 45^\circ$  in combination with longitudinal  $\pm 60^\circ$ . For this case the annual energy yield is 709.8 kWh/m<sup>2</sup>a.

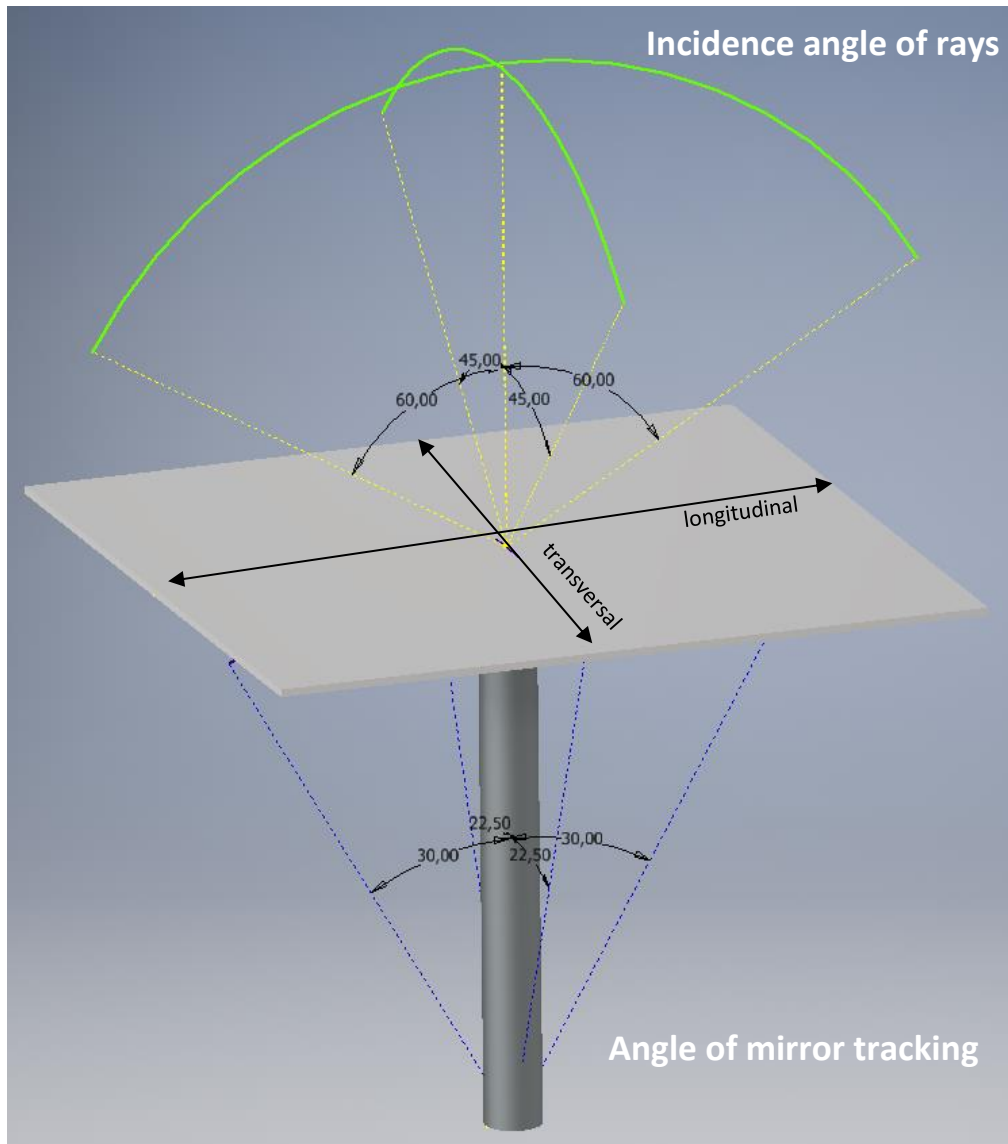


Figure 55: Sketch of mirror tracking path (yellow: angles of incidence, blue: pin/mirror movement)

The result of that simulation is, that the mirrors only have to move  $\pm 22.5^\circ$  in transversal respectively  $\pm 30^\circ$  in longitudinal direction.

### Results SCO\_4\_Micro-mirror concentrator concept UPatras

A series of optical simulations were conducted in an effort to validate COMSOL’s results with Tonatiuh software. Since the two programs are inherently different, we were not able to set all the simulation parameters identical to COMSOL.

Table 27 Tonatiuh simulation parameters

mirrorWidthX	0.14	m	Width of the mirror in X direction
mirrorWidthY	0.187	m	Width of the mirror in Y direction
gapX	0.0015	m	gap between mirrors in X direction
gapY	0.0015	m	gap between mirrors in Y direction
focalLength	1.5	m	Focal length of the mirror array and distance of receiver from array centre
numMirX	7		number of mirrors in X direction
numMirY	8		number of mirrors in Y direction
ref	1		mirror reflectivity
sundisk	4.65e-3		sun disk uniform random distribution
rec_width	0.2	m	receiver width
rec_length	0.25	m	receiver length
alpha	0	°	receiver tilt angle (rotation around y axis wrt array centre)

We define as transversal direction the solar azimuth plane and longitudinal the solar elevation plane with the system rotated in a way that normal incidence occurs at 180° and 0° respectively.

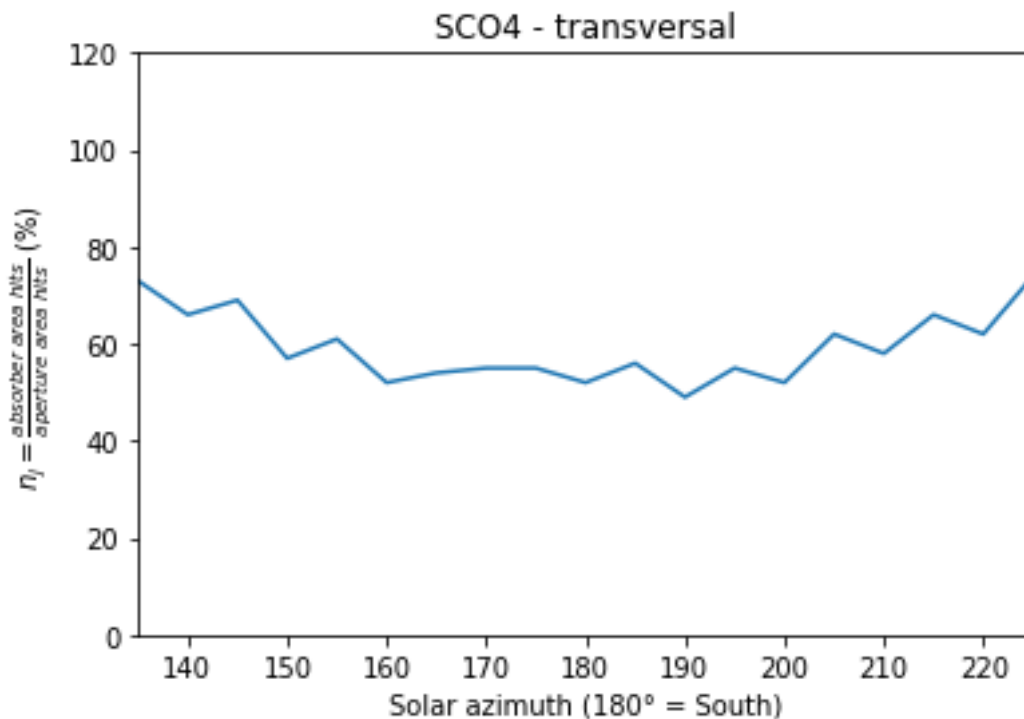


Figure 56 Theoretical intercept factor - azimuth angle (trasversal)



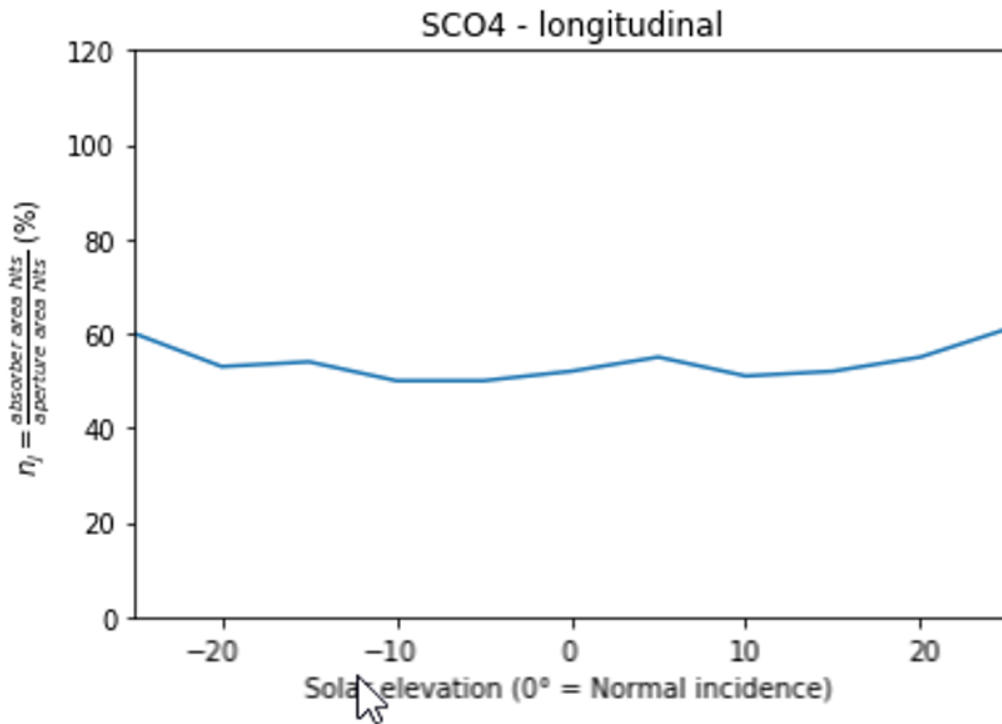


Figure 57 Theoretical intercept factor - solar elevation (longitudinal)

The theoretical intercept factor for 10.000 rays as displayed above is in agreement with the COMSOL results.

The intensity distribution on the receiver at 0° incidence (180 azimuth in Tonatiuh) is displayed in Figure 48

## Conclusion

The concepts **SCO\_1\_Tracking\_Sym** and **SCO\_1\_Tracking\_Asym** do not fulfill the criterion 2, mainly because of a poor intercept factor and a low performance at certain IAM's.

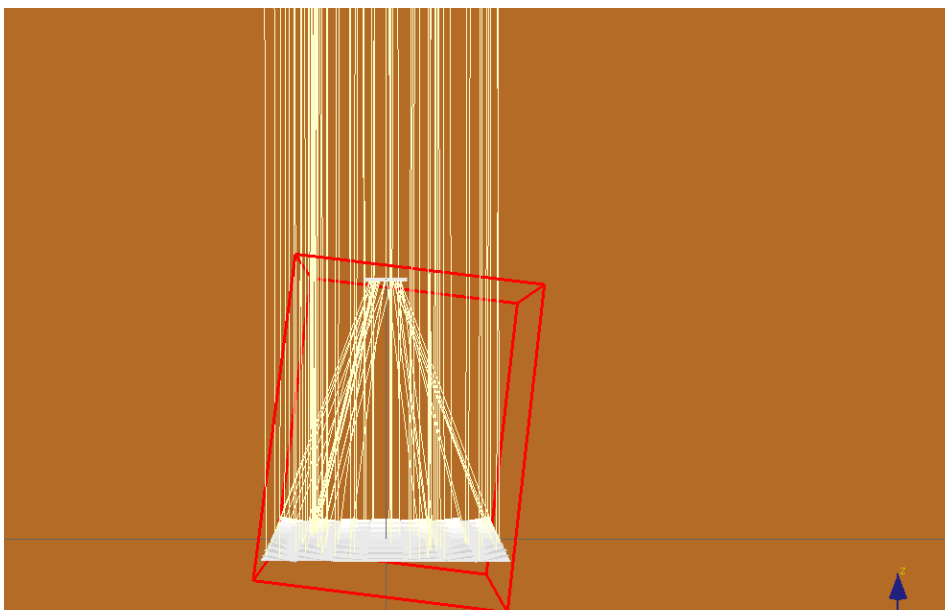


Figure 58 View of the raytracing elements of the micro-mirror system in Tonatiuh for incidence angle 180 (0° in Comsol)

Initially, the defined concept

**SCO\_1\_CYC\_CPC** can't reach the design point criterion (criterion 1) neither the annual yield criterion (criterion 2).

The concept **SCO\_1\_CYC\_CPC** fulfills the criteria 1 and 2 with the consideration of the redefined errors and with an improved reflector. Therefore, the pure geometrical setup is adequate regarding the defined criteria.

Other variants, like the best of breed version and the same version with a circular tracking path also fulfill the criteria. However, those variants imply high quality materials for reflector, transparent cover and absorber coating and a precise construction and accurate manufacturing.

For the concept **SCO\_1\_CYL\_CPC** a direct flow receiver, which is state of the art for medium temperature solar collectors, is required. The specifications of the receiver should be equal or better than the one's from Himin.

The concept **SCO\_4** with the initial parameter setup can't reach the setpoint criterion. Even if the instantaneous efficiency at 250 °C is only missed by 2%, the criterion is considered as a knock-out criteria. With improved error assumptions the **SCO\_4** concept fulfills the defined criterion.

Although the optical performance may increase when using smaller facets, the SIJ expects higher costs for the mechanical system if too many facets must be tracked. Therefore, the facet size of 14 cm appears to be a reasonable compromise without proof so far.

It appears that a small correction to the present tracking algorithm is necessary as the centre of the intensity distribution moves away from the receiver centre at larger angles of incidence. However, the development of this correction will take more time and effort.

Table 28 summarizes the results of the analysis by the SIJ.

Table 28: Overview SCO\_1 and SCO\_4.

Variant	Criterion 1 Design point ≥50% @250°C	Criterion 2 Yearly yield with specific Receiver  @Patras ≥700 kWh/m <sup>2</sup> a	Criterion 3 System performance solar fraction 80%	Criterion 4 Any other criteria
SCO_1_1xSym_37mm & SCO_1_2xSym_37mm & (without error assumptions)	NO	NO	not done	Costs receiver Division of tasks between partners Tracking pathway Requirements on materials and construction Manufacturing of reflectors
SCO_1_2xASYM_37mm (without error assumptions)	OK	NO	not done	
SCO_2 (3 tubes)	NO 43 %	NO 350 kWh/m <sup>2</sup> a		
1. Err. ~10mrd/refl initial parameter setup SCO_1_CYL_CPC	NO	NO	not done	
2. Red.err; refl=90 SCO_1_CYL_CPC	OK	NO 631 kWh/m <sup>2</sup> a	not done	
3. Red.err; refl=95 SCO_1_CYL_CPC	OK	OK 703 kWh/m <sup>2</sup> a	94 m <sup>2</sup>	
4. Red.err; refl=95, Tau97, a96 SCO_1_CYL_CPC	OK	OK 760 kWh/m <sup>2</sup> a	87 m <sup>2</sup>	
5. Red.err; refl=95, Tau97, a96, circular pathway SCO_1_CYL_CPC	OK	OK 744 kWh/m <sup>2</sup> a	90 m <sup>2</sup>	
1. SCO_4 [10mrad] initial parameter setup	NO	Ok 718 kWh/m <sup>2</sup> a	100 m <sup>2</sup> @SIJ [-]	
2. SCO_4 [7mrad]	OK 51.5 %	OK 759 kWh/m <sup>2</sup> a	96 m <sup>2</sup> @SIJ [-]	

## Annex

Manufacturers of vacuum receivers		Schott PTR 70	Rioglass UVAC 70 – 7G	HIMIN HSC 3420	Hofmann Receiver (intended)	ProTarget
Country of origin		Germany	Spain/Israel	China	Germany	Germany
Components						
Dimension	Length	4060 mm	4061 mm	3420 mm	2990 mm	2900/3000mm (cold/hot)
	Usable length	~96,7% of overall length at 350°C	~96,4% of overall length at 350°C	~93,9% of overall length at 350°C	~87% of overall length at 350°C Bellow outboard with:  Length: 80 mm  Diameter: 110 mm  Position: at one side	n.s.
Absorber tube	Outer diameter / WS	70mm	70mm x 2 mm	42 mm x 2 mm	38 mm x 2 mm	38 mm x 2 mm
	Coating	Selective coating  PVD Sputtering	Selective coating  PVD Sputtering	Selective coating  PVD Sputtering	Selective coating  PVD Sputtering [PolyCSP]	n.s.
	Emissivity	$\varepsilon \leq 9,5 \%$	$\varepsilon \leq 9,5 \%$	$\varepsilon \leq 11 \%$	$\varepsilon \leq 10 \%$	$\varepsilon \leq 0.00004 \cdot (\theta^t)^2 - 0.0093 \cdot (\theta^t) + 9.1331$
	Absorptance	$\alpha \geq 96 \%$	$\alpha \geq 96,2 \%$	$\alpha \geq 95 \%$	$\alpha \geq 95 \%$	$\alpha \geq 95.0 \%$ (at AM 1.5).
	Material support pipe	Stainless steel DIN 1.4541	k.A.	DIN 1.4401	DIN 1.4541	n.s.
Glas envelope tube	Material	Borosilicat	Borosilicat	Borosilicat	Borosilicat	n.s.
	Outer diameter	125 mm	115 mm	102 mm	70 mm	100 mm
	Antireflection coating	Yes	Yes	No	No	No

	Transmission	□ ≥ 97 %	□ ≥ 96,7 %	□ ≥ 92,0 %	□ ~ 92,0 %	□ ~ 91,0 %
Thermal losses		250 W/m [bei 400°C]	n.s.	170 W/m [bei 400°C]	250 W/m [bei 350°C]	n.s.
		165 W/m [bei 350°C]	not specified	113 W/m [bei 350°C]	180 W/m [bei 300°C]	
		110 W/m [bei 300°C]		71 W/m [bei 300°C]	110 W/m [bei 250°C]	
		70 W/m [bei 250°C]		48 W/m [bei 250°C]	75 W/m [bei 200°C]	
		Data from product specifications		29 W/m [bei 200°C]	[small annular gap]	
Operation temperature	Maximum	400 °C	400 °C	400 °C	350°C	n.s.
Vacuum	Annular gap	Yes	Yes	Yes	Yes	n.s.
Gas pressure	absolute	≤ 10 <sup>-3</sup> mbar	≤ 10 <sup>-4</sup> mbar	≤ 10 <sup>-4</sup> mbar	≤ 10 <sup>-3</sup> mbar	≤ 10 <sup>-3</sup> mbar
Heat transfer fluid	Medium	Conventional high temperature heat transfer oil, silicone HTF or water				
Operation pressure	absolut	≤ 41 bar	≤ 40 bar	≤ 40 bar	≤ 40 bar	≤ 35 bar
Retail price	about**€/ per receiver	800 – 1000 €/unit	800 – 1000 €/unit	450 €/unit for an order of > 100Pcs	300 €/unit target price Not available on market	Collector prize 250-235 €/m <sup>2</sup> Aperture

Table: Receiver [Check of References is necessary]

## References

- Tripanagnostopoulos, Y., and P. Yianoulis. 1996. "CPC Solar Collectors with Multichannel Absorber." *Solar Energy* 58(1–3): 49–61.